State of the Art in Transportation Geotechnics

État de l'art en géotechnique des transports

Richard Kelly
Chief Technical Principal SMEC & Conjoint Professor University of Newcastle, Australia, drrichard.kelly@smec.com

Buddhima Indraratna
Distinguished Professor & Director of Transport Research Centre, University of Technology Sydney, Australia

William Powrie
Professor, University of Southampton, United Kingdom

Claudia Zapata
Assoc. Prof., Arizona State University, USA

Yoshiaki Kikuchi
Professor, Tokyo University of Science, Japan

Erol Tutumluer
Professor, University of Illinois, USA

Antonio Gomes Correia
Professor, University of Minho, Portugal

ABSTRACT: Transportation systems are undergoing a period of substantial change. Vehicles are becoming larger, heavier, faster and longer. There is a desire to reduce environmental impact in construction and operations, and opportunities associated with digital advancements are being created. In this paper we report the current state of the art within this context, identify elements practitioners could adopt and opportunities for further research.

RÉSUMÉ : Les systèmes de transport traversent une période de changements substantiels. Les véhicules deviennent plus gros, plus lourds, plus rapides et plus longs. Il y a un désir de réduire l'impact environnemental dans la construction et les opérations, et des opportunités associées aux avancées numériques sont créées. Cet article passe en revue l'état actuel de l'art dans ce domaine et identifie les éléments que les praticiens pourraient adopter et les opportunités de recherches futures.

KEYWORDS: Port, Airport, Road, Rail

1 INTRODUCTION.

Transportation systems facilitate the operation of economies which supports the way of life for people and communities (National Academies of Sciences, Engineering, and Medicine 2019). Transportation systems are the arteries of global and local communities. Transportation systems are required to move goods and people from their source to where they are needed or wanted to be. Ports and airports tend to act as gateway and corridor infrastructures between countries while road and rail distribute people and goods more locally.

Roads and ports have existed for thousands of years. Rail has existed for about 200 years and airports for about 100 years. However, the world is in a period of significant change as a result of population growth, globalisation, technology development and environmental stresses. That is driving major changes in transportation systems and hence will require major advances in the geotechnical engineering that supports them.

Global growth is projected to increase to 2030 with the fastest growth in developing countries and more moderate growth in the developed countries (OECD, 2011). This growth will demand increased capacity from transportation systems and this is likely to translate into more infrastructure as well as larger ships, aeroplanes, trains and road vehicles. Reducing the carbon footprint of transportation infrastructure is contributing to increased load carrying capacity instead of high volume. Increased capacity has a major effect on geotechnical engineering behaviour of transport systems.

HSBC estimates the financial investment over the next 20 years (in US Trillions of dollars) in roads is $30.6, rail is $10.3, ports and airports are each $3.2. (HSBC Global Infrastructure Trends, 2019)

Delivery of transport infrastructure will require balancing competing socio-economic, political, cultural, demographic and increasingly, ecological factors. This balance is reflected in transportation strategies published by various countries. Each country has a different balance to achieve but there are many common themes. Some key themes are:

1. Financing and building cost effective infrastructure (National Academies of Sciences 2019, OECD 2011, ICE 2019, Australian DIRD 2016). Earthworks and

pavements often comprise a large percentage of construction and maintenance costs.

2. Building integrated transportation systems (OECD 2011, CPCCC 2019, BBC 2013, ICE 2019, Australian DIRD 2016). For example, greater marine traffic will require greater land transport capacity to move goods from the port before port storage capacity is reached and to turn boats around within 24 hours.
3. Connecting people within cities and between cities with reasonable commuting times and reduced traffic congestion (National Academy of Sciences 2019, CPCCC 2019, ICE 2019, Australian DIRD 2016) driving the need for fast 400km/hr to 600km/hr trains (CPCCC 2019)
4. Step change in capacity. For example freight trains with 30,000 tonne capacity travelling at 250km per hour (CPCCC2019) or container ships that are too large to navigate through existing transport routes or dock at some nation's ports (BBC 2013)
5. Improved environmental outcomes (National Academies of Sciences 2019, CPCCC 2019, BBC 2013, Australian DIRD 2016) such as more efficient use of materials, use of recycled materials or selecting routes away from high value ecological land which could favour construction through poor quality ground conditions.
6. Resilience in response to changing environmental conditions (National Academy of Sciences 2019, OECD 2011, ICE 2019, Australian DIRD 2016). Resilience is the ability to rapidly re-establish key transport infrastructure after some form of major disaster event.
7. Development of intelligent systems to assess the performance of infrastructure assets and inform maintenance requirements (National Academy of Sciences 2019, CPCCC 2019, ICE 2019, Australian DIRD 2016). This includes big data analytics and machine learning concepts (e.g. massive storage of wayside data that has been accumulated over many years to cover all aspects of construction quality and immediate performance, design validation and performance monitoring (short to medium term), and maintenance and repairs (medium to long term).
8. Further development of automated driverless systems (National Academy of Sciences 2019, CPCCC 2019, Australian DIRD 2016) and their implications on traffic volumes and pavement construction. Short distance commuter trains or light rail are relatively common in some countries and some iron ore trains and mining vehicles in Australia are driverless. The concept here is that automation of a large proportion or all traffic in large cities could occur in order to maximise traffic volume while minimising travelling times.

While there are many similarities in the engineering requirements for ports, airports, road and rail there are some key differences. The container trade is a high volume relatively low margin business (BBC 2013) where it is important to transport in bulk and to distribute goods to and from port efficiently. New airports require large areas and are often located in areas with poor ground conditions. In large countries such as Canada, Australia, Russia, China, India and USA, the distance between the source (or destination) and port (or airport) can be several hundreds of kilometers which favours large capacity heavy haul road or rail infrastructure. In contrast, for commuter transport, people will want to ensure the trains and buses stop at their doorstep when the timetable states that they will arrive and that roads are not too congested. This leads to construction of high speed, high volume transport systems to accommodate relatively low weight vehicles. Ports, airports, major roads and rail are required to be operational most of the time which means that disruption due to planned and unplanned maintenance should be consistent with the operational requirements of the infrastructure. This is driving utilisation of big monitoring and materials data sets to understand when and where future maintenance is required. Some systems are designed for periodic maintenance such as ballasted rail track and flexible pavements and some are designed to require minimal maintenance such as slab track or rigid concrete pavements. Maintenance in constrained corridors can require people to be in close proximity with traffic which increases safety risks. Overcoming these safety risks is a key driver for the development of remote sensing systems.

In this paper we address three themes:

1. The future of transportation: bigger, heavier, faster, longer;
2. Management of our environment; and
3. The digital age.

Based on this review, we discuss opportunities for practitioners and areas of research for academics.

2 THE FUTURE OF TRANSPORTATION: BIGGER, HEAVIER, FASTER, LONGER

2.1 *Reclamation for ports and airports*

Port facilities including seaports and airports have become increasingly important to drive economic growth worldwide. The expansion of these facilities is strictly controlled by the availability of suitable nearby land, due to their locations close to urban areas. As a result, new port or port expansion projects often rely on land reclamation or swampy land where ground improvement methods are required before the construction of facilities. The reclamation techniques mainly employ dredged or borrowed materials together with the additional improvement to achieve the required performance criteria. Additional challenges need to be addressed when dealing with the unacceptable geotechnical properties such as, low shear strength and excessive long term deformation which can affect the stability of built infrastructure.

2.1.1 *Kansai International Airport*

The Kansai International Airport is located 5km offshore from the mainland, as shown in Figure 1. Reclaimed zone is separated into two phases. The length of each zone is about 5km and the width of each zone is 500m. The ground conditions at the site are shown in Figure 2. The thickness of Holocene layer at the site is about 20 m, and there is more than 400 m of older compressible layers beneath the Holocene layer. The water depth is 18m to 20m. Reclamation of the 1st phase comprised an area of 510ha, a volume of 180Mm^3 and an 11km long sea wall, was started in 1988 and finished in 1991. The second phase had an area of 545Ha, a volume of 250Mm^3 and a 14km seawall (Furudoi, 2010).

For the first phase reclamation, the Holocene layer was improved using sand drains and the settlement of Holocene layer was about 6m, finished just after the reclamation. The Pleistocene layer beneath Holocene layer was not treated and the estimated settlement is about 9m, which is expected to continue for more than 50 years. Figure 3 show the time - settlement relationship of the 1st phase island. As the 1st phase of the airport was inaugurated in September 1994, an estimated 12m of settlement was expected in the period from the beginning of construction to the opening of the runway. An extra 6m of residual settlement was predicted over a 50-year period after the opening of the runway.

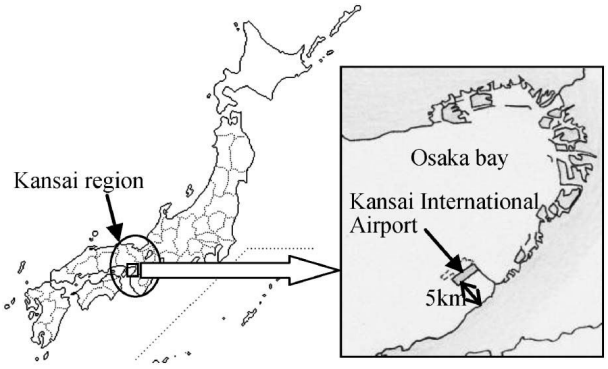

Figure 1 Location of Kansai International Airport (Furudoi, 2010)

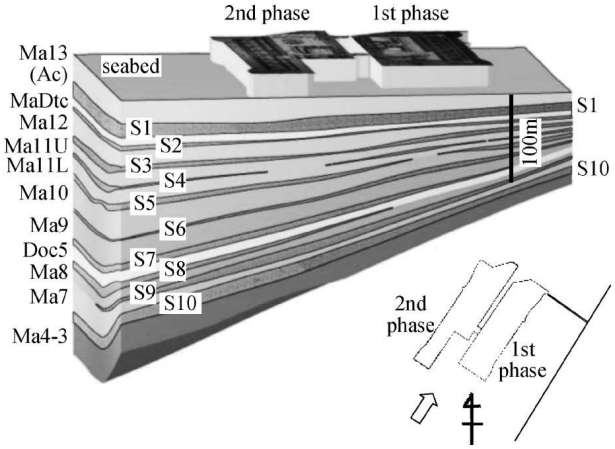

Figure 2. General overview of seabed under airport islands (Furudoi, 20 10)

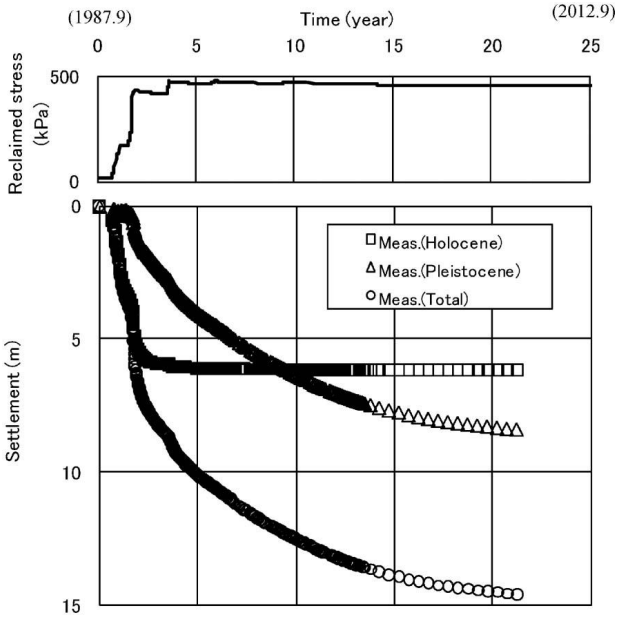

Figure 3. Settlement observed at Holocene and Pleistocene clay layers in the first phase reclaimed island (Furudoi, 2010)

The long-term settlement predictions were incorporated into the design of the airport island, which had a design life of 50 years. The reclamation was carefully performed to minimize uneven settlement and to ensure the thickness of reclaimed soils by properly managing the reclamation work.

In order to predict the amount of settlement, the geotechnical properties of the Pleistocene clay properties and layer configurations were investigated prior to the beginning of the first phase project. Among the boring explorations, two of which were at the minus 400m level, because the estimated consolidation layers were continued to that level.

The prediction of the long-term settlement was based on a one-dimensional consolidation analysis with the boundary conditions of pore water pressures in the Pleistocene sand layers, which were calculated separately by a two-dimensional seepage flow analysis. The constitutive model used for estimating the settlement of the second phase airport island was developed from the results of laboratory tests and observations of ground behavior at the first phase airport island and takes such factors as settlement and pore water pressure into account. In this model, the *e-log p* curve was simulated by two straight lines such that one for the overconsolidated region, and the other for the normal consolidated region. All the consolidation layers were slightly overconsolidated. As settlement data obtained during the construction of the first airport island showed the existence of a secondary consolidation, secondary consolidation was also considered.

A comparison of the measured and predicted settlements of the 2nd phase airport island is shown in Figure 4. The estimated data from the above model is named DB in the figure. Its validity was confirmed by the second island settlement data.

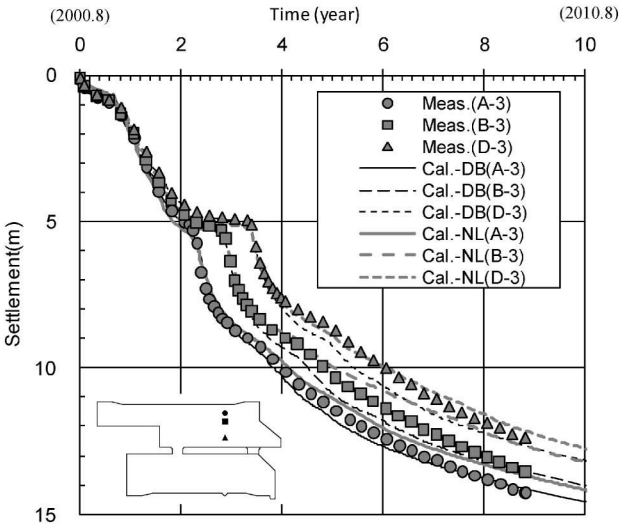

Figure 4 Comparison of measured and calculated settlement (total settlement DB: DB model, NL: Nonlinear model; Furudoi, 2010)

When total settlement is large, differential settlement becomes large. Minimizing the differential settlement was one of the important issues in constructing the second phase airport island. Figure 5 shows the change in settlement of the first and second phase islands with time. As shown in Figure 5, the settlement in the first island varied with the location. In contrast, the settlement in the second phase island showed almost the same tendency regardless of location. To avoid large differential settlements, it was important to continuously supply reclamation soil to the reclamation area from the initial stage of construction. As shown black line in Figure 5, there was especially small differential settlement, because of avoiding differences in the construction history.

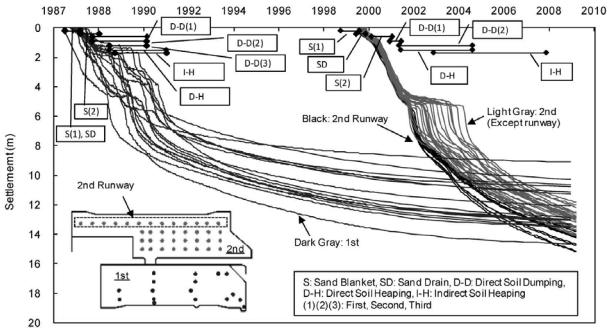

Figure 5. Settlement of 1st and 2nd islands (Furudoi, 2010)

2.1.2 *Tokyo International Airport*

An offshore extension project for Tokyo International Airport was conducted from 1984 to 2004. The offshore construction site was used for waste reclamation facilities for dredged clay. The surface ground condition of the site was extremely weak, essentially liquid. To enable construction, firstly shallow solidification was used to provide access to heavy ground improvement machinery (Figure 6). After the surface treatment, the ultra-soft dredged clay was improved by consolidation with vertical drains and preloading. This technology requires a long construction period.

Figure 6 To enable trafficability, a shallow solidification method was conducted with heavy machine on a barge (courtesy of Kanto Regional Development Bureau, MLIT, Japan).

At Kansai International Airport, prediction technology for consolidation settlement in a deep Pleistocene clay was significantly advanced. This experience aided the new runway project at Tokyo International Airport (TIA), shown in Figure 7. Because, incremental consolidation pressure at TIA new runway was 550 kPa or larger, which is almost the same as that in the second phase island of Kansai International Airport, prediction of long-term consolidation settlement derived from deep soil layers (without ground improvement) was very important.

Technologies used for soft clay/dredged clay in the previous airport projects were 1) vertical drains to accelerate consolidation, 2) replaced by good material: clay and sand, and 3) chemically strengthened (cement treatment)

In the TIA new runway project, 1) soft clay deposit inside the reclamation section was improved by Sand Drains (SD), 2) under the rubble seawall was improved by Sand Compaction Pile method (SCP) with low replacement ratio and 3) under the important seawalls the ground was improved by Cement Deep Mixing as shown in Figure 8.

Figure 7 View of the TIA new runway (courtesy of Kanto Regional Development Bureau, MLIT, Japan).

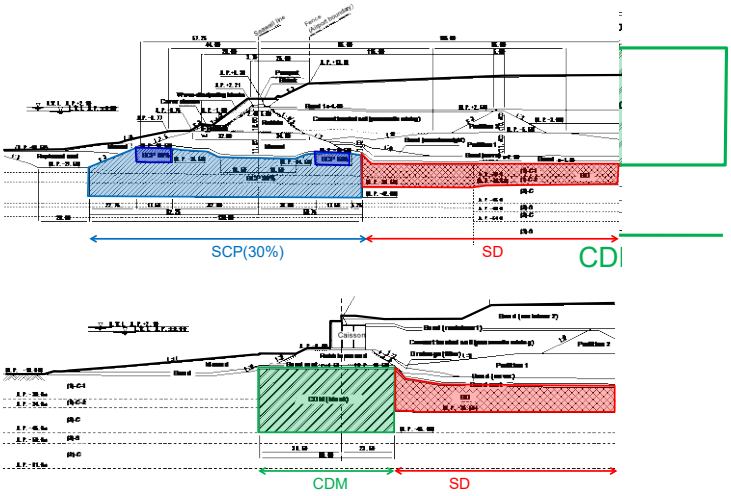

Figure 8 Ground improvement for TIA (courtesy Prof Kikuchi)

2.1.3 *Central Japan International Airport*

Central Japan International Airport was opened in 2005. The north region of the airport island was reclaimed by cement treated dredged clay (Figure 9, Figure 10). This cement treated method called Pneumatic flow mixing method was new technique at the time. In this method, dredged clay was placed as a cement mixture. This technology does not require a long curing time and cement treated soil itself has no settlement.

2.1.4 *Application of the deep mixing method to Tokyo/Haneda international airport expansion project*

Tokyo/Haneda International Airport was founded in 1931 as the first primary airport in Japan. The airport had been expanded several times to cope with the rapid increase in air transportation. In order to cope with the recent and expected future increase in air transportation, the construction of fourth runway was commenced in 2006 and completed in 2010 (Figure 11). As soft grounds were stratified at the construction site, various ground improvement techniques including the sand drain method, the sand compaction pile method and the deep mixing method were employed depending on the location and the requirements.

Figure 9 Satellite view of Central Japan International Airport.

Figure 10 Cement treated dredged clay method was used for the reclamation of the site (Courtesy Prof Yoichi Watabe).

Figure 11: Aerial view of construction site and existing airfield on March 15th, 2009 (Courtesy Prof Kitazume).

The ground condition and the major soil properties at the site were extensively studied and are summarized in Figure 12. The ground can be roughly divided into five layers. The most upper layer between -20 m and around -35 m has high plasticity index ranging from 60 to 100 and high water content ranging from 100 to 150 %. The undrained shear strength and the pre-consolidation pressure increased linearly with the depth, which indicated the clay was lightly over-consolidated condition of OCR of 1.3. The second upper layer from -35 to -60 m was a clay layer underlain locally by a sand layer. The upper two layers were improved to increase the stability of superstructures and to reduce the residual settlement of the man-made island for the fourth runway.

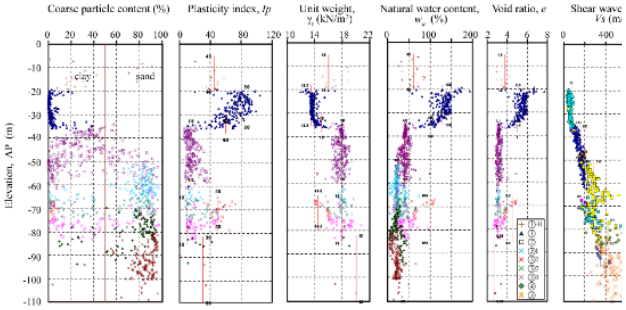

Figure 12: Soil properties at construction site (Kitazume and Terashi, 2013)

Almost all of the sea revetment embankment was constructed on ground improved by the sand compaction pile method. However, caisson type quays were constructed at two corners of the island (CW and CN revetments). The block type improvement of 60m in width was constructed to a depth of minus 45m, as shown in Figure 13 for the CW revetment. Table 1 summarizes the properties of the soil layers. The table shows that the properties of the four soil layers were much different to each other so that the mixing condition should be adequately determined for each layer to assure the design strength of stabilized soil. The mixing conditions were designed as tabulated in Table 1 based on the laboratory mix tests, where blast furnace slag cement type B of 110 to 165 kg/m^3 was mixed with the soil to obtain the average field unconfined compressive strength, q_{uf}, of 3,375 kN/m^2 at 28 days curing. The total of about 620,000m^3 soft soils was stabilized by four DM vessels within five months. Figure 14 shows the DMM vessels in operation.

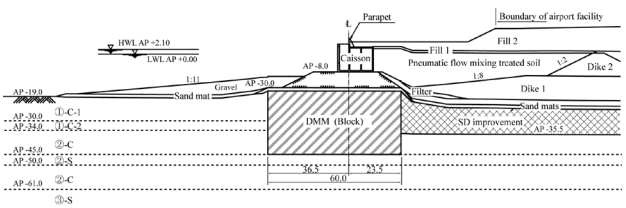

Figure 13: Cross section of DMM improvement at CW revetment (Kitazume and Terashi, 2013).

Table 1: Soil properties and cement content.

	soil property				binder content
	w_n (%)	w_l (%)	w_p (%)	Ip	(kg/m^3)
surface layer	168-177	-	-	-	165
clay 1-C1	132-145	132-137	51-54	78-85	140-145
clay 1-C2	42-117	41-118	22-47	19-70	130-135
clay 2-C	35-52	32-55	18-24	14-31	110-120
sand 2-S	37	-	-	-	

Figure 14: DMM vessels in operation (Courtesy of the Tokyo/Haneda International Airport Construction Office).

At 24 to 26 days after the construction, soil sampling was carried out at several points for quality assurance. The stabilized soils sampled were subjected to unconfined compression test to investigate the strength of in-situ stabilized soil. A summary of the test results is shown in Table 2. The data shows that the average of q_{uf} was 4,094 kN/m^2, 20% higher than the target value, and the coefficient of variation (COV) was 28.3%, lower than the design value, 35%. According to that, the mix design was modified for the subsequent construction in order to reduce the amount of ground heaving and the cost, where the amount of cement was decreased by 3 to 27%. Table 3 shows the q_{uf} values of the stabilized soils after the modification. The table clearly shows that the average strength of the stabilized soils was 4,066 kN/m^2 and the stabilized soil constructed in-situ satisfied the acceptance criteria.

Table 2: Original cement factor and field strength.

	no. of tests	Field strength, q_{uf28}		Binder content
		average (kN/m^2)	COV (%)	(kg/m^3)
surface	20	3,409	27.1	165
clay 1-C1	36	4,009	28.9	140-145
clay 2-C2	16	3,929	21.3	130-135
sand 2-C	44	4,534	26.4	110-120
Total	116	4,094	28.3	

Table 3: Modified cement factor and field strength.

	no. of tests	Field strength, q_{uf91}		Binder content
		average (kN/m^2)	COV (%)	(kg/m^3)
	30	3,568	35.8	160
Surface	16	4,010	31.7	160
clay 1-C1	72	4,410	29.8	120-125
clay 1-C2	32	4,561	33.9	110-120
clay 2-C	88	3,871	26.2	80-85
Total	238	4,066	31.4	

2.1.5 *Port of Brisbane*

The Port of Brisbane is the third largest container port in Australia. The Port is located at the mouth of the Brisbane River at Fisherman's Island (Figure 15). A new outer area (235ha) was reclaimed to provide the maximum number of berths suitable for bulk cargo and container handling. Part of the reclamation lay adjacent to a marine nature park have a constraint of zero impact from the works.

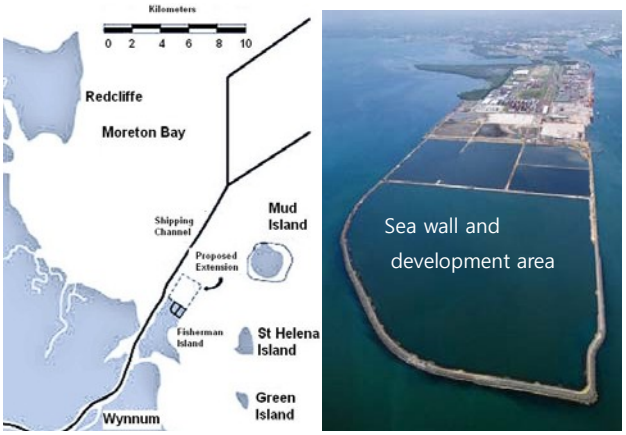

Figure 15: Expansion area of the Port of Brisbane (modified after Indraratna *et al*., 2011a)

The geological profile consisted of highly compressible clay with undrained shear strength less than 15 kPa. The same clay was dredged from the adjacent river and used as reclamation fill at moisture contents in excess of the liquid limit. It was predicted that the consolidation could take 50 years with vertical settlements up to 4.0m in the absence of ground improvement. Ground improvement via surcharging alone had a high risk of instability and consequent effects on the marine park.

Use of prefabricated vertical drains (PVDs) with vacuum consolidation was adopted adjacent to the park to enhance stability, accelerate the consolidation process, reduce the volume of imported surcharge fill and reduce lateral deformation (Indraratna *et al*. 2011a).

The stratigraphy consisted of an upper Holocene sand layer of approximately 2-3m thickness underlying the reclaimed soil (dredged mud), followed by the Holocene clay layer varying in thickness between 6m and 25m. An in situ and laboratory testing program was conducted including cone penetration/piezocone tests, dissipation tests, boreholes, field vane shear tests and oedometer tests to determine consolidation and stability design parameters. Conventional fill preloading system (WD1-WD5, Figure 16) and the membrane-type vacuum consolidation system (VC1 and VC2, Figure 16) with circular PVDs were adopted. The design criterion was that the maximum residual settlement should be no more than 0.25 m over 20 years under a service load of 15-25 kPa. In surcharge-only areas, both circular and band shape drains were installed in a square pattern at 1.1 to 1.3m spacing whereas, in the vacuum area, only circular drains were installed under a membrane system at a spacing of 1.2m in a square pattern.

Arrays of different instruments were used, including settlement plates, vibrating wire piezometers, magnetic extensometers, and inclinometers. Fill placement and associated settlements and excess pore pressures responses are shown in Figure 17.

Very similar settlement trends can be observed among the different sub-areas where the settlement rate is higher at the start of consolidation and the magnitude of settlement varies along with the clay thickness and embankment height. Excess pore pressures show the effect of surcharge loading and the pore pressure dissipation with time. For the same period, the reduction of excess pore pressure in vacuum areas (VC1 and VC2) was greater than that in the surcharge only areas. At this site, the circular drains propagated the vacuum pressure to depth without losing suction head.

Figure 16: Detail the proposed extension area at the Port of Brisbane (Indraratna *et al*., 2011a)

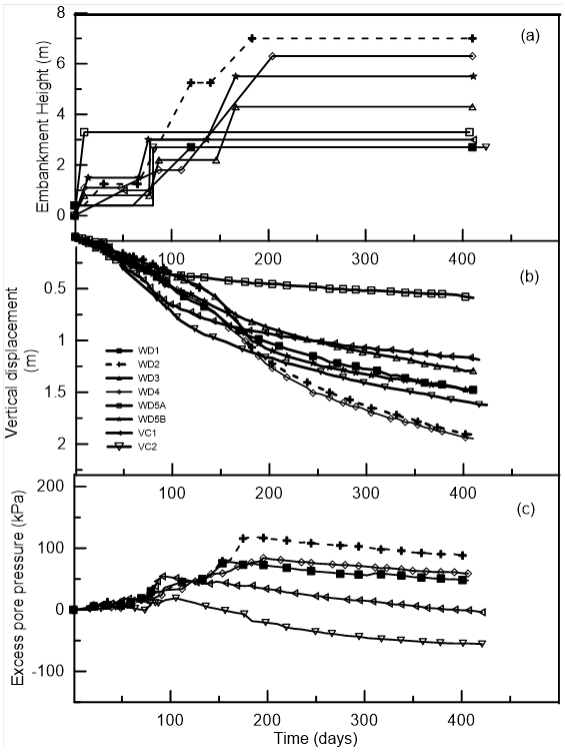

Figure 17: Embankment responses (a) staged construction, (b) settlements and (c) excess pore pressures (Indraratna *et al*., 2011a)

In order to separate the 'clustering' especially towards one year, the degree of consolidation was divided by a dimensionless beta factor (Indraratna *et al.*, 2013b), which is defined in Equation 1 by:

$$\beta = \left(\frac{l_d}{\alpha s_d}\right)\left(\frac{H}{h_c}\right) \qquad (1)$$

The β-factor is independent of soil properties and is designed to capture the drain and site loading conditions. The β-factor comprises (i) the drain length (l_d), (ii) the drain spacing (s_d) and its pattern (α = 1.05 for triangular and 1.13 for square spacing), and (iii) the surcharge load height including equivalent height of vacuum pressure as well as fill height (H) to consolidate the given clay thickness (h_c), represented by the ratio (H/h_c).

Although the value of β has no specific relationship to the target degree of consolidation (U), it can act as a 'filter' in distinguishing relative performance. Figure 18 shows the variation of U with time for the membrane and membraneless systems. Figure 19 shows U divided by β-factor with time.

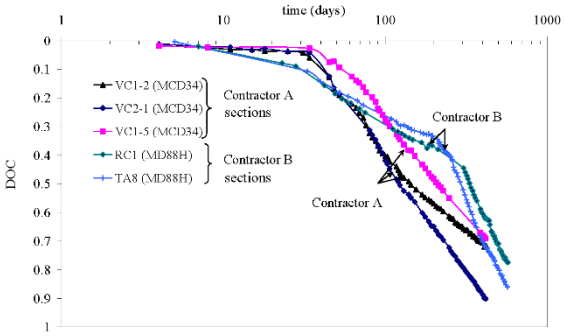

Figure 18: Computed degree of consolidation with time (Indraratna *et al.*, 2013b)

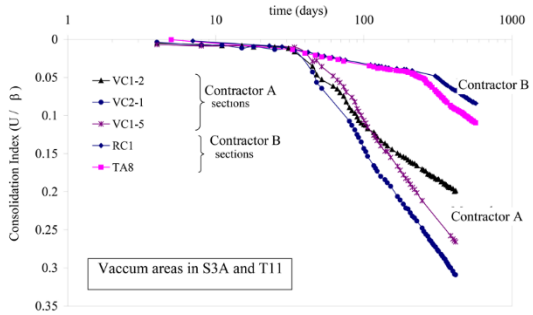

Figure 19: Computed U / β with time (Indraratna *et al.*, 2013b)

Extended running of vacuum pumps can become uneconomical. The optimal time for turning off the vacuum pumps depends on various factors such as degree of consolidation, vacuum-fill surcharge ratio and required time-cost to complete the improvement following switching off the vacuum pumps. Based on laboratory observation supported by field observation at the Port of Brisbane, Kianfar *et al*. (2015) showed that removal of the vacuum pressure can be decided based on flattening of the pore pressure response with time (Figure 20).

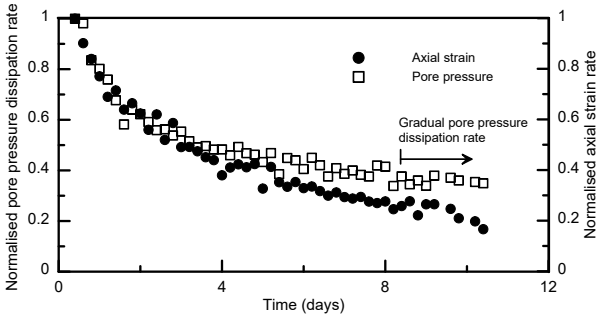

Figure 20: Determination of removal time of vacuum pressure (Kianfar *et al.* 2015)

2.1.6 *New Mexico International Airport*

López-Acosta *et al*. (2019) analysed the performance of an embankment stabilized by vacuum pressure with a membrane-less system for the New Mexico International Airport (Figure 21). PVDs were installed at 1.2m spacing in a triangular pattern before the horizontal drains were installed. A suite of instrumentation was installed including piezometers, settlement plates, magnetic extensometers, vertical and horizontal inclinometers. The monitored time-dependent performance comprising of vacuum pressure, expelled volume of water, and pore pressure is shown in Figure 22. The nonuniform vacuum pressure shows a possible leak at the connections (Figure 22b). Based on the measurement, the maximum applied vacuum pressure was approximately 72 kPa. The rate of water extraction at the site decelerates with time (Figure 22c). The measured pore pressures show that the vacuum can propagate to the depth where the PVDs were installed (Figure 22d). At this site, longitudinal cracks were observed around the embankment's perimeter. They suggested that the efficiency of vacuum consolidation of the site depended on the prevention of the vacuum loss at the connections and the elevation of vacuum pumps in relation to that of the horizontal drains.

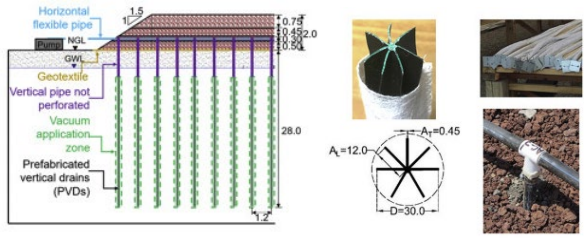

Figure 21: An embankment with vacuum preloading system (a) Vertical cross-section (b) circular drain and the connection between horizontal drain and circular PVDs (López-Acosta et al. 2019)

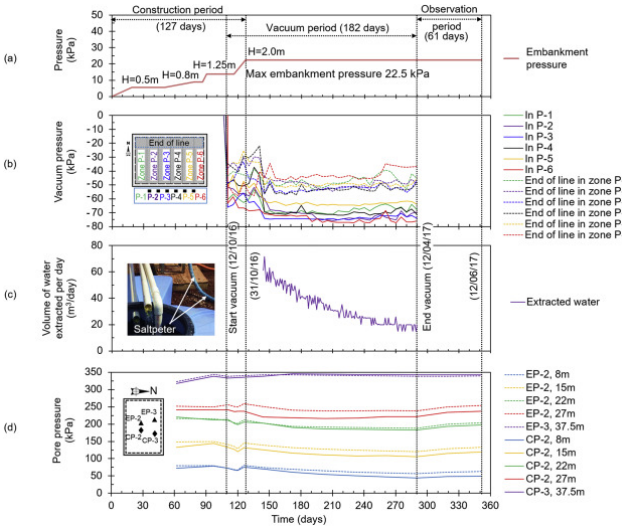

Figure 22: (a) staged construction (b) measured vacuum pressure (c) volume of discharged water (d) pore pressure (López-Acosta et al. 2019)

2.1.7 *Oufei sluice project, Wenzhou, China*

Cai *et al*. (2015) introduced a new approach to improve deep marine clay where a booster prefabricated vertical drain is employed to channel compressed air into the deeper soil layer to assist pore pressure dissipation close to the end of vacuum consolidation. Figure 23 shows a schematic diagram of the air booster vacuum consolidation where the booster PVDs are installed in between conventional PVDs. The performance of the system in comparison to conventional vacuum consolidation system was examined at the Oufei sluice project in Wenzhou, China which was one of the largest individual tideland reclamation projects in China. At this site, the marine soils included silt, silt clay, silty clay, and muddy–silty clay. A vacuum pressure of 85 kPa was applied with PVDs installed at 0.8m spacing in a triangular pattern. Figure 24 presents the variations of pore water pressure and settlement where the booster was activated after 72 days. It shows that the booster system can further increase the dissipation rate of the pore water pressure and settlement at the end of consolidation especially at depths greater than 20m.

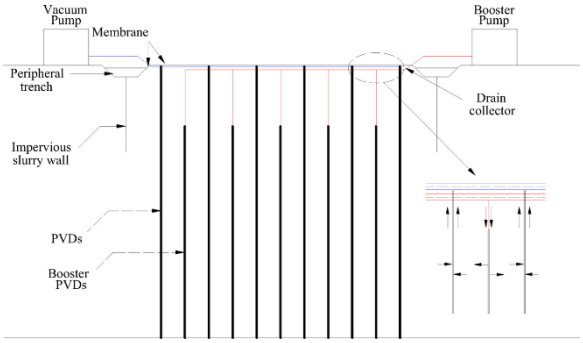

Figure 23: Cross-section of air booster vacuum system (Cai *et al*. 2015)

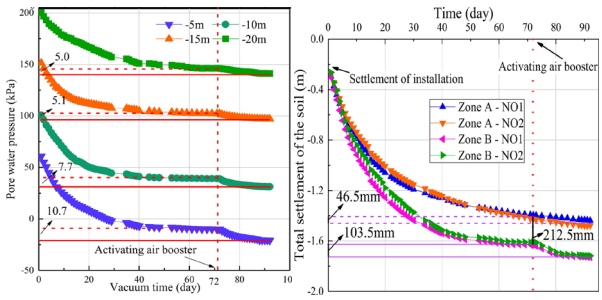

Figure 24: (a) pore water pressures and (b) settlements at different depths (Cai *et al*. 2015)

2.1.8 *Ningo port, China*

The High Vacuum Densification Method (HVDM) was applied at the land reclamation project at Ningbo Port, China (Xu *et al*. 2015). This technique combines the application of vacuum dewatering and dynamic compaction. Vacuum pressure facilitated by PVDs is applied to shallow depth of the dredged soil to increase the undrained shear strength. Subsequently, dynamic compaction can be applied to create positive excess pore pressures which can be dissipated after a second round of vacuum application. The process can be repeated until the desirable results in terms of shear strength and compressibility are obtained. At this site, the shear strength of soil was increased by 30-40kPa to a depth of 5m after the first cycle of the treatment. Figure 25 shows the CPT profiles before and after treatment. It can be seen that the cone resistance increased as a result of the treatment.

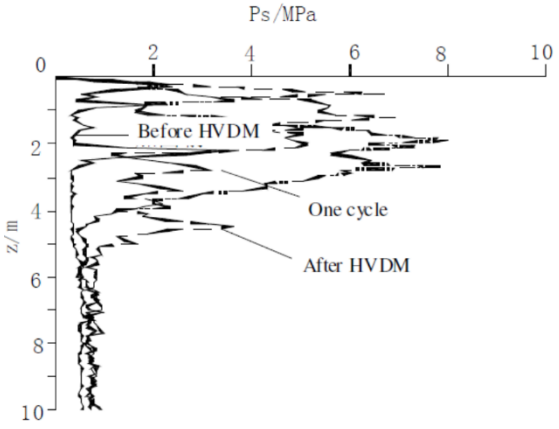

Figure 25: Cone resistance before and after treatment (Xu *et al* 2015)

2.2 *Airport pavements*

Airfield pavement represents almost 30% of initial airport construction cost and between 30% and 40% of annual airport infrastructure maintenance costs. Pavement is the biggest Airport airside asset (Fabre, 2021). Therefore, constructing durable pavement and extending the life of existing pavements are important considerations. Because both wide body passenger and cargo aircraft gear/wheel loads are quite heavy, protecting the pavement foundation, i.e. subgrade and granular subbase and base from excessive permanent deformation has been the key consideration in airport pavement design.

Recent airport pavement research has been linked to the concept of building airport pavements to protect the subgrade layer. Key elements in the work include better prediction of unbound aggregate base/subbase permanent layer deformations and their accumulation rates. This requires a better understanding of the magnitudes and variations of stress states in the granular layers, number of load applications, gear load wander patterns, previous loading stress history effects, trafficking speed or loading rate effects, and effects of principal stress rotation due to moving wheel loads.

State-of-art resilient and permanent deformation models have been developed based on the full-scale test data from Construction Cycles 1, 3, 5 and more recently 9 (CC1, CC3, CC5 and CC9) at the USA Federal Aviation Administration (FAA) National Airport Pavement Test Facility (NAPTF). NAPTF is an indoor facility for construction and testing of full-scale airport pavement test sections under actual full size multiple gear/wheel loading scenarios (Figure 26 and Figure 27).

Figure 26: NAPTF test vehicle (Sarker and Tutumluer, 2020)

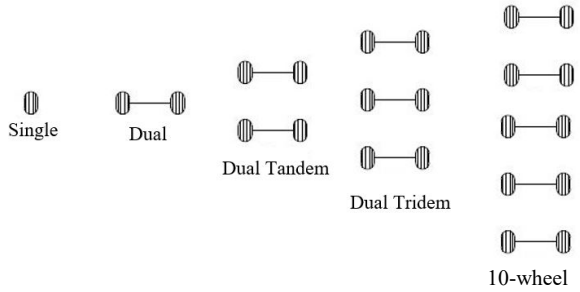

Figure 27: possible landing gear configurations (Sarker and Tutumluer, 2020)

Construction Cycle 5 (CC5) tests are summarized by Sarker and Tutumluer (2020). In these tests the complex deformation behavior of unbound layers due to heavy aircraft loading applied with wander was characterised. CC5 sections were built with 5in hot mix asphalt overlying 8in P209 granular base material overlying different subbase materials (crushed quarry screenings and dense graded aggregates) with 34in and 38in thicknesses over a low-strength subgrade. These pavement sections were instrumented with various sensors such as multi-depth deflectometer (MDD), pressure sensor, and asphalt strain gauge.

The MDD data indicated that load wander affected the residual (non-recoverable) deformation accumulations in the unbound aggregate layers. The first pass on each wander position in the west to east direction typically caused the highest deformation response and the return pass along the same wander position showed significantly less residual deformation. This shakedown behavior was more evident when the wander width was kept narrow (Figure 28). In contrast, accumulations of permanent deformation in the subbase layers appeared to increase as traffic progressed, however, this may have been a function of the relative positions of the sensors with respect to the load. Figure 29 shows that the subgrade layers in sections with 38in. subbase layers did not show any significant rutting but did occur to some extent in subgrade layers of sections that were built with 34in. subbase layers once the load exceeded 58kips. The HMA layer did not rut.

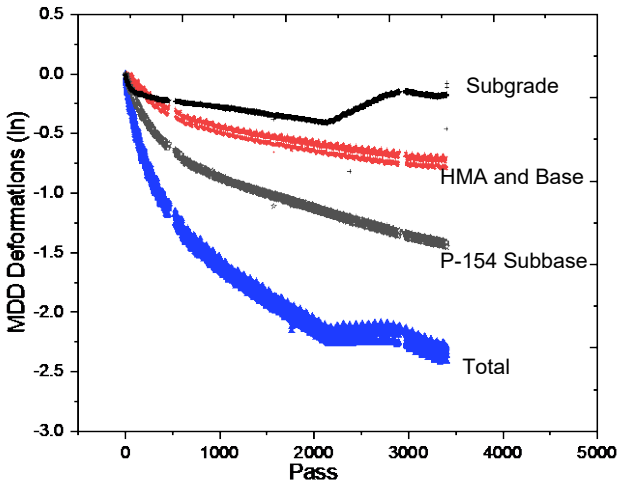

Figure 28: MDD permanent deformation accumulations, LFC1-SE section, 6-wheel (Sarker and Tutumluer, 2020)

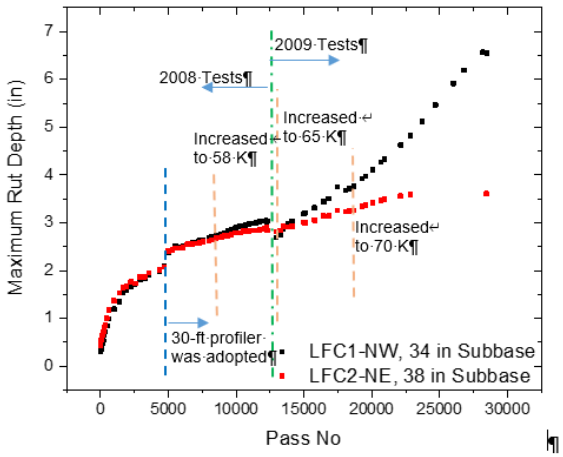

Figure 29: Maximum rut depth, section LFC1-NW, 34in subbase, and section LFC2-NE, 38in subbase (Sarker and Tutumluer, 2020)

A stress history approach (Donovan *et al* 2016) was developed to predict rutting. This approach considers that if there was rut due to a previous pass and if there was rut in same location due to current pass, then the incremental increase in rut depth would reduce. Similarly, incremental heave also decreases with subsequent passes. In contrast if the element was compressed in the previous pass, it would heave more in the next offset pass. Likewise, if the element heaved in the last pass, it would rut more in the next pass when the load was directly over the element. Multipliers for heave and rutting as a function of load offset were generated from the CC1 and CC3 tests and used to predict pavement response. However, the developed model showed somewhat limited success in determining the transverse surface profiles of the CC5 full-scale accelerated flexible pavement test sections. It was observed that while this approach could predict the deformations in the CC5 test sections at the most trafficked location on the pavement, it could not predict the complete transverse surface profiles of the pavement sections due to the complexities arising from factors such as random loading sequences, complex landing gear configurations, and load wanders.

This model was improved by Sarker and Tutumluer (2020). First, critical wander locations were established and their contributions to transverse rut profiles were studied for multiple passes. Then, by utilizing the measured MDD data, individual pavement layer deformations, and the periodic transverse field surface profiles, a rut prediction model was developed using general linear models in the forms of power and sigmoidal function distributions to determine realistic surface profiles of the CC5 test sections. A quadratic model was established based on the MDD calculated theoretical transverse rut basins and using general linear models, the relationships between the MDD and field transverse rut profiles were developed. Figure 30 shows the power model predictions were reliable up to 15,000 passes. However, at higher traffic, the rut prediction model using the sigmoidal function could result in more accurate predictions of the field rut depths.

These results confirm results of previous studies, that although wander reduces the number of repetitions of maximum load applied to the most heavily trafficked pavement location, wander does not necessarily increase the pavement life. Rather it causes constant particle shuffling and rearrangements in unbound layers, ultimately leading to a weaker and more unstable granular layer.

One limitation of this approach is that it requires at least 5,000 passes and/or a total of eight MDD residual basins calculated at different stages of traffic for accurate predictions, hence is not yet suitable for use in practice.

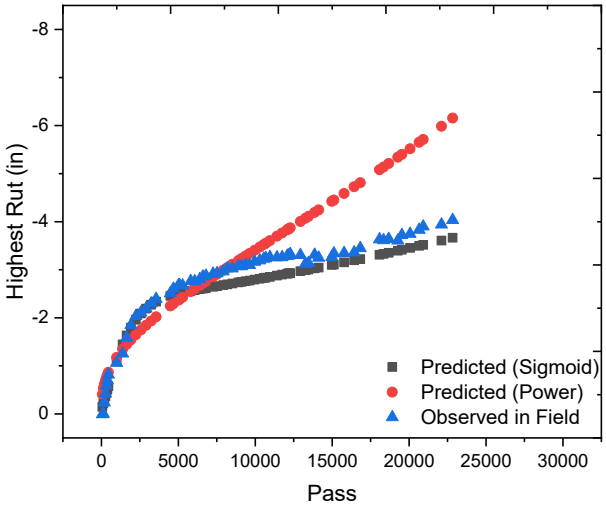

Figure 30: Comparison of observed and predicted highest rut amounts with traffic passes, section LFC3-N (Sarker and Tutumluer, 2020)

One of the objectives for the CC9 tests was to assess the performance of geogrids in airport pavements. Geogrids act by constraining aggregate particles from moving and hence increase their strength and their stiffness. The effect that geogrids have on small strain stiffness in the CC9 tests has been reported by Kang *et al* (2022). The pavement profile consisted of a 5in HMA layer underlain by an 8in granular base material which in turn was underlain by a 29in granular sub-base material. A biaxial geogrid was installed at the interface of the base and the sub-base layers. Bender elements (BE) were installed just above the geogrid layer and at the same depth in a control section constructed without the geogrid. A pair of bender element shear wave transducers attached at each end of the BE field sensors generates the shear wave and collects the shear wave velocity propagating through the constructed aggregate material.

Tests performed after pavement construction prior to loading showed that the shear wave velocity and small-strain modulus at the geogrid-stabilized section were 9.5% and 19.7% higher than that measured in the unstabilized section, respectively. After the moving wheel loading was applied the shear wave velocity reduced more in the unstabilized section than in the geogrid-stabilized section. The geogrid appeared to reduce the dilation caused by aircraft wander. During static load tests the stiffnesses with and without geogrid were similar. Kang *et al* (2022) suggested that this may indicate that the geogrid stabilization is less effective when the confining pressure is high.

2.3 *Railways*

2.3.1 *Loads and stresses*

Considerable advances have been made over the past 10-15 years in our understanding of the loads and stresses applied to the subgrade by trains as they pass. Six key areas are (1) the understanding that stress paths in the field involve a rotation in the direction of principal stresses during load cycling, which may affect subgrade; (2) the role of trackbed stiffness and propensity for plastic settlement on the performance of railway track; (3) appreciation of the role of grain shape and mineralogy on ballast performance, and the implications for re-using ballast; (4) the ability to characterize and reproduce in experiments the complex loading associated with passage of a complete train; (5) recognition of the role of train speed in enhancing track deflections as a result of resonance or so-called "critical velocity" effects; and (6) environmental loads, the need for resilience to climate change, and to be aware of the greenhouse gas emissions

("carbon footprint") associated with new geotechnical transportation infrastructure and maintenance strategies.

2.3.1.1 *Principal stress rotation*

Brown (1996) recognized that elements of soil below a pavement or a railway are subjected to complex loading involving shear as well as normal stresses, resulting in a rotation of the direction of principal stress as a vehicle or train approached and receded. Only when the axle load is directly above the soil element is the major principal stress vertical, as in a conventional triaxial apparatus. This led to a concern that soils exhibiting stability or shakedown under conditions of uniaxial cyclic loading might be susceptible to fatigue failure when loading cycles involving the application of a shear stress and rotation of the major principal stress direction are applied. Investigation of the stress paths to which soil elements below railway tracks are subjected as trains pass using finite element analysis by Yang *et al* (2009) showed that principal stress rotation, which arises from the interaction of individual axle loads at moderate depths, was potentially an issue mainly near the top of the subgrade. The ballast is generally shallow enough for interaction of loads and hence principal stress rotation not to be significant, while at greater depths the stresses associated with train passage are small. Yang *et al* (2009) also showed how stress paths comprising cycles of deviatoric and torsional stress 90° out of phase with each other could be imposed in a laboratory hollow cylinder test to simulate those experienced by soil elements in the field.

The effect of principal stress rotation during load cycles has been investigated by a number of researchers, including Yang *et al*., (2009); Gräbe and Clayton (2009, 2014), Xiao *et al*., (2014), Qian (2016), Wu *et al*., (2017), Mamou *et al* (2017, 2018, 2019a,b, 2021), Guo *et al*. (2016, 2018), Blackmore *et al*. (2021), Fedekar *et al*. (2021), and Zhang *et al*. (2021). Mamou *et al*. (2017, 2018, 2019a,b, 2021) showed how the susceptibility of a saturated mixed material (comprising sand, clay and silt sized grains) to failure during cyclic loading with principal stress rotation depended on the magnitude of the cyclic shear stress (Figure 31), the clay content of the material and the drainage conditions.

When shear stresses were below a threshold stress, the material was found to reach a stable state during load cycling. Above the threshold shear stress, strains would increase gradually (ratchet) with increasing number of load cycles, until eventually failure occurs. The cyclic threshold stress was found to increase with an increase in clay content up to 14% and was higher in free to drain than in undrained conditions. Tests by Guo *et al*. (2016, 2018) confirmed that, above certain critical cyclic stress ratios, principal stress rotation accelerates excess pore water pressure and permanent strain development in saturated, intact, K_0-consolidated soft clay. Blackmore *et al*. (2021) showed that unsaturated materials were much less susceptible to adverse effects of principal stress rotation.

2.3.2 *The role of trackbed stiffness and propensity for plastic settlement on the performance of railway track*

Field measurements at a number of sites have demonstrated that even on well-performing railways, the track support stiffness is likely to vary from sleeper to sleeper (e.g. Figure 32, from Le Pen *et al*. 2020 and/or Figure 33, from Track Stiffness Working Group 2016). Numerical modelling has suggested that significant variations in dynamic wheel load are associated with variations in the initial track level rather than minor variations in sleeper support stiffness (Milne *et al*. 2019). This also applies at under-track crossings, where the difference in track support stiffness may be more pronounced; however, if the change in track support stiffness over a relatively short distance (a few sleeper spacings) is too high, a perceptible increase in vehicle dynamic load becomes apparent (Powrie *et al*, 2019a). Translating this into the evolution of increased differential settlement in a vehicle-track interaction (VTI) model through the use of an appropriate plastic settlement law for the trackbed is feasible, but the quantitative outcome depends crucially on the model and parameters adopted. While we probably have, in principle, the computing power needed to predict the evolution of track geometry over tens of thousands train passes, experimental (field) validation and model parameterisation will be the key challenges for the next few years.

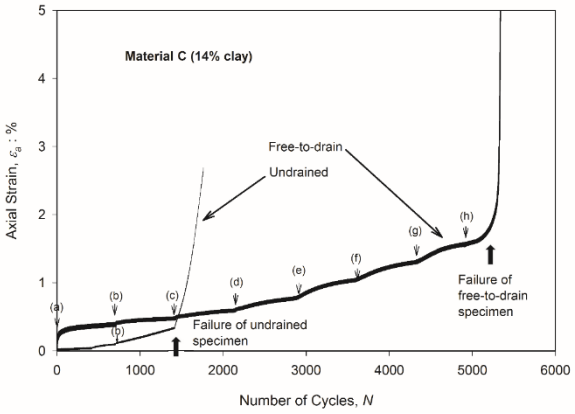

Undrained stages

Test stage	$\Delta\tau_{\theta z}$
a	$\Delta\tau_{\theta z} = +8{\cdot}5 \rightarrow -8{\cdot}5$ kPa
b	$\Delta\tau_{\theta z} = +11{\cdot}5 \rightarrow -11{\cdot}5$ kPa
c	$\Delta\tau_{\theta z} = +14{\cdot}5 \rightarrow -14{\cdot}5$ kPa

Free-to-drain stages

Test stage	$\Delta\tau_{\theta z}$
a	$\Delta\tau_{\theta z} = +8{\cdot}5 \rightarrow -8{\cdot}5$ kPa
b	$\Delta\tau_{\theta z} = +11{\cdot}5 \rightarrow -11{\cdot}5$ kPa
c	$\Delta\tau_{\theta z} = +14{\cdot}5 \rightarrow -14{\cdot}5$ kPa
d	$\Delta\tau_{\theta z} = +17{\cdot}5 \rightarrow -17{\cdot}5$ kPa
e	$\Delta\tau_{\theta z} = +20{\cdot}5 \rightarrow -20{\cdot}5$ kPa
f	$\Delta\tau_{\theta z} = +23{\cdot}5 \rightarrow -23{\cdot}5$ kPa
g	$\Delta\tau_{\theta z} = +26{\cdot}5 \rightarrow -26{\cdot}5$ kPa
h	$\Delta\tau_{\theta z} = +29{\cdot}5 \rightarrow -29{\cdot}5$ kPa

Figure 31: Axial strain vs number of cycles for a typical engineered trackbed material in cyclic loading with principal stress rotation; cyclic axial stress was constant $\Delta\sigma_z$=30kPa and the cyclic shear stress, applied 90° out of phase to the axial stress, was increased in steps (Mamou *et al*., 2017)

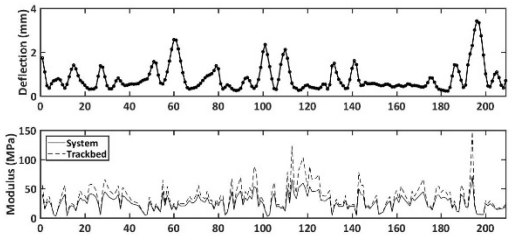

Figure 32: Average of 12 trains (a) sleeper deflections and (b) system modulus and trackbed modulus (assuming pad stiffness of 84 MN/m and 0.6m sleeper spacing). (after Le Pen *et al*., 2020)

Transition zones are areas where the track stiffness changes rapidly such as at the locations of structures or level crossings. Typically, problems related to railway transitions are enhanced dynamic load, differential settlement and accelerated track degradation (Indraratna *et al*., 2019). These problems are highly inter-related, so any increase in one parameter causes a corresponding increase in the others, especially when faster

speeds and increased axle loads are involved. The behaviour of a track transition subject to dynamic load, rail deflections and track acceleration is summarised in Figure 34.

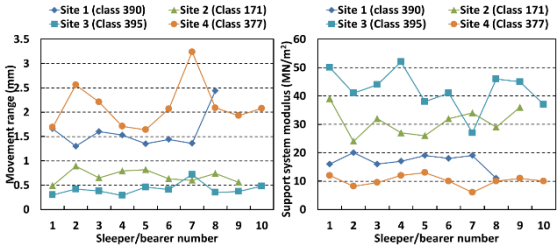

Figure 33: Data from well performing track: (a) measured sleeper movements (b) inferred support system modulus seen by the rail (after Track Stiffness Working Group, 2016)

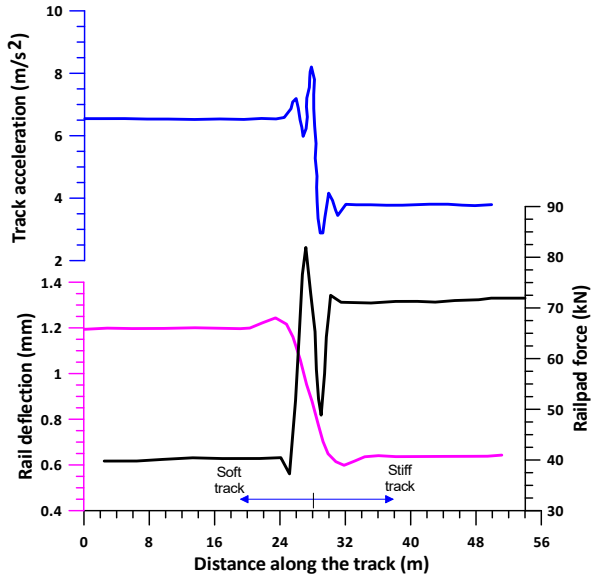

Figure 34: Variation in track acceleration, rail deflection and railpad force at track transition under moving loads (Indraratna *et al*. 2019a)

The theory of beams on elastic foundations (BOEF) has been extensively used to model railway tracks and transitions (e.g. Kang *et al*. 2008). Some studies used BOEF theory considering Euler-Bernoulli beam on a Winkler foundation for transition zone modelling. Others adopted a Timoshenko beam for this purpose. The BOEF model, in spite of some limitations and the lack of a comprehensive model for predicting track response for complex track substructures, is widely used in practice and offers considerable insights. Its main shortcoming is the limited ability to represent sudden, large variations in track support stiffness, such as a hanging sleeper or as may occur at transitions onto or off stiff substructures.

Dynamic impact loads are commonly caused by wheel or rail abnormalities such as flat wheels, imperfect rail welds, rail corrugations, expansion gaps between two rail segments, and transition zones (e.g. Priest *et al*. 2010). When a train passes through a rail crossing and through turnouts or transition zones, the rapid change in wheel rail contacts coupled with sudden variations in track stiffness causes the wheels to displace up and down, giving rise to impact loads (e.g. Paixão *et al*. 2014). At transition points such as bridge approaches, road crossings and slab track to ballasted track, a considerable change in track stiffness causes high impact forces that accelerate track deformation.

Rubber mats have recently been trialled for track substructure having stiff foundations to reduce deformation and degradation of ballast, while enhancing the overall track stability (Costa *et al*. 2012a, Lakuši *et al*. 2010). These studies found that the rubber mats could provide better load distribution by increasing contact areas, reducing the contact forces, thus reducing track damage. A high-capacity drop weight impact testing equipment was used to evaluate the ability of rubber mat to attenuate dynamic impact loads and mitigate ballast degradation (Figure 35) where a schematic diagram of a ballast assembly is shown. Tests were conducted on ballast with and without the inclusion of rubber energy absorbing mats (READS) placed on a soft subgrade and a stiff base (concrete) subjected to varying impact loads.

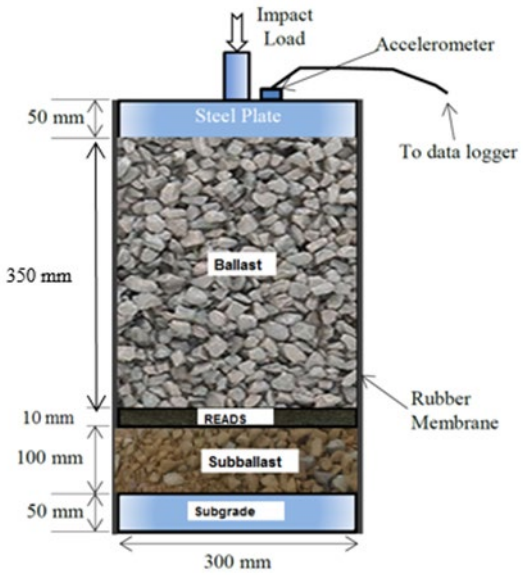

Figure 35: High capacity drop weight impact apparatus: schematic diagram of ballast sample (Ngo *et al.*, 2019)

Measured test data shows that the inclusion of rubber mats helps to reduce the dynamic impact load transferred to the ballast layer resulting in significantly less permanent deformation and degradation of ballast, as well as significant attenuation of load magnitude and vibration to the underlying subgrade layers (Ngo *et al*. 2019). The beneficial effects of the mats are more pronounced on the stiff subgrade, and this corroborates the energy absorbing nature of rubber mats whereby less energy is transferred to the ballast and other substructure components, thus reduced deformation and degradation.

Typical acceleration of ballast under soft and stiff subgrade (with and without READS) measured at the 10th drop (N=10) subjected to a drop height of h_d = 100mm is shown in Figure 36. It is seen that the inclusion of recycled rubber mats reduces the peak acceleration. Measured accelerations for stiff subgrade are always larger than those for the soft subgrade indicate higher levels of vibration at the sleeper-ballast interface, as expected. With soft subgrade, maximum accelerations are around 66 g and 105 g for the ballast assembly with and without rubber mat, respectively. The accelerations measured approximately 110 g (with shock mat) and 169 g (without shock) for stiff subgrade. In addition, the inclusion of rubber mat helps to attenuate vibration faster, as shown in Figure 36b. Based on these results, rubber mats could be used at track transition zones to reduce vibration and prevent excessive ballast deformation and breakage.

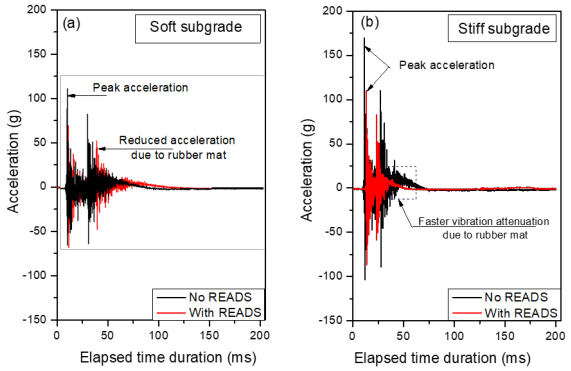

Figure 36: Measured acceleration of ballast under a drop height of h_d = 100mm, at the 10th drop (N=10) placed on: (a) soft subgrade; and (b) stiff subgrade (Ngo *et al.* 2019)

2.3.3 *Characterising train loading*

Advances in the measurement and analysis of railway track deflections as trains pass have led to the ability to quantify train loading as the superposition of a series of different magnitudes and frequencies, as illustrated in Figure 37. When normalised with respect to the vehicle or car passing frequency, the load spectrum depends on the characteristics of the train including axle and bogie spacing, axle loading, and car length and number. Characterisation of train loading in this way has implications for soil element, ballast and component testing. For example, tests in which a specimen is subjected to the full axle load at a frequency based on the passage of adjacent axles will likely significantly overestimate the actual response. Furthermore, the higher frequencies of loading attenuate rapidly with depth (Powrie *et al.* 2019b).

The dominant frequency for pore pressure generation, and the ability to calculate realistic residual pore pressures during and after train passage, remain an ongoing debate and challenge.

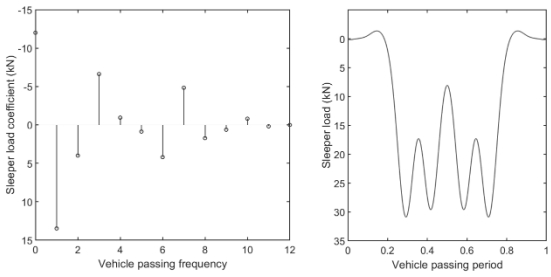

Figure 37: Disaggregation of train loading at the sleeper into a series of loads of different magnitude and frequency, for a 20m long vehicle with 14.2m bogie centres and 2.6m axle spacing, 75 kN wheel load, 25 MPa rail support system modulus and UIC 60 rail (Milne *et al.* 2017)

2.3.4 *Resonance (critical velocity) effects*

The amplification of dynamic track deflections below trains as the train speed approaches that of (surface) Rayleigh waves in the underlying ground, owing to a resonance effect, is well established. A train speed at which dynamic response is significantly amplified due to resonance is called the 'critical speed'. Several semi-analytical and numerical approaches have been implemented to predict the dynamic response of high-speed railway track at the critical speed. In the semi-analytical methods, the track and foundation are modelled as variants of beam, masses and spring-dashpot assemblies to represent rail, rail pads, sleeper, ballast and foundation (Kouroussis and Verlinden, 2015; Walker and Indraratna, 2018). These models have been used to study the instantaneous response of railway track under moving load in the frequency and time domains. However, these models do not capture the wave propagation and mechanical response of the track-ground system.

In order to better understand the effect of wave propagation, several studies have considered the track as a beam resting on an elastic half-space or layered half-space. Though various solutions have been implemented, they are mostly based on a Fourier transform in the frequency-wave number domain. These methods are widely applied ground vibration predictions due to their computational efficiency, they are rarely applied to study the complex dynamic response of in the track due to geometric and material complexities (Dong *et al.*, 2018).

In order overcome the limitations of semi-analytical techniques, advanced numerical modelling for moving loads using Finite Element Method (FEM) or Discrete Element Method (DEM) can be used. The FEM has been employed to study the effect of increasing train speed on ground vibration and instantaneous track deflection (Connolly *et al.*, 2013; Costa *et al.*, 2012b; El Kacimi *et al.*, 2013; Kouroussis *et al.*, 2014; Sayeed and Shahin, 2016; Shih *et al.*, 2016), and dynamic stress amplification (Li *et al.*, 2018; Tang *et al.*, 2019a; Varandas *et al.*, 2016), among others. In addition, the FEM allows complex geometries and implementation of advanced constitutive relationships in order to incorporate non-linear response and long-term settlement and track degradation (Correia and Cunha, 2014; Li *et al.*, 2016; Nguyen *et al.*, 2016; Varandas *et al.*, 2020). The FEM considers ballast as an elastic or elasto-plastic continuum, while semi-analytical spring-mass-damper models considers all track layers as multi-rigid body dynamics. Mesomechanical behaviours, such as discontinuity, angularity, breakage, randomness, of the ballast layers are highly simplified (Bian *et al.*, 2020; Zhang *et al.*, 2017). The DEM has also been successfully implemented to study particle breakage/degradation and subsequent settlement of ballast layer under moving load (Zhang *et al.* 2017, Indraratna *et al.* 2014a). In summary, the choice of analytical and numerical prediction approach should be aligned with the expected outcomes that to be investigated.

These various forms of model have been developed in recent years in an attempt to capture aspects of the critical velocity problem. Models that account for the development of strains during train passage are perhaps the most comprehensive but are very computationally demanding and time consuming. A method gaining in popularity for large-scale infrastructure is based on the dispersion curve, which inverts the process followed by geophysical investigations. A phase velocity *versus* wavelength relationship is estimated from an expected profile of shear wave velocity *versus* depth for the ground and earthworks, together with other basic soil characteristics. The minimum estimated phase velocity is then taken as representative of the critical velocity of the ground and earthworks system

An approach developed by Sheng *et al.* (2004) involves plotting the dispersion curves (i.e., the frequency-dependent wavenumbers or wave speeds of free waves that can occur at the ground surface in the absence of damping) for the ground and for the track with a free base. The point at which the wave speeds for the track and the ground coincide gives the wavenumber / frequency at which waves can propagate in the coupled structure; hence the critical velocity of the system and the frequency of oscillations ("resonance") seen behind the load. This approach has recently been taken up by others (e.g. Alves Costa *et al.* 2015, 2020; Connolly *et al.* 2015), while Kausel *et al.* (2020) showed how a dispersion curve could be developed for layered ground. However, it is difficult to apply in practice because of the information required and the stage in the design process at which it is needed (for example, ground improvement, should it be necessary, can only be applied prior to the placement of the track

form). This and other practical design issues are discussed by Duley (2021).

2.3.5 *Dynamic amplification*

As the train speed increases, the dynamic loading due to acceleration from the components of the vehicles becomes more significant. Irregularities at the wheel-rail interface amplifies the acceleration the unsprung masses (the wheels and axles). Acceleration of both sprung and unsprung masses also occur due to longer wavelengths irregularities such as track support stiffness and unsupported sleepers (Esveld, 2001; Powrie *et al*., 2019b). These dynamic loads are taken into account in track design by the Dynamic Amplification Factor (DAF), which is the ratio of dynamic to the static response (deflection and stress). In DAF calculations the track substructure is modelled with a single parameter called track modulus. Measurements for field and full-scaled laboratory tests have shown that the dynamic amplification is primarily affected by the Rayleigh wave propagation speed, type of track (ballasted and slab track) and stiffness variation (Bian *et al*., 2014; Indraratna *et al*., 2010).

Figure 38(a) shows that the DAF of the vertical displacement of the rail as a function of the ratio of the train speed, c, to the shear wave speed of homogeneous ground for an elastic modulus of 200MPa. Figure 38 (b) shows the DAF of the same track structure modelled with a softer subgrade layer of 3m thickness is introduced (E_{top} = 50MPa, E_{bottom} = 200MPa). The amplification increases with flexibility of the track (bending stiffness of slab track V3 is twice of slab track V2).

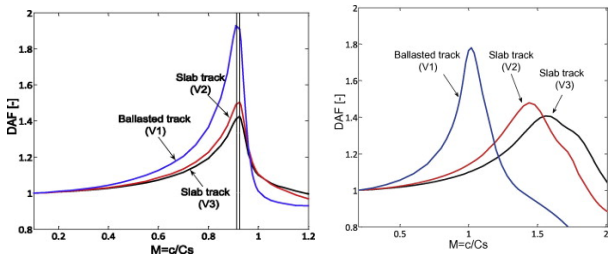

Figure 38: Dynamic amplification factor of vertical rail displacement (a) homogeneous subgrade (b) layered subgrade (M = c/CS, upper layer) (Costa *et al*., 2015)

A comparison of Figure 38 (a) and (b) shows track stiffness and type of track have a significant effect on the DAF and critical speed, in addition to the influence of subgrade stiffness. The relationship between CR (Rayleigh wave speed) and CS (Shear wave speed) is approximately CR = 0.934CS. According to Sayeed and Shahin (2016) and Dong *et al*., 2018, the critical speed increases with the top subgrade stiffness while the DAF exhibits a decreasing trend. Therefore the performance of the track can be improved by stiffening the subgrade using ground improvement in soft soil deposits, and installation of piles.

New data from Gravel Hole on the UK West Coast Main Line confirm the overall trend of normalised displacement against train speed shown in Figure 39.

Presentation of the data in normalised form masks the fact that, at low train speeds on a soft subgrade a dynamic amplification factor of 3 applied to a static displacement of 5 mm would be a problem; whereas the same factor applied to a static displacement of 0.5 mm on a much stiffer subgrade at a much higher train speed would probably not.

Further challenges remain relating to the accurate determination of effective soil stiffnesses, Rayleigh wave speeds and system critical velocities, which depend on a combination of the characteristics of potentially multiple and / or discontinuous soil strata, the track form and any earth structures (embankments or cuttings) that may be present.

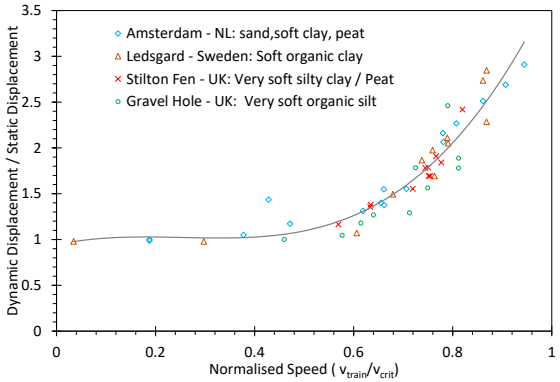

Figure 39: Normalised plot of track vertical displacement (dynamic displacement ÷ static displacement) against normalised train speed (train speed ÷ Rayleigh wave speed) for various case study sites. Data from Woldringh & New (1999) and Duley (2018)

Other studies conducted on the field and prototype models have shown an increase in vertical, lateral stresses and subsequent deformation with increase in the speed of the train (Bian *et al*., 2014; Hendry *et al*., 2010; Indraratna *et al*., 2010; Lamas-Lopez *et al*., 2016; Tang *et al*., 2019b). As a result, the track layers not only experience amplified vertical stresses, but also longitudinal and shear stresses (Malisetty *et al*., 2020; Powrie *et al*., 2007; Yang *et al*., 2009). The magnitude of these stresses is found to increase with the speed and axle load of the train. This complex stress conditions in the track layers leads to excess deformation and settlements in track substructure layers including ballast and subgrade soils (Grossoni *et al*., 2020; Varandas *et al*., 2020). Therefore, an accurate prediction of the complex behavior of railway tracks subjected to an increasing speed of trains must be achieved through rigorous field measurements, analytical and numerical analysis.

2.3.6 *Novel multi-laminate model for estimating permanent deformation at high speeds*

A novel constitutive model in multi-laminate framework has been developed by Malisetty *et al*. 2020a and Malisetty *et al*. 2020b. By considering the evolution of plastic strains at the contact planes, the multi-laminate model incorporates stress induced anisotropy caused by principal stress rotation inherently in its framework (Lee and Pande, 2004). The model assumes that deformations are induced at the inter-particle contact planes irrespective of the loading condition. The overall behaviour of the material is captured by numerical integration.

Train induced stress paths can be characterized by Cyclic Stress Ratio (CSR), shear tress ratio η_τ and modified CSR*, where, $\Delta\sigma_z'$ is the amplitude of cyclic vertical stress, p_0' is the initial mean effective stress and $\Delta\tau_{xz}$ is the amplitude of cyclic shear stress.

$$\left(CSR = \frac{\Delta\sigma_z'}{2p_0'}\right) \quad (2)$$

$$\left(\eta_\tau = \frac{\Delta\tau_{xz}}{\Delta\sigma_z'}\right) \quad (3)$$

$$\left(CSR^* = CSR\sqrt{1+\eta_\tau^2}\right) \quad (4)$$

The shear stress ratio η_τ is 0 for triaxial compression with no principal stress rotation and CSR^* reduces to CSR. Based on the model predictions from Malisetty *et al*. (2020a), the

permanent axial strains ($\epsilon_{a,sh}$) of ballast at shakedown under these stress paths are replotted along with CSR* in Figure 40. For a typical passenger train with sleeper-ballast interface vertical stress amplitude of $\Delta\sigma'_z = 230\ kPa$, increasing the CSR^* reduces the stability of ballast leading to a steady increment of permanent axial strains at shakedown. The permanent axial strains which reached a stable shakedown state at low CSR^* do not tend to reach shakedown, eventually reaching ratcheting failure at $CSR^* = 5.4$. It is evident that the rotation of principal stress axes at higher train speeds can induce instability without changing the amplitude of vertical stress. Further, increasing the vertical stress amplitude ($\Delta\sigma'_z > 230\ kPa$) led to quicker failure (steep slope) when compared to low $\Delta\sigma'_z$ which signifies that heavy axle loads imparted by freight trains increases instability when compared to passenger trains travelling at the same speed. The modelling outcomes show that if the influence of Raleigh waves and principal stress rotations are not incorporated in the design of tracks for high speed trains, the deformation of ballast can be underestimated and can affect track stability causing unevenness of the track profile, ultimately increasing the frequency and cost of maintenance operations.

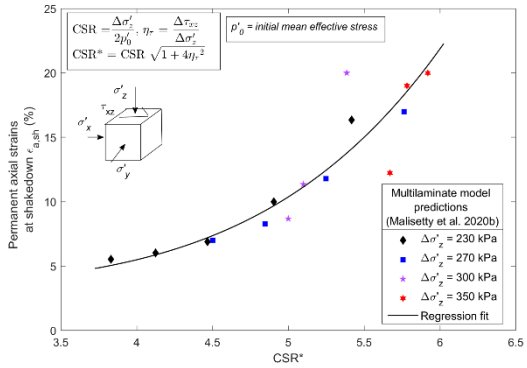

Figure 40: Influence of cyclic principal stress rotation on shakedown axial strain response of ballast (data sourced from Malisetty *et al*. 2020a)

2.3.7 *Estimation of critical train speed for different axle loads*

Using the multi-laminate model predictions from Malisetty *et al*. (2020a), the critical train speed for a ballasted railway track can be analyzed for different axle loads. The axle loads considered for analysis represent passenger (P=15 tonnes), coal freight (P = 25 and 30 tonnes) and iron ore freight wagons (P = 40 tonnes). The dynamic stresses in the ballast layer were analysed using beam on layered elastic half-space model, considering Rayleigh wave propagation and dispersion in the ballast and underlying subgrade layer. The elastic modulus for ballast (E_b=100 MPa) and alluvial subgrade (E_b=30 MPa) are adopted from field data (Nimbalkar and Indraratna, 2016). Two approaches for estimating the critical speed are discussed here using: peak static shear strength of ballast and maximum allowable permanent axial strains under repeated loading.

For each axle load, the stress response at the mid-depth of the ballast layer was calculated and the ratio of dynamic shear stress, q_{dyn}, to peak static shear stress, q_{sta_peak}, (ψ) developed for a confining stress of 30 kPa. This ratio computed for different train speeds is shown in Figure 41.

The dynamic shear stress amplifies with increasing the train speed for all axle loads. At a train speed of V=270 kmph, the Raleigh waves generated by the train reached a resonance state causing maximum stress amplification and this speed was found to be unique for all axle loads. However, when the train speeds lie in the sub-critical zone (V<270 kmph), the value of ψ exceeded 1 for all axle loads. The train speed for which $\psi \geq 1$ decreased with increasing axle loads. This implies that freight trains with higher axle loads must be limited to lower speeds than that of passenger trains to avoid a rapid increase of shear stress within the ballast.

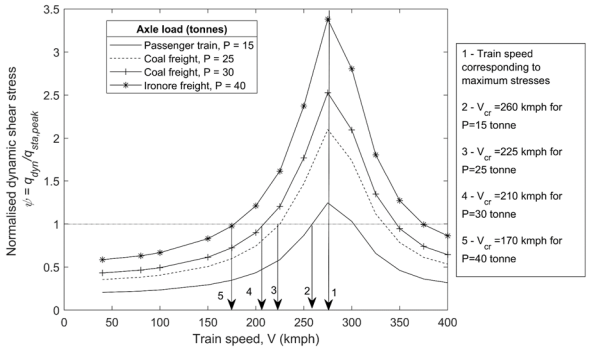

Figure 41: Dynamic stress amplification in the ballast layer at different train speeds (Malisetty *et al.*, 2020a).

The corresponding CSR* was computed for all the stress path at different train speeds and axle loads the results are plotted in Figure 42. Using the multi-laminate model predictions of ballast (See Figure 40), the CSR* corresponding to greater than 20% permanent axial strains was considered as failure and is shown in Figure 42. The region below the failure plane can be considered as a stable loading zone and the region above the failure plane as an unstable loading zone. The intersection line represents the critical train speed for different axle loads. The critical train speeds corresponding to 20% axial strain for different axle loads are very close to that of those estimated for $\psi \geq 1$, which indicates that failure or excess deformations occur when the peak stress applied on the material is exceeded.

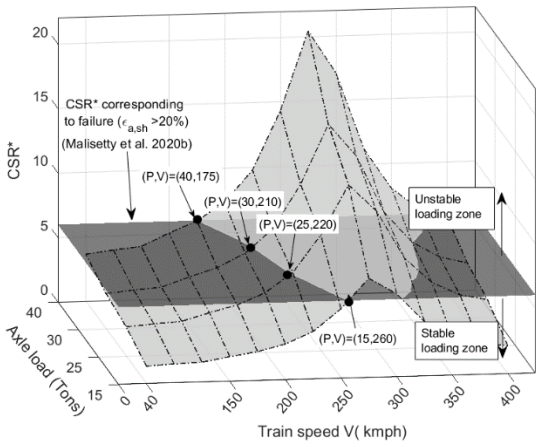

Figure 42: Critical speed estimation in ballasted railway tracks for different axle loads based on multi-laminate model predictions (Malisetty *et al*. 2020a)

While the amplification factor is same for all axle loads, the high magnitude of dynamic stresses at high axle loads plays an important role in determining the critical speed. In essence, it can be interpreted that the critical train speed of the track not only depends on the track material properties and geometry, but also on the axle load; higher the axle load, lower will be the allowable maximum train speed.

However, these critical speeds were only determined for the shakedown performance of ballast. The influence of wave

propagation on the number of loading cycles after which this shakedown state is reached needs further research. The influence of Raleigh waves on the instability of undrained subgrade soils needs to be addressed in more detail using the multi-laminate constitutive model and needs to be integrated with Finite Element Modelling. This is required to investigate the influence of principal stress rotation due to moving trains on mud pumping behavior and stability of subgrade soils, where excess pore water pressures play an important role.

2.3.8 *Dynamic stresses in the track under high-speed train loading*

The state of stress in the track subjected to moving train load exhibits a complex stress path as the load approach and passes a given location. As the train moves towards an observation point, the shear stress gradually increases, and then decreases to pass through zero when the load is exactly above the observation point, while the vertical stress peaks. The shear stress then changes its sign and increases as the load moves away from the observation point before gradually returning back to almost zero. This makes the shear stress to be 90 degrees out of phase with the normal stress, which in turn results continuous rotation of principal stress axis. Several studies have shown that principal stress rotation accelerates permanent deformations compared to a single point cyclic loading (Bian *et al*., 2020; Cai *et al*., 2018).

Yang *et al*. (2009) showed, using a 2D FE model, that the vertical and longitudinal shear stresses increase with the train speed . Numerical results indicated that the vertical and shear stresses at the critical speed are about 20% and 80% higher than those calculated in a static analysis, respectively. The shear stress at 50% of the critical speed was underestimated by 30% while the error in the vertical stress was about 15% in static analyses.

Three dimensional FEM has been used to compare the stress state in the ballast layer at low and high speed (Indraratna *et al*. 2010). The axle load configuration mimics the RAS 210 Australian Standard Wagon equivalent to 20.5t axle load. The ballast and capping material parameters were adopted from triaxial test results reported by Indraratna *et al*. (2010) while the subgrade was assumed to have a resilient modulus of 50MPa. The track was modelled with solid elements and infinite element boundaries were applied at the all sides except the centerline (Figure 43a). Figure 43b and 43c show the difference in deformation contours when the speed of moving load changes from slow speed to high speed, where the critical speed of the track ground system which is about 85m/s. At low speed the vertical transient vibration is symmetrical while asymmetrical transient displacement is observed at high speed (e.g. Connolly *et al*., 2013).

Figure 44 shows the corresponding stress changes at low speed ($0.2V_c$) and near the critical speed of the track-ground model computed at the middle of the ballast layer (Point A of Figure 43a). Simulated results show that at the critical speed the vertical stress increased about 50% while the shear stress along the longitudinal direction increased about 200% in the opposite direction.

For low speed, almost all the stress curves are symmetrical as shown in Figure 45. For high speed, the peak value of each stress is higher indicating the existence of vibration amplification. The symmetry of stress response is lost except for the vertical normal stress. Yang *et al*. (2019) and Dong *et al*. (2019) reported similar asymmetry of stress responses which is attributed to the load reaching the reference point before the stress wave has fully propagated to the same point. Comparison of dynamic stress path from the double-bogie load in Figure 44 shows that the deviatoric stress and shear stresses increase significantly with the train speed. Similarly, high speed results in significant upward displacement and negative mean stress, which could lead to loss of confinement and instability (Dong *et al*., 2019).

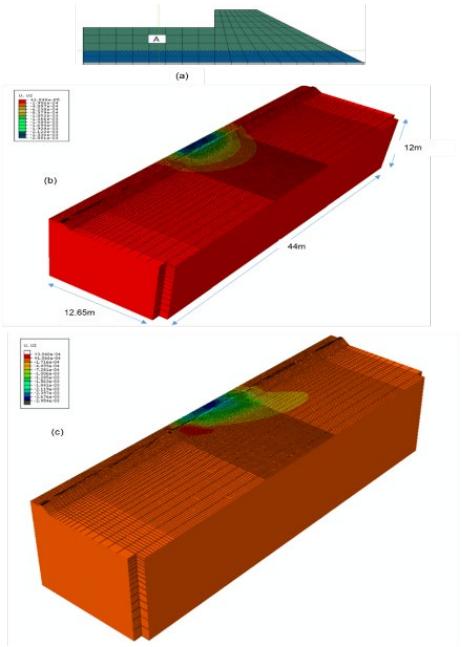

Figure 43: Finite Element Modelling (a) Section (b) Deformation contours at 60km/h (c) Mach effect (vertical deflection) at 300km/h (unpublished part of a current program at the University of Technology Sydney through funding from the Australian Research Council, courtesy A. Tucho, PhD student)

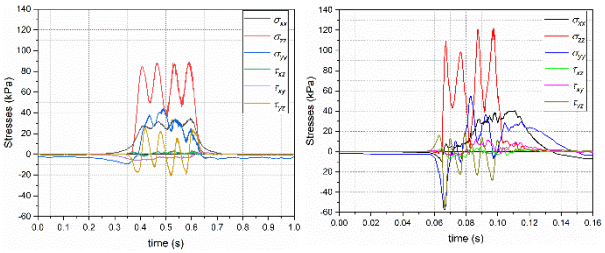

Figure 44: Stress Distribution at a speed of 60km/h and 300km/h (unpublished part of a current program at the University of Technology Sydney through funding from the Australian Research Council, courtesy A. Tucho, PhD student)

2.3.9 *Ballast structure, grain shape and mineralogy*

Ballast is gravel to cobble-sized hard granular material that is placed below and surrounding sleepers. The ballast provides the following functions (Li *et al*, 2015):

- Supports the rail and sleepers by providing vertical, lateral and longitudinal resistance
- Transmits and reduces rail wheel forces
- Provides drainage
- Provides resilience and damping of wheel/rail forces

Heavy cyclic loads cause progressive deterioration and breakage of ballast, and consequently the loss of track geometry leading to frequent track maintenance. During train operations, ballast deteriorates due to the degradation of angular corners and sharp edges, the intrusion of fines, and mud-pumping from the underlying soft soil layers. In addition, impact forces generated by wheel and/or rail irregularities or imperfections or at transitions zones (e.g., bridge approaches and exits, road crossings) may exacerbate track deterioration (Powrie *et al*. 2007; Indraratna *et al*. 2019a). As the sharp corners of aggregates

break and weaker particles are crushed under heavy cyclic loading, differential track settlement can occur (Indraratna *et al*. 2014a). As the ballast assembly becomes degraded its grain angularity, overall strength and drainage capability may be reduced (Indraratna *et al*. 2011b, Tutumluer *et al*. 2012, Tennakoon *et al*. 2012).

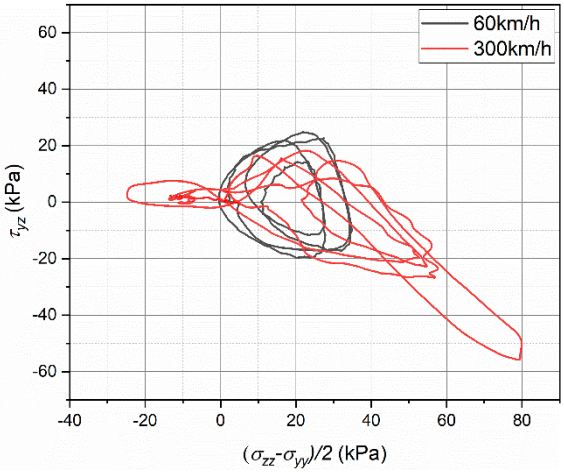

Figure 45: Stress paths at a speed of 60km/h and 300km/h based on the stresses shown in Figure 44 (courtesy A. Tucho)

The past decade has seen a significant number of studies investigating the performance of railway ballast at the grain scale. These have included experimental investigations of structure using X-ray computed tomography (CT scanning) of samples whose structure was fixed by impregnation with resin, detailed assessment of grain mineralogy and shape, and numerical analysis using the discrete element method.

Studies such as those reported by Le Pen *et al* (2014) and Aingaran *et al* (2018) have shown that during trafficking, ballast develops a dense structure through a reduction in void ratio and an increase in average coordination number. Maintenance by tamping disrupts this structure by disturbing the grains; subsequent trafficking does not then ever quite recover the maximum bulk density originally attained.

Ballast grain shape may be characterised by three measures (in decreasing order of scale) of form, angularity and roughness. Grain shape influences the density, void ratio and hence the stiffness and (peak) strength of the assembly.

Le Pen *et al* (2013) showed that form and angularity varied slightly but not significantly across particle scale and introduced the concept of "ellipseness" (rather than the traditional "roundness") to quantify angularity. Potticary (2018), Potticary *et al*. (2014, 2015, 2016) and Harkness & Zervos (2019) quantified ballast form by combining the Longest (L), Intermediate (I) and Shortest (S) orthogonal dimensions of ballast grains into two parameters they termed platyness (α) and elongation (ζ) (defined in Figure 46). This results in individual grains plotting onto a triangular diagram (Figure 46), which is considered to be an advance on the conventional Zingg plot of I/L vs S/I because (i) each grain is characterised as one of three distinct shape types (spherical, columnar or platey: the Zingg plot distinction between platey and blade-like is rather subtle), and (ii) each of the shape parameters include all three of the principal dimensions.

Recent work on ballast degradation has focused on how the three measures of grain shape change with loading. Mineralogy is important: much empirical evidence of the nature and timescale of ballast degradation by grain attrition and breakage is based on relatively low quality ballast (particularly limestone), and is unlikely to be applicable to modern high quality ballast such as granite. For granite ballast, trafficking seems to result in changes in both angularity and form. Abadi *et al*. (2021) quantified angularity from the dimensions and volume of solid ellipsoids fitted to 3D images of ballast grains captured using a laser scanner. Figure 46 shows data of form for fresh and used ballast grains; the used ballast is generally more spherical than the material.

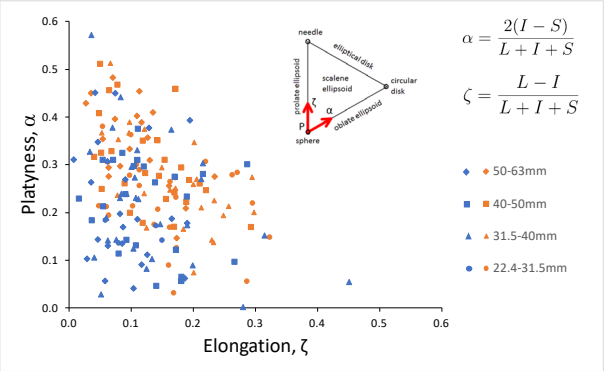

Figure 46: Plot of Platyness vs Elongation (Potticary *et al*., 2015) for fresh and used ballast. Orange data points represent fresh ballast and blue data points represent used ballast of different sizes (data extracted from Abadi *et al*. 2021)

On loading, the local surface roughness seems to be affected immediately at the inter-grain contacts (Gupta *et al*. 2021); Figure 47.

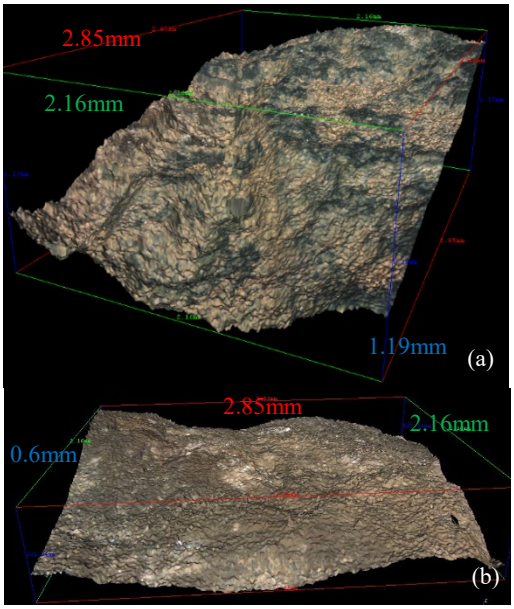

Figure 47: Surface characterization of ballast particles using varying focus microscopy. a) fresh ballast surface (average surface roughness = 50μm); b) used ballast surface (average surface roughness = 20μm) (after Gupta *et al*. 2021)

Monotonic triaxial tests, and cyclic loading in sleeper rig tests, show no appreciable difference between fresh and recovered granite ballast, suggesting considerable potential for re-use (Abadi *et al*., 2021).

Ballast fouling is a potential concern and has been investigated through triaxial and laboratory rig tests and discrete element analysis (e.g. Indraratna *et al*. 2014a, Ngo *et al*. 2014). Experience in the field and physical test data suggest that dry fouling, for example by sand grains small enough to fall through the voids to the bottom of the ballast bed, makes no difference to the resilient stiffness until the voids in the ballast are filled to

sleeper soffit level. At this point, the resilient stiffness increases significantly and ongoing plastic settlement substantially stops (University of Southampton, 2013). However, fouling by wet, fine (clay-like) particles is generally held to reduce the resilient stiffness and accelerate plastic settlement. This could be a result of associated subgrade deterioration, and / or the fine, wet fouling particles reducing the stiffness and strength of the ballast grain contacts. While there have been several individual or case specific studies, a unified theory of the effects of ballast fouling accounting for the presence or absence of water has not as yet been postulated.

2.3.10 *Ballast confining pressure*

The confining pressure is a significant factor in ballast performance. Large-scale cyclic triaxial tests have been performed to investigate how confining pressures affect ballast breakage under high cyclic loading (Lackenby *et al*. 2007, Sun *et al*. 2019). Ballast was tested under different effective confining pressures (σ_3') ranging from 10kPa to 240kPa with deviator stresses up to 500kPa. Figure 48 shows the effect of confining pressure on the axial and volumetric strains in the ballast; here the axial strains decrease with an increasing confining pressure and the ballast assemblies dilate at a low confining pressure (σ_3' < 30 kPa), but become progressively more compressive as the confining pressure increases from 30 kPa to 240 kPa. The effect of σ_3' on particle breakage is shown in Figure 49, where breakage is divided into three regions: (I) a dilatant unstable degradation zone (DUDZ); (II) an optimum degradation zone (ODZ); and (III) a compressive stable degradation zone (CSDZ).

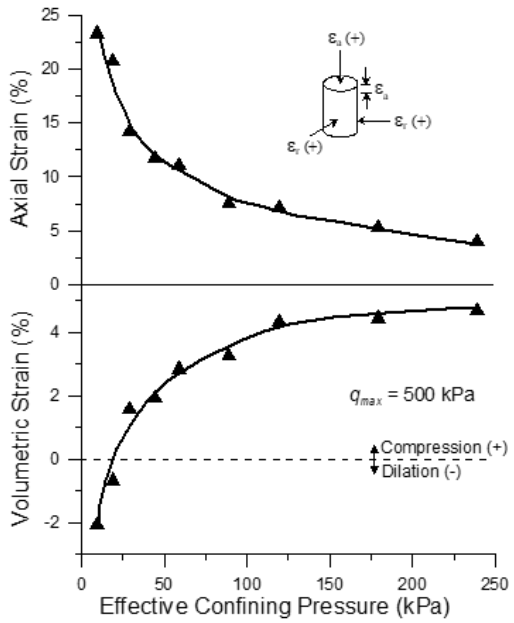

Figure 48: Effect of confining pressures on axial and volumetric strains (Lackenby *et al*. 2007)

2.3.11 *Ballast permanent settlement*

It is well known that railway track gradually settles over time with trafficking. Both the subgrade and the ballast may contribute to this settlement; but it should be possible to minimise at least the component attributable to the ballast by appropriate methods of installation and maintenance. After initial densification (which may occur because the track is lifted to above its final geometry by tamping), ongoing settlement is usually attributed to ballast grain breakage (often due to maintenance tamping) and lateral spreading of the ballast bed. Measures that have been shown to reduce the rate of development of permanent settlement of the ballast bed, at least in full-scale laboratory rig tests (Abadi *et al*. 2016, 2019; Navaratnarajah *et al*. 2018; Jayasuriya *et al*. 2019) include the following:

- under sleeper pads (which increase the ballast to sleeper contact area when a standard concrete sleeper is used, providing a more stable and less aggressive interface)
- the use of duoblock rather than monoblock sleepers (which eliminates the possibility of "centre binding", but for other reasons seems to be falling out of favour in railway administrations around the world)
- changing the grading to include a greater proportion of slightly finer grains, improving mechanical interlocking.

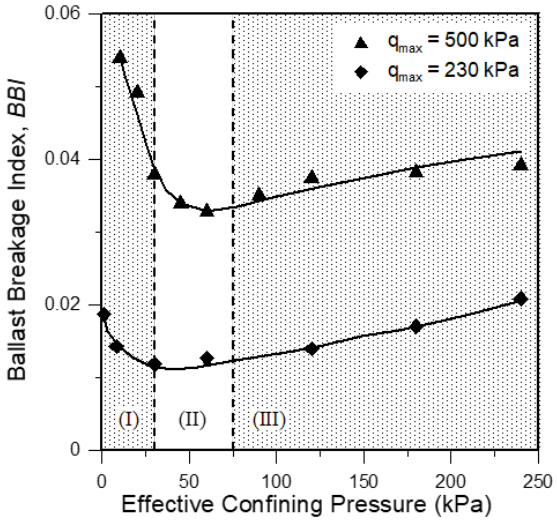

Figure 49: Effect of confining pressures on particle degradation (Lackenby *et al*. 2007)

Methods of reducing ballast settlement by preventing or restricting lateral spread include

- reinforcement with random fibres (Ajayi *et al*. 2017); the development of tensions in the fibres increases the effective confining stress on the ballast
- reinforcement with geogrids (Indraratna *et al*. 2011b)
- physical confinement
- reducing sleeper spacing, widening the sleeper at the ends or using intermittent lateral restraints (Indraratna et al. 2011b) to increase resistance to ballast lateral movement and possibly the confining stress
- Increasing the height of a ballast shoulder raised above the level of the sleeper surface (Lackenby *et al*. 2007), or
- reducing the slope of a ballast shoulder that falls away below sleeper surface level, where (as is almost invariably the case) the ballast bed is raised (Abadi *et al*. 2016).

With the possible exception of under sleeper pads, few if any of these techniques have been adopted in practice. This may be a result of concerns regarding cost, interference with maintenance by tamping (e.g. the use of geogrids), the lack of available land along the trace width (reducing the ballast shoulder), or a lack of field demonstration of the efficacy of the technique.

2.3.12 *Characterising fouled ballast*

Methods to quantify the degree of fouled ballast include Selig and Waters (1994) and Feldman and Nissen (2002). These methods do not account for the differences of specific gravities of various contaminants (e.g., coal, clay, mud, pulverised rock). A void contaminant index (VCI) (Tennakoon *et al*. 2012) was developed to include contributions from various materials.

$$VCI = \frac{1+e_f}{e_b} \times \frac{G_{sb}}{G_{sf}} \times \frac{M_f}{M_b} \times 100 \quad (5)$$

where, e_f, e_b are void ratio of fouling and ballast; G_{sb}, G_{sf} are specific gravity of ballast and fouling; M_f, M_b are weight of fouling and ballast.

Tennakoon *et al*. (2012) studied the effect of the degree of fouling on the overall hydraulic conductivity of fouled ballast using a large scale permeability apparatus. Based on test results, a relative hydraulic conductivity ratio (k_b/k) was introduced to understand how the overall hydraulic conductivity (k) varies in comparison to clean ballast (k_b), as shown in Equation 6.

$$\frac{k_b}{k} = 1 + \frac{VCI}{100}\left(\frac{k_b}{k_f} - 1\right) \quad (6)$$

The study showed that a 5% increase in VCI decreases the hydraulic conductivity by a factor of at least 200 and 1500 for ballast contaminated by coal and fine clayey sand, respectively.

Variations of relative hydraulic conductivity of ballast with VCI are shown in Figure 50. The drainage ranges are subjective and will vary depending on the local climate, track use, etc. For example, a hydraulic conductivity of 10^{-5} m/s for a section of track may be acceptable (due to the low rainfall etc.), but unacceptable for a track section subjected to very heavy rainfall.

Figure 51 shows the variation of hydraulic conductivity for fouled ballast with increased VCI. The overall hydraulic conductivity always decreases with an increase in VCI. When the VCI > 75%, further reduction in hydraulic conductivity becomes marginal as it approaches the hydraulic conductivity of the fouling material itself. These observations agree with the laboratory measurements of sand-gravel mixtures reported by Jones (1954), whereby a high percentage of sand (greater than 35%) in gravel provides a hydraulic conductivity close to that of the sand alone.

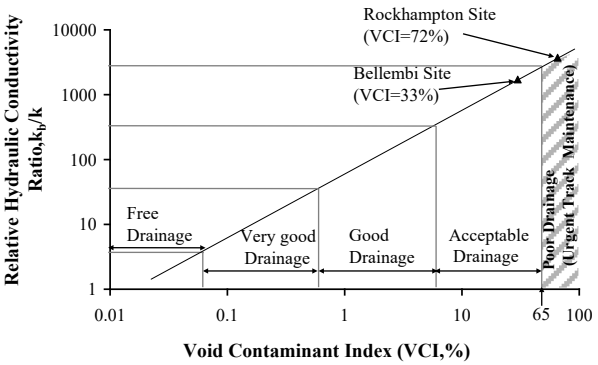

Figure 50: Variation of relative hydraulic conductivity with Void Contaminant Index for coal fouled ballast (Tennakoon *et al*., 2012)

VCI has also been related to the shear strength of fouled ballast (Indraratna *et al*. 2013a).

$$\frac{q_{peak,f}}{q_{peak,b}} = \frac{1}{1+\beta\sqrt{VCI}} \quad (7)$$

In Equation 7, $q_{peak,b}$ and $q_{peak,f}$ are peak deviator stresses for fresh and fouled ballast respectively, and β is an empirical parameter for fouled ballast. The values of β for different fouling agents can be determined from permeability tests.

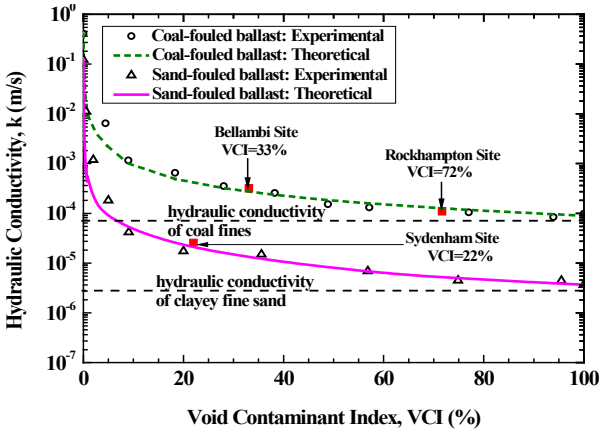

Figure 51: Variation for hydraulic conductivity *vs*. void contaminant index for coal/clayed fine sand (Tennakoon *et al*., 2012)

The allowable train speed V_f for fouled ballast can be estimated as:

$$V_f = \left[\frac{q_{peak,f}\left(B+\frac{h}{2}\right)\left(\frac{l}{3}+\frac{h}{2}\right)}{\frac{P_s}{2}} - 1\right]\frac{D_w}{0.0052} \quad (8)$$

Where P_d is the design wheel load, q_r is the rail seat load, B is sleeper width (m), l is sleeper length (m), h is ballast thickness, D_w is the diameter of the wheel (m) and V is the velocity of the train (km/h). Figure 52 shows the predicted maximum train speed for coal-fouled ballast at varying levels of VCI. Both the confining pressure and level of fouling affect the operational train speed (V_f). Train speed can be slightly increased with increased track confinement but is significantly reduced with an increase in fouling, in particular when VCI is greater than 30% at which stage track maintenance could be initiated to avoid potential track problems and to increase passenger comfort (Indraratna and Ngo 2018).

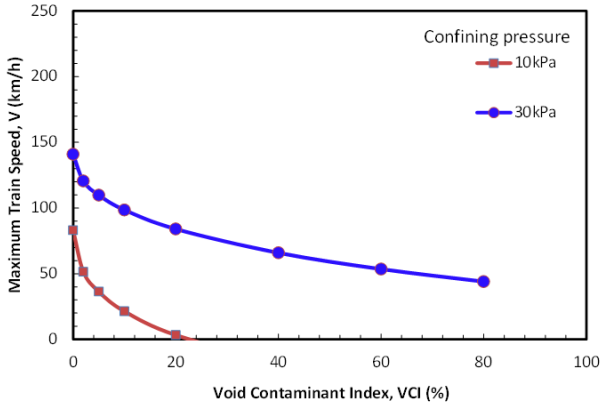

Figure 52: Predicted allowable train speed with VCI for a heavy haul of 30 tonne axle load (Tennakoon *et al*., 2012)

2.3.13 *Measurement and modelling of ballast particles*

Settlement of ballasted tracks occurs due to rearrangement of ballast particles as well as their lateral spread under cyclic train loads. The mechanisms controlling ballast settlement have been investigated by experimentally and using the numerical discrete

element method (DEM). Zhai *et al*. (2004) placed multiple accelerometers in ballast layer to measure the particle accelerations for modelling ballast vibrations under moving trains. Kumara and Hayano (2016) used a method of particle image velocity (PIV) to track local deformations induced by tamping tools. A series of studies have been recently conducted to monitor the movement of ballast particles using a wireless device called "Smart Rock". Liu *et al*. (2016a) developed this device by encasing a motion-sensing unit in a ballast shaped PLA plastic object and used it to study the motion of ballast particles reinforced with different geogrids. Zeng *et al*. (2019) used small cubes with embedded motion sensors to monitor ballast movement for the identification of its condition. In these studies the SmartRock did not either have the density of an actual rock or the shape of a realistic ballast particle as shown in Figure 53.

Ballast particles with realistic geometry and density have been created by 3D printing using a special kind of filament infused with metal powder to provide a realistic weight. The final product as compared to actual ballast particle is shown in Figure 54.

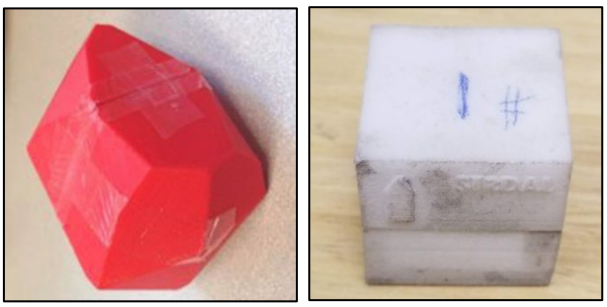

Figure 53: Smart Rock Liu *et al*. (2016a) Zeng *et al*. (2019)

Figure 54: Smart Ballast particle (unpublished part of a current program at the University of Technology, Sydney through funding from the Australian Research Council), courtesy A. Siddiqui, PhD student)

Liu *et al*. (2016a) used the "Smart Rock" particles in a ballast box representing half section of a rail track structure and concluded that the particle translation and rotation are important modes of ballast particle movement that affect ballast performance.

The discrete element method (DEM) has been widely used to study the micro-mechanical behaviour of ballast (e.g. Zhang *et al*. 2017). In DEM, irregularly-shaped ballast aggregates can be modelled by connecting and overlapping several spherical balls of different sizes and positions via a clump approach. Indraratna *et al*. (2014a) adopted the clump approach and simulated the angular ballast aggregates in DEM. The simulated particles were generated in a simulated shear box at random orientations to resemble experimental conditions. Huang and Tutumluer (2011) presented a method to simulate fouled ballast in DEM by reducing the surface friction angle of ballast. Indraratna *et al* (2014a) introduced an approach to model fouled ballast by injecting various amounts of fine particles into the voids to represent different values of void contaminant index (VCI).

Liu *et al* (2016a) compared the particle displacement and orientation data with their distinct element model (DEM) and found both to be in good agreement as shown in Figure 55. In another study, they have also shown that their DEM model was able to capture the ballast particle accelerations that could compare well with the data obtained through "Smart Rock" as shown in Figure 56.

Discrete element analysis (DEM) has become increasingly popular for modelling the behaviour of railway ballast at the grain scale, not least because the relatively large grain size compared with soils means that a realistic number of individual grains can be included in simulations. Modelling approaches have moved from 2D to 3D, and away from simple single or bonded pairs of spheres to include agglomerates of large numbers of spheres clustered together to represent "catalogues" of ballast grain shapes obtained by 3D scanning (e.g. Ngo *et al*. 2016, Li and McDowell 2019, Shi *et al*. 2020); polyhedra (e.g. Tutumluer *et al*. 2013); or level-set defined "potential particles" (Harkness 2009), which take the form of slightly rounded polyhedra, and super-ellipsoids (e.g. Duriez & Galusinski 2021).

Ways of modelling the effects of ballast attrition in DEM have been developed, primarily involving the breakage of asperities (McDowell and Li, 2016) and the "conical damage" approach (Harkness *et al*. 2016), also adapted by Suhr *et al*. 2018. Modelling attrition in some way seems necessary in DEM to replicate the transition from dense to loose behaviour of a granular medium as the confining effective stress is increased (Ahmed *et al*. 2016).

DEM has been used to investigate various aspects of ballast behaviour: geogrid reinforcement (Ngo *et al*. 2014, 2016, Qian *et al*. 2015), effects of layers of differently-sized particles (Li and McDowell, 2020), lateral resistance (e.g. Chen *et al*. 2015), differences between fresh and recycled ballast (e.g. Jia *et al*. 2019), ballast settlement (e.g. Tutumluer *et al*. 2013), under-sleeper pads (Ngo and Indraratna, 2020) and tamping (e.g. Shi *et al* 2020, Guo *et al*. 2021).

With DEM simulations and other advanced geotechnical modelling studies, the computed behaviour is increasingly dependent on the underlying constitutive models and input parameters used. In the case of DEM, there is an evidence gap between a phenomenon and how it is represented in the simulation (for example, representing ballast grain attrition by a change in surface roughness, although both the conical damage model and the breakage of asperities does do offer a more direct link); with the result that DEM may often indicate a plausible rather than a definitive explanation. As is often the case, empirical validation through high quality field measurements made over a long period of time remains both essential and a major challenge.

DEM simulations can assess the evolution of contact force distributions within the fresh and fouled ballast assembly. Distributions of contact force chains of fresh and fouled ballast (VCI=25%, and 50%) at an axial strain of ε_a=10% under a given confining pressure of σ_3=30 kPa are shown in Figure 57. Contact forces between grains are plotted as lines whose thickness is proportional to the magnitude of the force. Contact forces were distributed non-uniformly throughout the assembly and transmitted vertically from the top plate to the bottom of the simulated triaxial apparatus which was aligned in the loading

direction. The number of particle contacts increased significantly with an increase of VCI and consequently the magnitude of the contact forces decreased hence decreasing ballast strength.

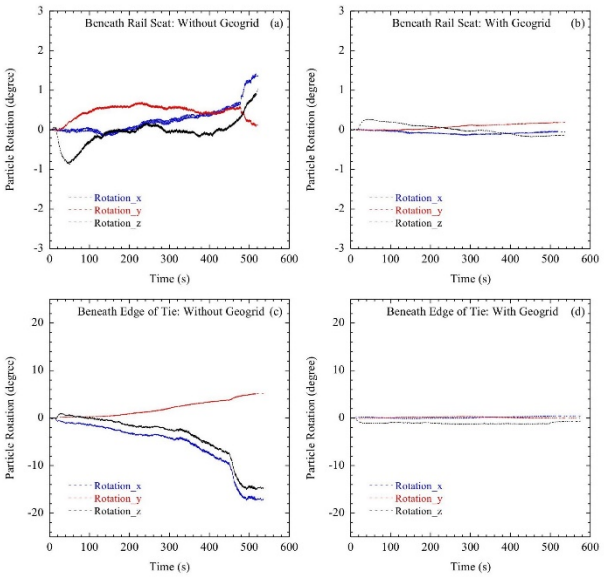

Figure 55: Comparison of Ballast Particle Displacement and Orientation Data with DEM (Liu *et al*. 2017a)

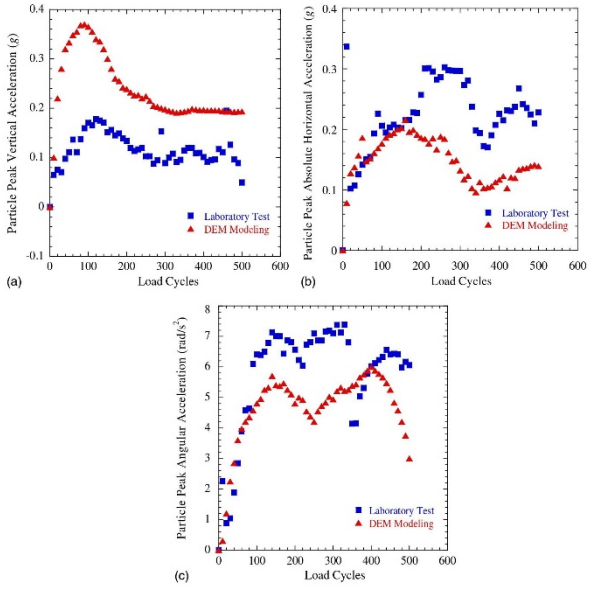

Figure 56: Comparison of Ballast Particle Accelerations with DEM (Liu *et al*. 2016b)

DEM simulations of complete track systems are too computationally intensive for practical (or academic) use. The method can be extended by coupling it with the finite element method (FEM). The coupled DEM-FEM method has been used to study the load-deformation response of the ballast assembly while considering interaction between the ballast aggregates and the subgrade layer. In this coupled model, the discrete ballast grains were modelled by DEM and the capping/subgrade layers are modelled as a continuum by FEM. Interface elements are introduced to transmit the interacting forces and displacements between adjoining material domains. The DEM transfers contact forces to the FEM, and then the FEM updates the displacements which provide a subsequent input to the DEM (Ngo et al 2017). The coupled DEM-FEM model was used to analyse the load-deformation responses of an instrumented track and the numerical predictions are compared with the field data in Figure 58. The field study was carried out along a section of instrumented track constructed over general fill and rock subgrades. The track substructure consisted of a 300 mm thick layer of ballast placed over 150 mm thick capping layer, overlying structural fill (thickness varying from 500 to 900 mm).

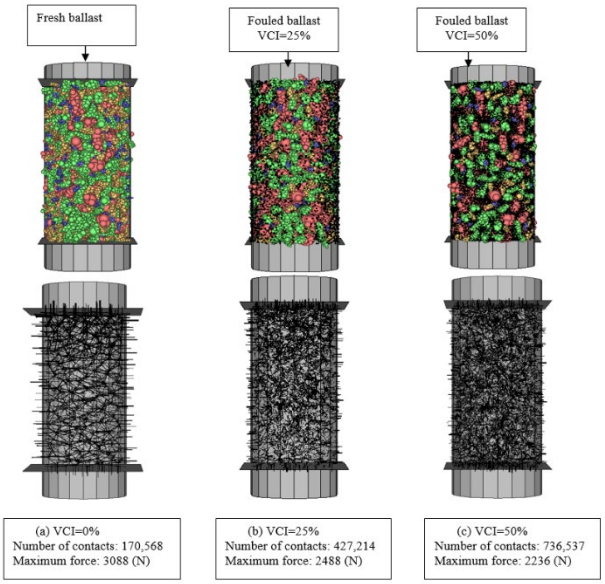

Figure 57: Contact force distributions of fresh and fouled ballast in simulated triaxial tests (Ngo *et al*. 2017)

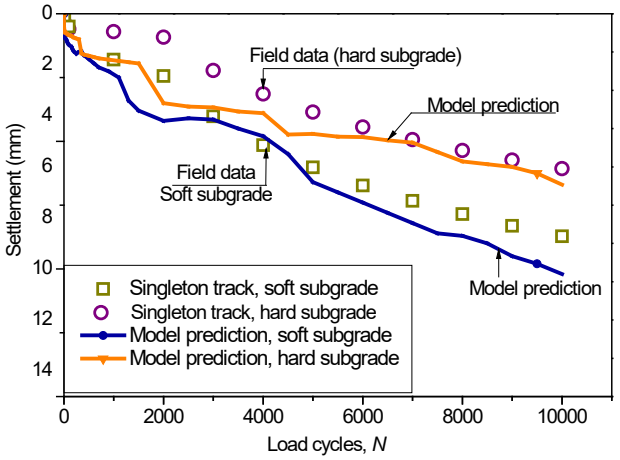

Figure 58: Comparisons of settlement between the combined model and field data (Ngo *et al.* 2017)

Comparisons of predicted settlement (Sv) of ballast for two types of subgrades obtained from the model and field observations are presented in Figure 58. It is seen that the model predicts the vertical deformation of ballast well in relation to the measured field data. The larger settlement predicted for soft subgrade (Sv =10.2mm) compared with the field observation of Sv = 8.7mm can be attributed to inevitable discrepancies between the field conditions and simplified boundary conditions applied for the coupled DEM-FEM model.

The simulation also showed that ballast directly underneath the sleeper experienced higher contact forces than ballast at the shoulder of the embankment. This caused vertical stress at the

interface between the ballast and capping to be distributed non-uniformly along the interface and was greatest towards the centreline of track. These simulations were consistent with the data measured in the field by Indraratna *et al*. (2014b).

2.3.14 *Effect of load frequency on ballast*

A series of large-scale triaxial cyclic tests on ballast was conducted to study the load-deformation behaviour of railway ballast under varied loading frequencies. Tests were carried out for ballast under different frequencies of *f*=10-40Hz subjected to a confining pressure of 20kPa, mimicking low confinement in the field. Cyclic tests were conducted within the bounds of $q_{cyc,max}$ =230kPa and $q_{cyc,min}$ =30kPa. Fresh latite basalt was used in this study. Stress-controlled cyclic loading was applied and the tests were ceased after N=500,000 cycles. During these tests, the axial strain, ε_a and volumetric change, ε_v were recorded by automated data loggers. Ballast aggregates were recovered at the end of each test, and the changes in particle size distributions were measured to analyse the extent of breakage.

The axial strain increases with an increase in loading cycles and frequency. The rate of increase in axial strain reduces with the number of cycles. When the ballast aggregates were compressed to a threshold packing arrangement, subsequent loading would initiate volumetric dilation and particle breakage.

Figure 59 presents volumetric strain versus number of cycles and shows that all tests exhibited volumetric compression at initial loading cycles (N=1000) progressing to a threshold compression, followed by a decreasing rate of compression at subsequent loading cycles. Under low frequencies of *f*=10, 20Hz, ballast exhibits volumetric compression throughout the tests. On the other hand, at high frequencies of *f*=30 and 40Hz, ballast shows dilation behaviour after N=10,000 cycles.

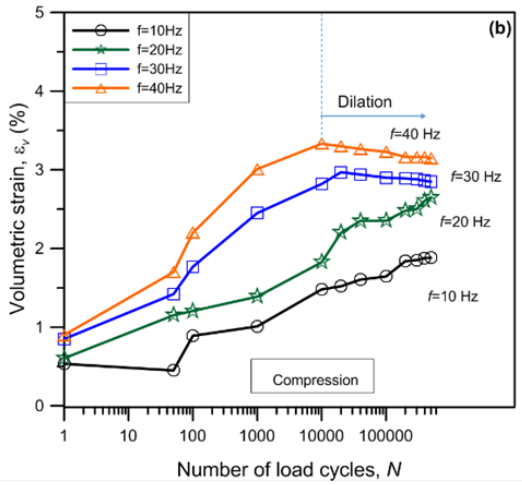

Figure 59: Measured volumetric strain of ballast and ballast breakage index with frequency (Indraratna *et al*. 2019b)

Ballast breakage can be reduced by installing rubber mats below the ballast. The amount of ballast breakage with and without the inclusion of a rubber mat is presented in Figure 60 for various frequencies. The ballast breakage increases with an increase in frequency and the ballast assemblies having the rubber mat show a decreased breakage compared to those without rubber mats. The reduction of ballast breakage is primarily caused by the energy absorbing characteristics of the mat which results in less load being transferred to ballast grains (Navaratnarajah *et al*. 2018). The inclusion of a rubber mat decreases the BBI up to 30.8% and 35.3% for ballast subjected to a frequency of f=10 and 20Hz, respectively.

The resilient modulus (MR) is also frequency dependent. MR is the ratio of the applied deviator stress (Δq_{cyc}= $q_{cyc,max}$ - $q_{cyc,min}$) to the recoverable (resilient) axial strain ($\varepsilon_{a,rec}$) during unloading.

$$MR = \frac{\Delta q_{cyc}}{\varepsilon_{a,rec}} \quad (9)$$

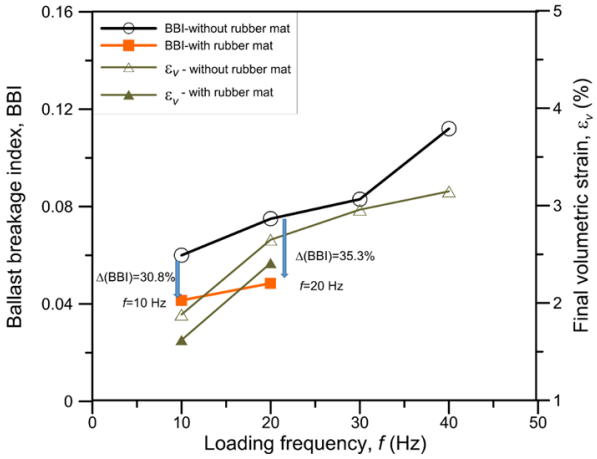

Figure 60: Measured ballast breakage subjected to varying loading frequencies *f*, with and without the inclusion of recycled rubber mats (Indraratna *et al*. 2019b)

The resilient modulus of granular materials can be expressed by a simple hyperbolic model as a function of the bulk stress, θ which is the sum of the principal effective stresses $\sigma_1'+\sigma_2'+\sigma_3'$. In Equation 10, k_1 and k_2 are empirical coefficients.

$$MR = k_1\theta^{k_2} \quad (10)$$

Figure 61 presents the variation of MR at different load steps with different frequencies for comparison with data conducted earlier by Lackenby *et al* (2007) at *f*=20 Hz. It is seen that Equation 10 can be used to estimate the strain hardening and softening of ballast at various frequencies.

For example, a standard gauge track with 25t axle load ($q_{max,cyc}$=230kPa) operating at 220km/h (*f*=30 Hz) often has a designed track confinement of less than 30kPa. With θ=420kPa and *f*=30Hz, the ballast layer will experience strain softening; for example, k_1=4.10 and k_2=0.55 is selected to calculate a value of MR =113.65MPa. The study also indicated that at a higher stress level, the increased contact area between particles decrease the freedom of ballast aggregates to deform elastically, which is strain hardening. As frictional failure occurs and significant particle sliding and rotating results in a more open structure causing a larger elastic strain indicating strain softening.

2.3.15 *Substructure Capping (sub-ballast) Layer: Role of Permeability, Drainage and Filtration*

A capping layer is required for protecting erodible subgrade fines while performing its normal function of sustainable load transfer to the underlying subgrade. Most compacted capping layers tend to be very stiff after construction and become even stiffer over time due to cyclic (repeated) loading. Increased compaction of sub-ballast (capping) materials can lead to a higher propensity for tensile cracking as well as reducing its permeability thus preventing the dissipation of any dynamic excess pore water pressures that may inevitably build up during the passage of very heavy (e.g. 40t axle load) and very long freight trains (up to

5km). This situation may be exacerbated if the cracks retain infiltrated water.

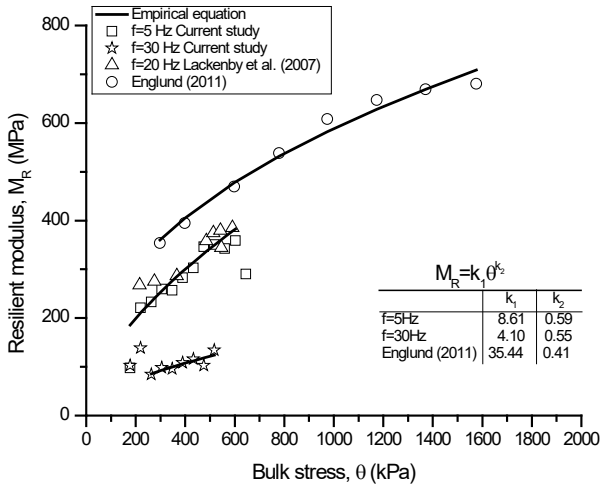

Figure 61: Measured resilient modulus of ballast (Sun *et al*. 2019)

An alternate approach is to provide capping with a more open grading so that it drains freely. The capping needs to act as a filter to prevent subgrade pumping and the subgrade needs to be relatively insensitive to water.

For a compacted sub-ballast material to act as an effective filter, it must satisfy three conflicting requirements: (a) sufficiently fine to arrest the pumped subgrade fines without clogging, (b) sufficiently coarse to avoid development of excess pore water pressure, and (c) to ensure that the finer fraction from the compacted material itself is not washed out under elevated hydraulic gradients induced by dynamic loads (Indraratna *et al*. 2018). The original filter selection criteria were established for static conditions based on soil gradations alone and they cannot always ensure effective filter performance for severe dynamic conditions imposed by heavy haul trains (Indraratna *et al*. 2018).

Sinusoidal loading up to 25Hz frequency (175km/hr) was simulated in the laboratory. The time-dependent reduction in permeability of subballast acting as a filter due to captured subgrade fines and compaction due to cyclic loading was quantified. Based on these results, the following retention criterion was proposed to select effective subballast filter (Trani and Indraratna, 2012).

$$\frac{D_{c35}}{d_{85}} \leq 3-4 \qquad (11)$$

where, D_{c35} represents the particle size in the filter corresponding to the 35th percentage passing by mass and d_{85} the particle size of the underlying material corresponding to the 85th percent passing.

Having examined the effects of compaction and loading conditions on various specimens of sands, sand-gravel mixtures, and silt-sand-gravel mixtures under internal erosion tests (Israr and Indraratna, 2019), two major phenomena have been identified as governing factors of internal erosion under cyclic loading; (1) excessive perturbation due to dynamic loading, and (2) accumulation of excess pore pressure. The former causes constrictions to vary between the loosest and densest states, while the latter causes the local hydraulic gradients to exponentially increase and reach the critical hydraulic gradient causing internal instability. The ratio of controlling constriction size of the stable coarse fraction in the loosest state of compaction and representative particle size by surface area of the potentially erodible fraction must satisfy Equation 12 for a sub-ballast capping material (designed to act as an effective filter) to be internally stable.

$$D_{c35}^{cL}/d_{85,sa}^{f} \leq 1 \qquad (12)$$

2.3.16 *Subgrade response to high-speed train loading*

Subgrade plays an important role in maintaining satisfactory performance of railway track. Experimental investigations on its cyclic behavior have been performed by many researchers under undrained conditions in the past several decades (Liu and Xiao 2010; Cai *et al*. 2018; Indraratna *et al*. 2020a), among others. Test results show that soft subgrade mainly exhibits stiffness degradation and plastic strain accumulation under cyclic loading induced by passage of moving trains, which become more critical when freight trains with higher speed and heavier axle loads are introduced.

The load induced by a moving train on a saturated fine grained soil results in principal stress rotation and accumulation of pore water pressure, which in turn results stiffness degradation and plastic strain accumulation (Dareeju *et al*., 2017; Gu *et al*., 2019; Jefferies *et al*., 2015). Some drainage and dissipation of excess pore water pressures may occur during and after the train load passage. The time rate of dynamic pore pressure accumulation is influenced by train speed/frequency, soil permeability and stiffness of the subgrade (Bian *et al*., 2019; Powrie *et al*., 2019b; Wang *et al*., 2019). Therefore, the speed of the train relative to the time scale of pore water pressure dissipation/ permeability is important to understand the mechanism. In Figure 62, as the ratio of load speed, *c,* to subgrade Darcy permeability, k_D increases, the maximum excess porewater pressure in the subgrade increases then decreases after the critical speed (Bian *et al*., 2019). Little excess pore pressure develops when the non-dimensional ratio (c/k_D) is less than about 100. Above this value train speed starts to generate additional excess pore pressure.

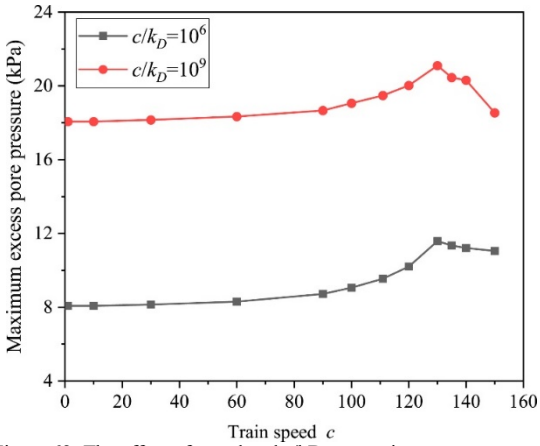

Figure 62: The effect of speed and c/kD on maximum pore water pressure (Bian *et al*., 2019)

The dynamic response of saturated subgrade has been studied using poro-elascticiy (Bian *et al*., 2019; Li *et al*., 2019). However, poro-elastic dynamics cannot capture the stiffness degradation and plastic strain accumulation caused by a moving load. Zhao *et al* (2021) presented a numerical study using finite element method that investigated the dynamic performance of saturated subgrade under moving train loadings, in which a two-phase porous medium consists of soil skeleton and pore fluid was considered in the analysis. Figure 63 shows the model predictions in terms of normalized pore water pressure versus vertical strains. The simulation results show that the model can capture the build-up of pore water pressure with increased loading cycles that have been widely observed in the laboratory

tests. Figure 64 presents the stress path that showing a continuous rotation of principal stress orientations. This kind of heart-shape envelope has also been reported by other studies via numerical investigations or analytical approximations (Li *et al*., 2019, Bian *et al*., 2019), among others. With continuous passage of moving trains, the stress path gradually moves to a lower stress state due to the build-up of pore water pressure.

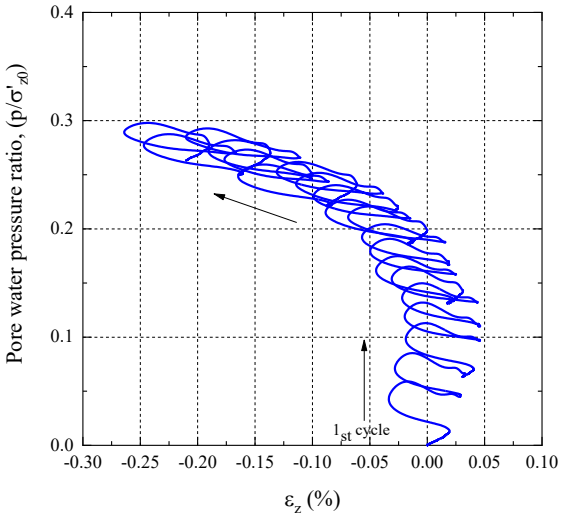

Figure 63: Pore pressure ratio with vertical strain (Zhao *et al*. 2021)

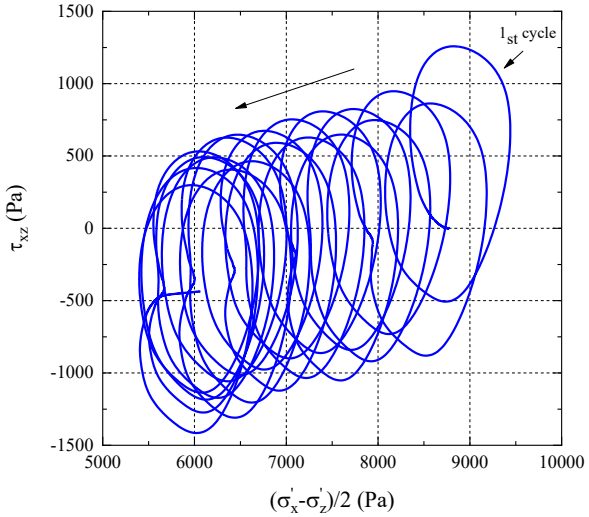

Figure 64: Deviatoric stress path (Zhao *et al*. 2021)

2.3.17 *Mud pumping*

With the continuous passage of trains on ballasted tracks, the upper layers of a saturated subgrade can soften and form a slurry near the ballast interface. Repeated application of railway loads pushes the softened subgrade slurry upwards and can reach the top of the ballast layer. The upward migration of soft subgrade fines into the coarser ballast layers under the action of moving loads is termed as mud pumping or subgrade fluidisation. The increased hydraulic gradient due to the high excess pore pressures results in subgrade fluidisation which then triggers an upward migration of fines under cyclic railway loading (Duong *et al*., 2014; Indraratna *et al*., 2020a).

In most cases, poor drainage of railway ballast is found to be the leading source of accumulated excess pore pressure and is associated with softening of the subgrade (Tennakoon *et al*., 2012). While this external loading is vital in initiating the fluidisation of fine particles, some studies indicate the role of varying accelerating factors such as the degraded contact between ballast and the subgrade, freeze-thaw cycles causing the ponding of water under the tracks in cold regions and stress-strain concentrations under rail joints, switches and transition zones in exacerbating mud pumping (Powrie, 2014; Nguyen *et al*., 2019).

Subgrade with low-to-medium plasticity is more vulnerable to mud pumping. Figure 65 shows that the plasticity chart for vulnerable subgrade lie in close vicinity of the A-Line, and high plasticity soils have not exhibited signs of mud pumping. It is believed that highly plastic clays undergo undrained shear failure as opposed to subgrade fluidisation. With the addition of 10% plastic fines (artificial kaolin) by dry weight, Indraratna *et al*. (2020b) observed the change in the mode of failure of subgrade from fluidisation to undrained shear failure.

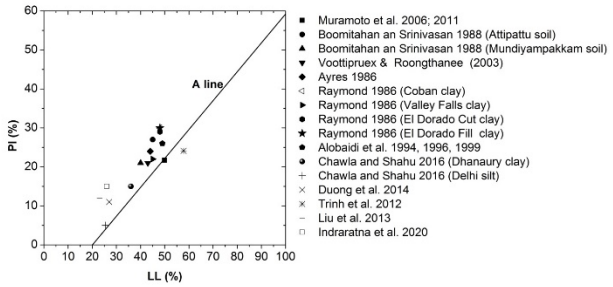

Figure 65: Plasticity chart of subgrade that experienced mud pumping (Indraratna *et al*. (2020a))

Indraratna et al. (2020a) investigated the undrained cyclic response of saturated subgrade compacted at different initial dry densities and subjected to varying cyclic stress ratio (CSR) and loading frequency (*f*). CSR is defined as the ratio of the applied cyclic stress to twice the effective confining pressure during the consolidation stage. When the specimen was subjected to higher CSR values there was a rapid accumulation of cyclic axial strains and mean excess pore pressure. For example, when the specimen compacted at an initial dry density of ρ_d = 1790kg/m^3 was subjected to a CSR = 1.0 and f = 1.0Hz, the residual strains increased to 5 % in about 10 cycles and the mean excess pore pressure ratio increased to 0.6 in the same time Figure 66. In addition, there was an increase in the fines content towards the top of the sample owing to the formation of slurry at the top of the sample Figure 67.

Figure 68 indicate that presence of plastic kaolin fines can significantly reduce the build-up of excess pore pressure and associated subgrade fluidisation. After adding 10% kaolin, the subgrade soil does not experience an early softening and fluidization with a CSR of 0.2. When the specimen subjected to a cyclic stress ratio of 0.4 it fluidised. Figure 69 shows that the change in liquidity index at the top of the specimen subjected to a CSR of 0.5 is about 75%. On the other hand, when the specimens were stable (at CSR ≤ 0.3), the specimens had a small uniform liquidity index throughout the sample.

Rapidly increasing excess pore water pressure (EPP) in the subgrade under cyclic loads is the main reason causing mud pumping beneath rail tracks. In order to gain some micromechanical insight into this phenomenon, a numerical simulation based on the discrete element method (DEM) coupled with computational fluid dynamics (CFD) where the soil is discretised in the form of a granular fabric subjected to fluid pressure can be used. Soil particles are simulated in DEM obeying Newton's law while the fluid flow behaviour is governed by Navier-Stokes theories following computational fluid dynamics. The mutual interaction between soil particles (i.e., solid phase) and pore water (i.e., fluid phase) is best carried

out in a manner whereby the variables of the solid and fluid phases are updated constantly over time.

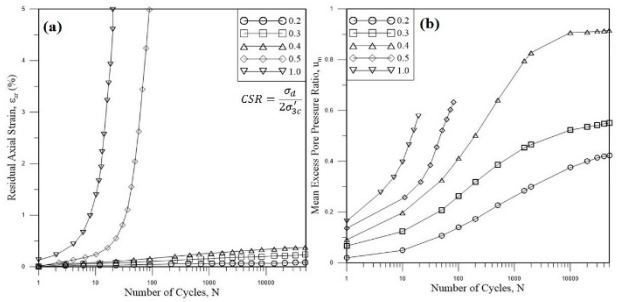

Figure 66: Development of (a) Residual axial strain and (b) mean excess pore pressure ratio at different cyclic stress ratio (ρ_d = 1790kg/m^3, f = 1.0Hz) (Indraratna *et al*. (2020a))

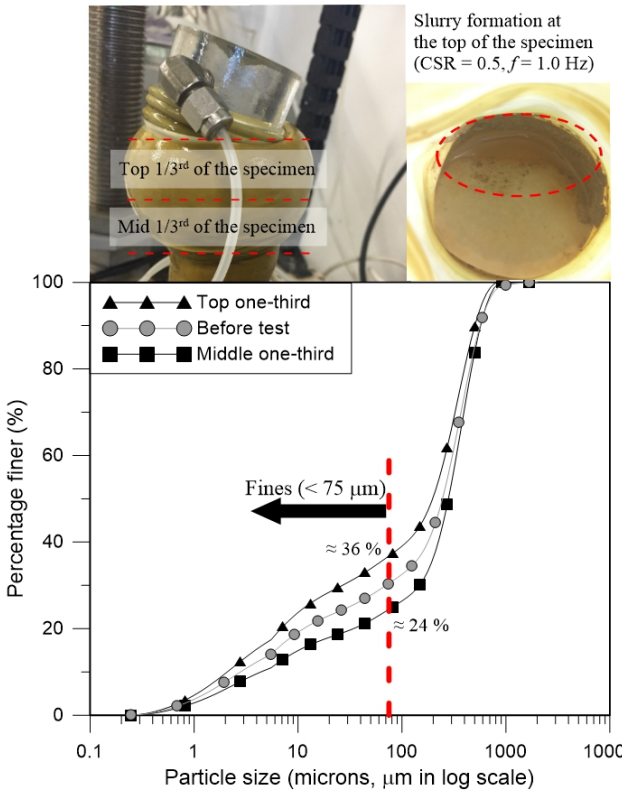

Figure 67: Subgrade soil fluidisation with the migration of fines under undrained cyclic triaxial loading (Indraratna *et al*., 2020a)

Nguyen and Indraratna. (2020) modelled a 6 mm wide and 17.5 mm high specimen of soil was modelled in DEM Figure 70. For computational simplicity, the particle size distribution (PSD) of a typical Ottawa sand (cohesionless) was used. In this approach, a periodic boundary is applied on the soil specimen in DEM (i.e., infinite soil element) while the adopted slip fluid-wall interaction enables the boundary effects to be eliminated. The hydraulic gradient (i) is assumed to increase gradually with time, which mimics the accumulated excess pore water pressure under a constant cyclic load. The increasing excess pore water pressure along the depth of soil results in increasing hydraulic forces acting on the particles. The densities of solid particles and fluid are taken as 2650kg/m3 and 1000kg/m3, respectively, while a Young's modulus of 6.8x10-9Pa is assumed for the granular assembly. The coefficients of sliding and rolling friction are taken as 0.5 and 0.1, respectively.

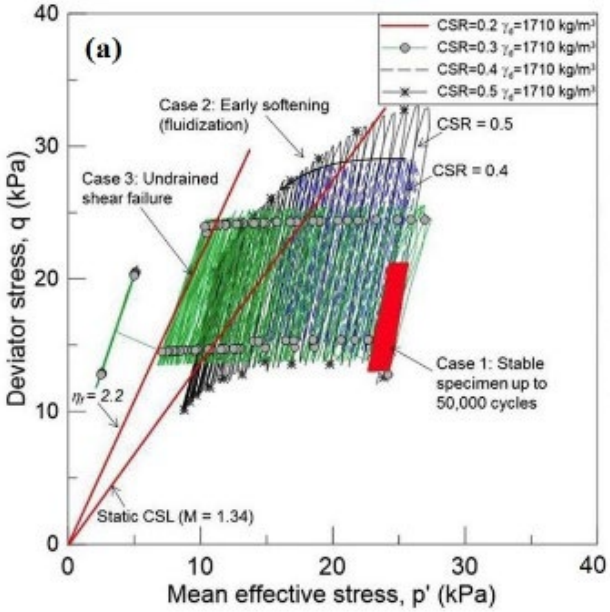

Figure 68: q-p' plots of the test specimen subjected to undrained cyclic triaxial testing (Indraratna *et al*., 2020b)

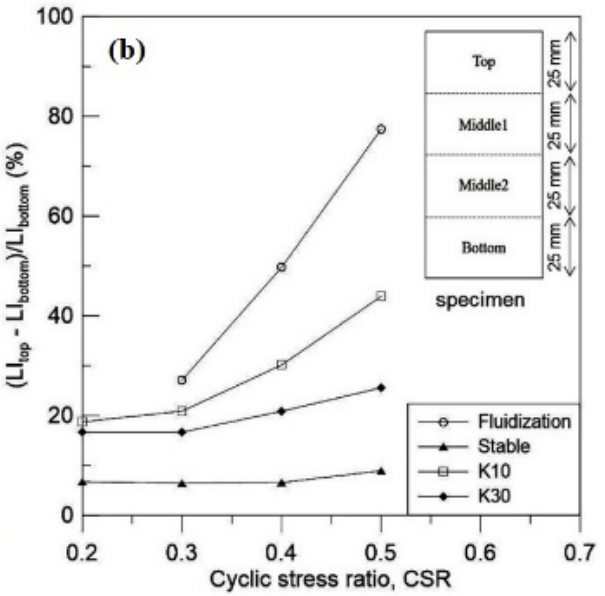

Figure 69: Change in the liquidity index throughout the height of the specimen (Indraratna *et al*., 2020b)

Figure 71 shows the axial strain developed with increasing hydraulic gradient. In this analysis, the vertical displacement is computed over the simulated time while increasing the hydraulic gradient, *i*, thus enabling the axial strain to be obtained. The axial strain begins to rise gradually with increasing *i*, and there is a swift change when *i* reaches approximately 1.4 where soil particles move rapidly. Increasing the hydraulic gradient results in correspondingly elevated hydraulic forces acting on the soil particles, causing their instability and internal migration.

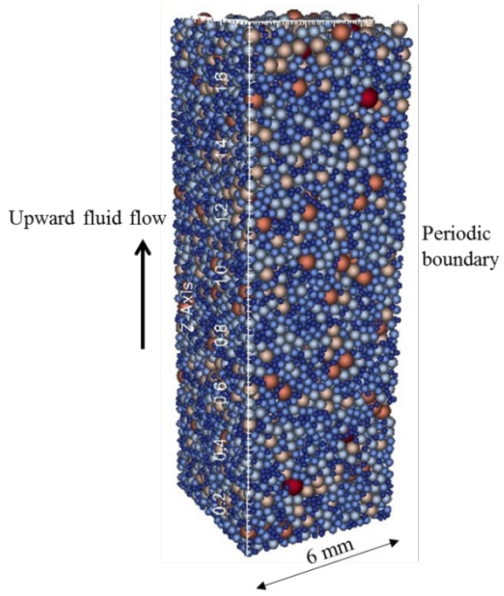

Figure 70: 3D soil specimen established in DEM coupled with CFD (Nguyen and Indraratna, 2020)

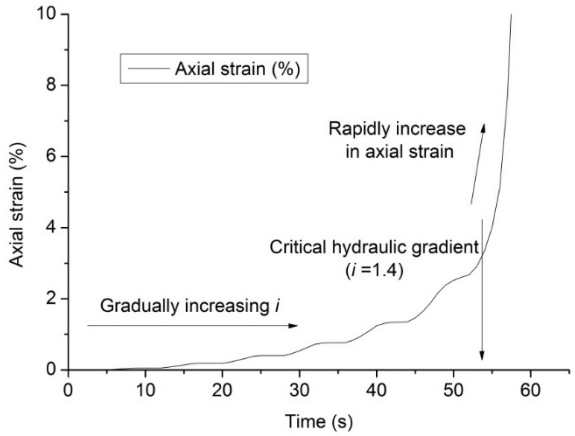

Figure 71: Axial strain development of specimen with increasing hydraulic gradient (Nguyen and Indraratna, 2020)

Figure 72 shows how the contact network of soil particles degrades under an increasing hydraulic gradient. For example, when the hydraulic gradient reaches 1.4, the maximum contact force drops severely from 14N to around 5.6N. When the contact forces become equal to the hydraulic forces soil fluidization occurs. Despite sustaining a certain degree of particle contact forces when i reaches the critical level, these contacts are shown to be in a chaotic state, hence do not necessarily represent the directional shear strength in a soil which we often assume in continuum mechanics.

2.4 *Roads*

2.4.1 *Overview*

Empirical pavement design by CBR procedures (soaked sample for 4 days to take care for the worst moisture conditions after construction) were originally evaluated by a field study (Corps of Eng. 1948, 1955) showing that this procedure (4 day soaked samples) was satisfactory or slightly conservative for the plastic materials, but conservative for non-plastic or slightly plastic materials. Additional studies of the predictions of subgrade moisture conditions for purpose of pavement design was reported by Gomes Correia (1996a).

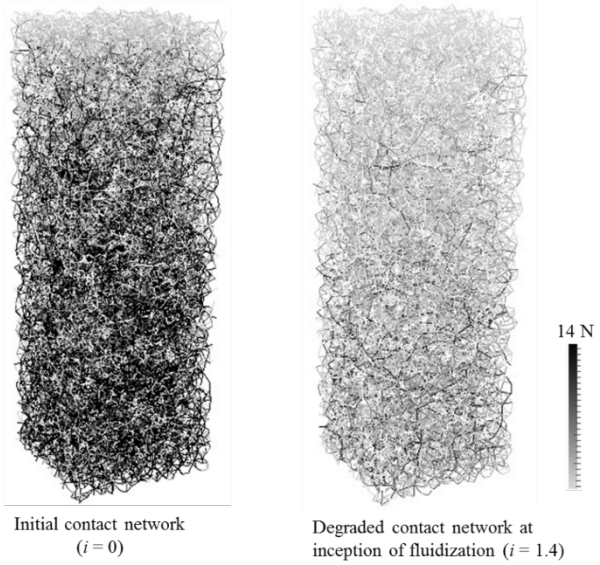

Figure 72: Degraded contact network of soil particles (i.e., soil fabric) at the inception of fluidization (Nguyen and Indraratna, 2020)

A first step for a rational design of flexible pavements was developed by Burminster (1943) who introduced the study of stress distribution that subsequently was extended to multi-layer systems and numerical modelling by FEM (*e.g.*, Balay *et al.*, 1997). From this point, the state of the art moved from empirical rules used in routine design of pavements to a mechanistic approach making use of the knowledge of the mechanical behaviour of soil mechanics framework, non-saturated soil mechanics and soil dynamics. Several contributions were promoted by ISSMGE related activities and particularly in the framework of ECTC11, TC3/ TC202. Some pioneer contributions include Brown (1996), Gomes Correia (1996b, 1999, 2001), Gomes Correia and Lacasse (2006). Zapata (2018) notes that most of all pavement layers will not exist in a fully saturated state and that the initial Mechanistic Empirical Pavement Design Guide (MEPDG) by the American Association of State Highway and Transportation Officials (AASHTO) has incorporated a design methodology for pavement systems that considers unsaturated material response and prediction techniques based upon the site-specific environmental conditions. This effort represented a huge step forward from the empirical Structural Number used in the AASHTO 1993 pavement design guide. However, and despite many efforts and advances through the world, there exists and important gap between the state of the art and the state of practice.

Environmental conditions affect fatigue and thermal cracking, permanent deformations, and the smoothness of flexible pavements. In rigid pavements, faulting and fatigue cracking, curling, warping, shrinkage, punchouts, and roughness are affected by moisture and temperature gradients. Mechanisms of failure such as the initial crack width are also directly related to these factors (Zapata, 2018).

Although the bound pavement layers act as a cover of the unbound materials, external factors such as precipitation, temperature, wind speed, solar radiation, relative humidity, and depth to groundwater table are environment parameters that affect pavement performance, as the internal stress state is continuously seeking an equilibrium condition. In a pavement structure, moisture and temperature gradients and also

freeze/thaw cycles are environmentally driven variables that can significantly affect the pavement layer and subgrade properties and, hence, its stiffness (Zapata, 2018).

Ward Wilson (1990) proposed a one-dimensional coupled thermo-hydro-mechanical model that incorporates the conservation of mass, allows the use of flow equations such as those proposed by Sheng *et al.* (2008) and imposed boundary conditions (Caicedo 2019). However, the model is complex, requires high computational effort and it is difficult to implement. A simplified set of mechanistic-empirical models to estimate the equilibrium moisture (suction) conditions beneath a pavement as a function of the Thornthwaite Moisture Index (TMI) were proposed by Zapata *et. al.* (2009). The model for granular materials is presented in Figure 73 as a function of percent passing the #200 sieve and the model for subgrade materials is presented in Figure 74 as function of the percent passing the #200 sieve and wPI, which is the product of the passing #200 (in decimal form) and the Plasticity Index. Mathematical models are available for implementation (Perera *et al.* 2004).

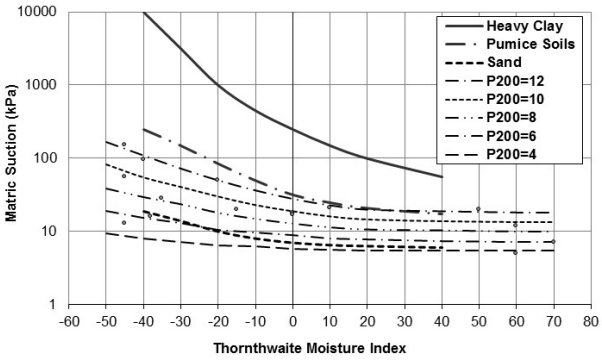

Figure 73: Suction at equilibrium for granular base materials (Zapata *et al.*, 2009)

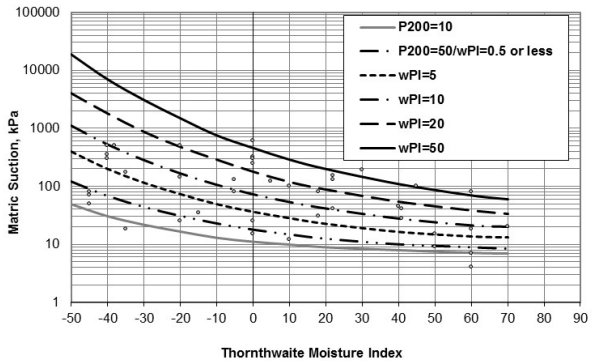

Figure 74: Suction at equilibrium for subgrade materials (Zapata *et al.*, 2009)

The suction obtained with these models can now be related to the soil degree of saturation (or any soil water content measurement) via the Soil-Water Characteristic or Retention Curve (SWCC). An empirically predicted model available is that proposed by Torres-Hernandez (2011). This model is based on information for more than 1,227,000 soils collected and grouped in a catalogue of properties for 31,876 plastic soil units and 4,518 non-plastic soil units collected as part of the NCHRP 9-23A project for the implementation of the MEPDG.

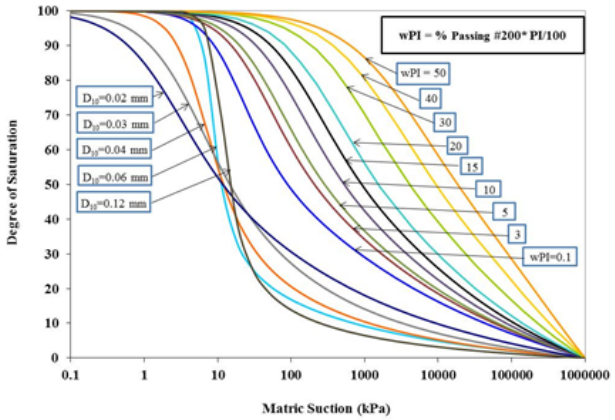

Figure 75: Combined family of SWCCs when using the Torres-Hernandez (2011) D10 model for nonplastic soils and Zapata (1999) model for plastic soils (Fredlund *et al.* 2012)

2.4.2 *Resilient modulus of subgrades*

A recent summary of the empirical relationships established for the resilient modulus has been presented by Gomes Correia and Ramos (2021), including the effects of stress variables and state conditions. Cary and Zapata (2011) extended the universal model to include effects of suction on resilient modulus, as shown in Equation 13.

$$M_R = k_1' p_a \left(\frac{\theta - 3u_a - 3\Delta u_{uw-sat}}{p_a}\right)^{k_2'} \left(\frac{\tau_{oct}}{p_a} + 1\right)^{k_3'} \left(\frac{(\psi_{m0} - \Delta\psi_m)}{p_a} + 1\right)^{k_4'} \quad (13)$$

Where p_a is the atmospheric pressure; $k_1' \geq 0$, $k_2' \geq 0$, $k_3' \leq 0$ and $k_4' \geq 0$ are regression constants; θ is the bulk stress, u_a is the pore air pressure, $\Delta u_{w\text{-}sat}$ is the build up of pore water pressure under saturated conditions; τ_{oct} is the octahedral shear stress; ψ_{m0} is the initial matric soil suction; $\Delta\psi_m$ is the relative change of matric soil suction with respect to initial suction due to build up of pore water pressure under unsaturated conditions. This model has been validated and compared to back-calculated stiffness obtained from Falling Weight Deflectometer (FWD) tests conducted at different moisture conditions (Salour *et al.* 2014, Salour *et al.* 2015).

Alternatively, changes of resilient modulus with moisture content can be estimated using Equations 14 and 15.

$$M_R = F_U M_{Ropt} \quad (14)$$

$$log\, F_U = (\alpha + \beta e^{-wPI})^{-1} + \left[(\delta + \gamma\sqrt{wPI}) - (\alpha + \beta e^{-wPI})^{-1}\right] / \left[1 + e^{\left(ln\left(\frac{-(\delta+\gamma\sqrt{wPI})}{(\alpha+\beta e^{-wPI})^{-1}}\right) + \sqrt{(\rho+\omega e^{wPI})}\left(\frac{S-S_{opt}}{100}\right)\right)}\right] \quad (15)$$

where, F_U is the ratio of MR at a given time to a resilient modulus at optimum conditions MR_{opt}, α = -0.600, β = -1.87194, δ = 0.800, γ = 0.080, ρ = 11.96518, ω = -10.19111, S is the degree of saturation, S_{opt} is the saturation at the optimum moisture content, and wPI is the product of the passing #200 (in decimal form) and the Plasticity Index.

A simplified model was developed for non-plastic materials in Equation 16 where $F_{U\text{-}STD}$ refers to materials prepared at standard compaction conditions.

$$log\, F_{U-STD} = -0.40535 + \frac{1.20693}{1 + e^{\left(0.68184 + 1.33194\left(\frac{S-S_{opt}}{100}\right)\right)}} \quad (16)$$

Results of Equations 15 and 16 are summarised in Figure 76 where it can be seen that F_U increases (i.e., *MR* increases) as the degree of saturation reduces below the saturation at optimum moisture content and vice versa. Although the model predicts that the resilient modulus under unsaturated conditions can be much greater than at optimum moisture content, care should be taken before adopting these values in design. Firstly, the equilibrium moisture content and potential variations in moisture should be estimated. Secondly, soils compacted dry of optimum tend to have a bi-modal void structure that can collapse on wetting (*e.g.* Alonso *et. al.*, 2012). It is preferable to compact soils near to the optimum moisture content to avoid this problem.

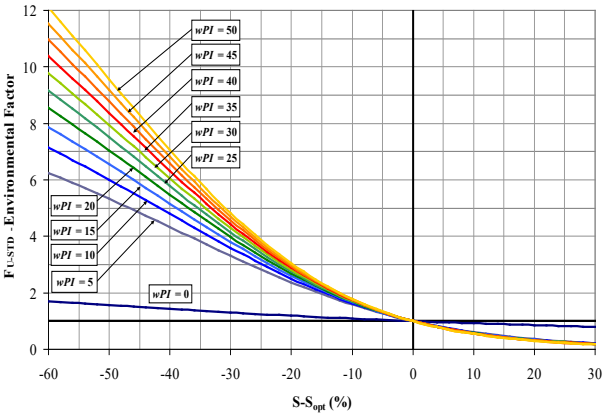

Figure 76: Variation of the Environmental Factor (F_U) as Function of Degree of Saturation and Soil Index Properties (Cary and Zapata, 2011)

Suctions are estimated from moisture content using the soil water characteristic curve (SWCC). Currently the MEPDG uses the drying arm of the SWCC and does not consider hysteresis. Rosenbalm and Zapata (2013) presented a stochastic evaluation of the models used in the MEPDG to estimate the water content of the unbound/granular materials considering the hysteretic behavior of the SWCC. They found that the prediction of the resilient modulus is overly conservative for any climatic condition when hysteresis is not considered and therefore, consideration of the SWCC hysteresis in pavement design and analysis is necessary and recommended, particularly in areas with lower TMI (arid climate).

Clearly, the resilient modulus changes as moisture and suction changes. Build-up of pore pressures in unsaturated soils as a result of traffic loading will have an effect on the resilient modulus. Cary and Zapata (2016) performed laboratory testing where a dynamic load was applied to unsaturated soil samples. The form of the pore pressure response is shown in Figure 77 and the accumulation of peak and residual excess pore pressures is shown in Figure 78. Figure 79 shows a plot of the predicted global peak pore water pressure curves obtained as a result of fitting the data to a nonlinear function. Note that the values plotted in the figure correspond to the actual pore water pressure rather than the excess pore pressure. For the unsaturated specimens, the origin of the predicted excess pore pressure was translated to the initial negative pore water pressure imposed on each specimen as the initial equilibrium condition.

Figure 79 shows that, for constant initial matric suction (c_{m0}) and dwelling time (t_D), the greater the bulk stress (u_{net} or u_{eff}) applied, the greater the pore water pressure developed. Also, under unsaturated conditions, the shorter the dwelling time, the greater the pore water pressure build-up, which means less dissipation between cycles.

It is a common belief that specimens under saturated conditions develop higher excess pore pressures than those under unsaturated conditions, because pores available for water pressure dissipation are scarce. However, Figure 79 shows that exactly the opposite effect was obtained. Specimens 3 and 4 tested under saturated conditions with a dwelling time (t_D) of 4 s and effective bulk stresses (θ_{net}) of 509 and 344 kPa, respectively, developed lower pore water pressures in excess than Specimens 1 and 2, (which were tested at the same t_D and θ_{net}), respectively, but under unsaturated conditions. Explanations for this include the presence of pressurized air within the pores exerting pressure on the pore water (suction stress), a reduction in voids as pore air compresses during the test increasing the chances for higher excess pore pressure build-up and low hydraulic conductivity in unsaturated specimens hindering excess pore pressure dissipation compared with saturated specimens.

The pore water pressure build-up gradually reached an asymptotic value for all specimens tested under the conditions of the study. The unsaturated specimens did not develop positive pore water pressures even after thousands of repetitions. However, under extreme loading conditions (i.e., under unusual high loads), it cannot be ruled out that the rate of pore pressure build-up becomes high enough to transition into the saturated regime and significantly reduce the effective confining stresses leading the specimen to failure.

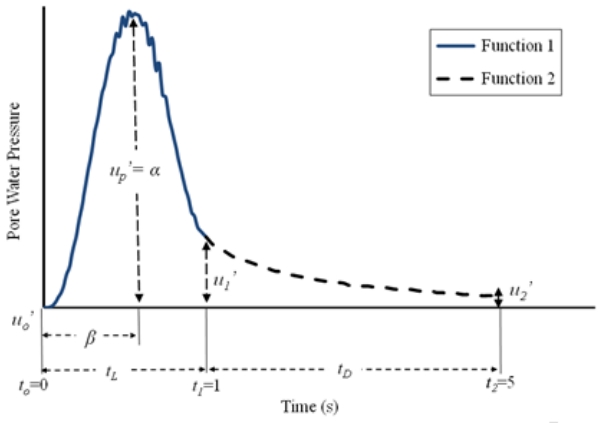

Figure 77: Pore Water Pressure Response to One Traffic Loading Cycle (Cary and Zapata, 2016)

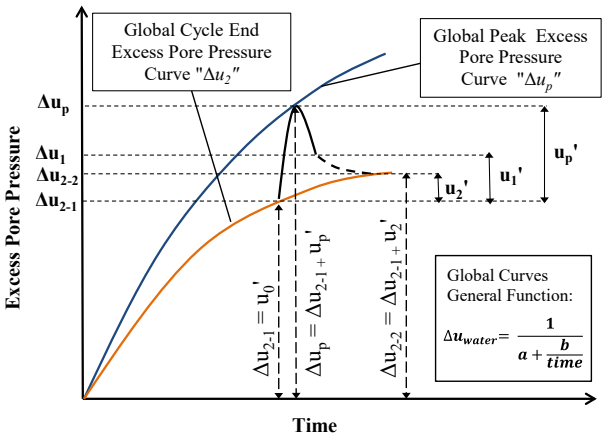

Figure 78: Excess and Peak Pore Water Pressures in Response to Traffic Loading (Cary and Zapata, 2016)

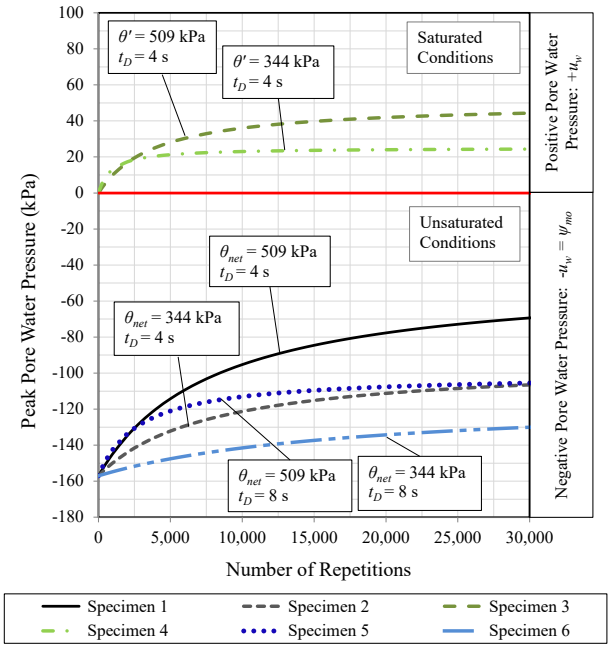

Figure 79: Peak Pore Water Pressures Observed on Samples Tested at Different Bulk Stresses, Dwelling Times, and Saturation Conditions (Cary and Zapata, 2016)

The results of the study were used to develop functions to assess changes in pore water pressure under saturated conditions ($\Delta u_{(uw\text{-}sat)}$) and suction changes ($\Delta\psi_m$) for unsaturated soil conditions with the number of cycles, that can then be used in Equation 13 to estimate the resilient modulus.

The results suggest that compacting unbound materials at or near optimum conditions could allow generation of pore pressures that degrade the resilient modulus. It is possible that compacting subgrades at conditions below optimum might be a better practice, albeit factoring in other effects of compacting materials at low moisture contents.

2.4.3 *Plastic deformations*

The resilient modulus of road materials has been extensively assessed because it is related to fatigue cracking of pavements (Caicedo, 2019). Research into permanent plastic deformations is more limited. A review of mechanistic-empirical permanent deformation models, including laboratory testing, modelling and ranking was recently presented by Ramos *et al*. (2020). Caicedo (2019) states that accumulation of plastic strains results from particle displacements caused by shear and compressive stresses and controlled by friction and suction pressure. Similar to other materials there are three ranges of behaviour, the boundaries of which are controlled by stress level and water content. These are:

1. Plastic shakedown range where plastic strains stabilise after a number of cycles;
2. Intermediate range where plastic strain increases at a decelerating rate but does not stabilise; and
3. Plastic failure range where strains increase until failure occurs.

Motorway roads would aim for the plastic shakedown range, more lightly trafficked roads could aim for the intermediate range and ideally, the plastic failure range would be avoided. Quantification of these ranges can be difficult because suction is an important parameter and hence drainage and infiltration are also important. When pavement materials become undrained, the air voids reduce, the degree of saturation increases, the suction reduces and hence the resistance to stress reduces. All this is also affected by the fine and coarse contents of the soil (Su *et al*., 2022).

The general state of practice is to adopt empirical laws relating permanent strain to strain after one cycle and various material parameters, shear and mean stresses and a power function of the number of cycles (Caicedo, 2019, Ramos *et al*., 2020). The power function is generally stabilising and the ratio of stress to strength is often used to assess a plastic failure range. Using these approaches in normalised conditions is possible to rank materials against permanent strains, what can be a very practical tool in the selection of materials (Ramos *et al*., 2020). Coupling this behaviour with the resilient modulus (both parameters controlling the pavement behaviour), it is possible to rate subgrade performances, as illustrated for pavements and railroad by Coronado *et al*. (2011) and Gomes Correia and Ramos (2021).

These empirical models are still commonly used in routine pavement design addressing the problem of rutting of flexible pavements. However, with the advance of numerical pavement modelling, the permanent deformations occurring mainly in subgrade and unbound layers are taken into account by constitutive modelling of cyclic plasticity of these geomaterials. Several of these constitutive laws have been developed with both isotropic and kinematic hardening, as well as using shakedown theory, to take account for the mechanical behaviour of these materials for large number of cycles, which is very different to the conventional soil dynamics modelling (Jing *et al*., 2018, Allou *et al*. 2007, Chazallon *et al*., 2006).

2.4.4 *Volume change behaviour of expansive soils and reactive fills*

Shrinking and swelling of fills and subgrade soils causes cracking of road shoulders, potentially tension cracking of pavements and settlement of fills, which can affect pavement shape and create bumps at the approach to bridges and culverts. Whether or not a material compresses or swells, its magnitude and time rate of volume change, is a function of its mineralogy, density, load, grading, compaction moisture content, and subsequent changes in moisture content (Muttuvel *et al*., 2020). A soil compacted at low density may expand when soaked at low applied stress but will collapse when the load increases. Soils compacted at intermediate densities may expand or collapse when loaded albeit to a lesser extent. Soils compacted to high densities may expand when soaked (Caicedo, 2019). In addition, soils and rocks derived from shales may break down over time as a result of changes in humidity or water content (Cardoso *et al*., 2012; Pineda *et al*., 2014) and microstructural changes (Alonso *et al*., 2012).

While trends in qualitative behaviour are reasonably clear, quantification of the magnitudes of swell or settlement and time rate of swell or settlement for engineering purposes is difficult to assess. In recent years, unsaturated soil models have been developed that can account for some of these behaviours such as the Barcelona Basic Model (Alonso *et al*., 1990) and the Sheng, Fredlund, Gens model (Sheng *et al*., 2008).

2.4.4.1 *Approaches to Estimate Shrink/Swell*

Methods for estimating shrink/swell soil volume change can be generally subdivided by empirical approaches using soil index properties such Atterberg Limits, particle size distribution, etc., and mechanistic approaches using engineering properties such as SWCCs, hydraulic conductivity, and results of 1-D oedometer tests.

Published studies which empirically relate soil index properties to shrink/swell soil volume change potential include but are not limited to: Seed *et al*. (1962), van der Merwe (1964), Ranganatham and Satyanarayana (1965), Nayak and Christensen

(1971), Schneider and Poor (1974), Chen (1975), Johnson and Snethen (1978) Weston (1980), Picornell and Lytton (1984), Dhowian (1990), Basma and Suleiman (1991).

Direct laboratory measurements of the soil volume change potential help improve the estimation of volume change used for design (Olaiz, 2017; Houston and Zhang, 2021). The 1-D oedometer "Response to Wetting Test" (ASTM D4546, 2014) is a common laboratory test for volume change determination. The following published studies include 1-D oedometer test-based relationships to unsaturated soil volume change: Jennings and Knight (1957), De Bruijn (1961, 1965), Burland and Jennings (1962), Sampson et al. (1965), Nobel (1966), Sullivan and McClelland (1969), Komornik and David (1969), NAVFAC (1971), Wong and Yong (1973), Gibbs (1973) Jennings *et al*. (1973), Smith (1973), Teng *et al*. (1972, 1973), Teng and Clisby (1975), Porter and Nelson (1980), Fredlund *et al*. (1980), Sridharan *et al*. (1986), Erol *et al*. (1987), Shanker *et al*. (1987), Nelson *et al*. (1992, 2001), Al-Shamrani and Al-Mhaidib (1999), Basma *et al*. (2000), Subba Rao and Tripathy (2003)

One key difference from the laboratory oedometer test compared to the field conditions the unsaturated soil will experience is the final degree of saturation. The response to wetting test inundates the sample, driving to saturation. However, with proper drainage, the probability that the soil will reach this moisture level over the period of the pavement design life is very low (Houston and Houston 2017). Suction-based volume change approaches are required for the estimation of the unsaturated soil volume change at moisture levels below saturation.

Several methods which account for the moisture/suction state of the soil include the Barcelona Basic Model (Alonso *et al*. 1990), the Lytton *et al*. (2005) approach adopted by the Texas DOT and the Post-Tensioning Institute (PTI, 2004, 2008), the Sheng, Fredlund, Gens model (Sheng *et al*. 2008), the Modified State Surface Approach (MSSA) first introduced by Zhang and Lytton (Zhang and Lytton, 2009), and the Surrogate Path Method (Singhal 2010; Vann *et al*. 2018).

2.4.4.2 *Incorporating the Effect of Shrink/Swell on Pavement Ride Quality*

The ability to estimate soil volume change as a function of time is a valuable tool in the design of pavement structure as it allows for the estimation of the cumulative International Roughness Index (IRI) impacted by environmental factors (Olaiz *et al*. 2021). Time-dependent estimations of shrink/swell soil volume change must quantify the changes in soil moisture/suction due to the varying climate. For a relatively near-surface groundwater table, significant potential exists for capillary rise into subgrade soils. The conventional assumption that negative pore water pressures (i.e., soil suction) can be estimated by backward extrapolation above the groundwater table of a line of slope equal to the depth times the unit weight of water, is appropriate in a thin region above the groundwater table, where soils are wetted to a degree of saturation of 85% or more (Zapata *et al*. 2007). When the groundwater table is relatively deep, the environmental factors such as precipitation, temperature, wind speed, solar radiation, and relative humidity affect the moisture state of the soils near the surface, commonly referred to as the active zone (Nelson *et al*. 2001).

Given the complexity and large number of climatic parameters affecting the climate-driven flux boundary conditions, the Thornthwaite Moisture Index (TMI) (Thornthwaite 1948; Thornthwaite and Mather 1955, Witczak *et al*. 2006) is commonly used by geotechnical engineers as an index that quantifies climate variability at a given location (McKeen and Johnson 1990). The TMI represents the aridity or humidity of a soil-climate system by summing the effects of annual precipitation, evapotranspiration, storage, deficit, and runoff. To a significant degree, the TMI index balances lateral infiltration and evapotranspiration for a particular region. TMI can be found from the map for the continental United States presented by Lytton *et al*. (1990) or from the models presented by Perera *et al*. (2004) and Witczak *et al*. (2006). Olaiz *et al*. (2016) reviewed the differing published procedures which attempt to simplify the TMI calculation from the original proposed by Thornthwaite in 1948 and concluded that the simplified equation by Witczak *et al*. (2006) provides values similar to those determined by the original Thornthwaite (1948) procedure.

The TMI has been used by geotechnical engineers to estimate soil suction envelope parameters, required for suction-based shrink/swell soil volume change estimations, such as the depth to stable (commonly referred to as equilibrium) suction, magnitude of stable suction, and total potential suction change at the surface. Published studies which relate TMI to suction envelope parameters include but are not limited to: Mitchell (1980, 2008, 2013), McKeen and Johnson (1990), Fityus et al. (1998, 2004), Barnett and Kingsland (1999), Cameron (2001), Jaksa *et al*. (2002), Briaud *et al*. (2003), Aubeny and Long (2007), Chan and Mostyn (2008), Vanapalli and Lu (2012), Karunarathne *et al*. (2012), Li *et al*. (2013), Sun *et al*. (2017), Lopes and Karunarathne (2017), the Post-Tensioning Institute 2nd and 3rd editions (2004, 2008), Vann (2019), Vann and Houston (2021), and Olaiz *et al*. (2021). Figure 80 below presents an example of TMI correlations to depth to stable suction using a TMI contour map for Australia (Mitchell 2008).

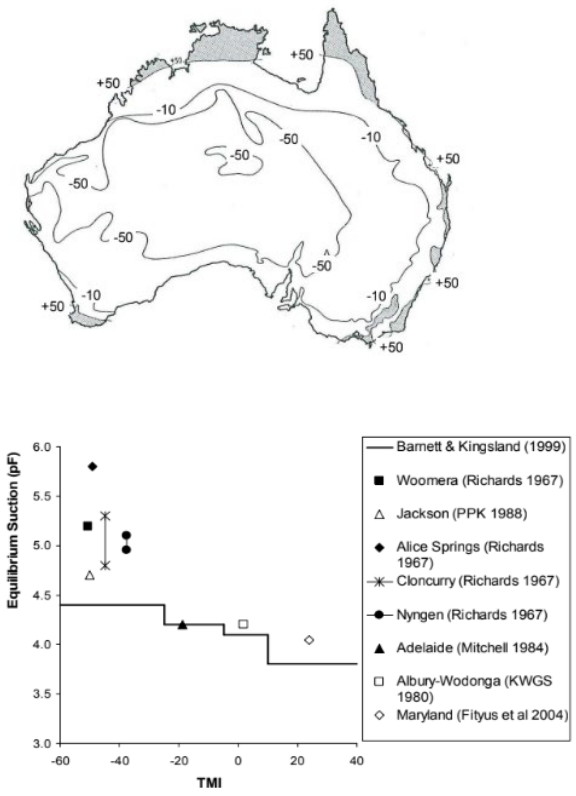

Figure 80 Distribution of TMI through Mainland Australia and the General TMI versus Equilibrium Soil Suction Relationship (Mitchell, 2008).

Further complications arise when soils are subjected to cycles of wetting and drying. Rosenbalm and Zapata (2017) reported the results of laboratory tests showing that shrinking and swelling increased with number of cycles, albeit at a decreasing rate Figure 81 and that the swell pressure reduced with the number of cycles Figure 82. The vertical deformations observed on the soils subjected to multiple wetting and drying cycles appeared to reach an equilibrium condition. At lower net normal stresses, the

vertical deformation is recoverable and at higher net normal stresses the vertical deformation is irrecoverable. The recoverability of the vertical deformation can be attributed to the soil fabric and changes in the void ratio. As the cycles progressed, the soil reached an equilibrium swell strain (recoverable) or an equilibrium collapse strain (irrecoverable) due to the applied net normal stress and changes in matric suction. In general, it was observed for the soils evaluated as part of this study that an equilibrium condition was reached after the fourth or fifth cycle for the wetting cycle, depending if the vertical deformation was swell or collapse, respectively. Conversely, the shrinkage strains reached an equilibrium state around the second or third drying cycle.

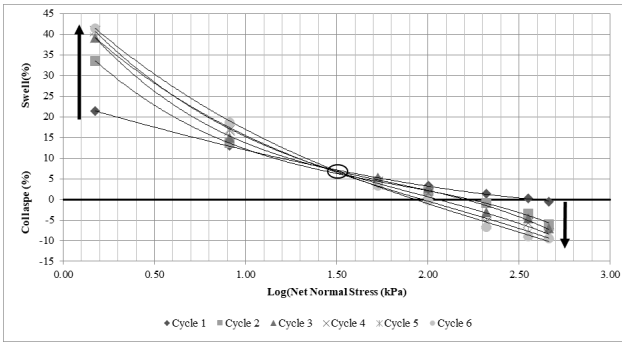

Figure 81: Swelling/collapse Results Observed on Soils Subjected to Wetting and Drying Cycles (Rosenbalm and Zapata, 2017)

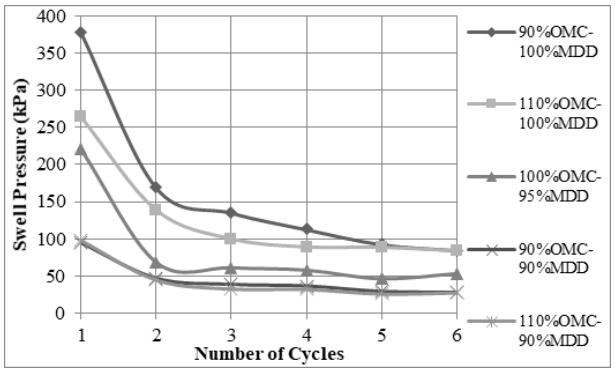

Figure 82: Swelling Pressure for Soils Subjected to Wetting and Drying Cycles at Different Initial Compaction Conditions (Rosenbalm and Zapata, 2017)

Practical solutions aimed at minimising volumetric changes of compacted fills are provided by BRE (1998) and Hopkins and Beckham (1998). Some recommendations are:

- Compact the lowest soil layers to modified maximum dry density. Increasing density has been shown to reduce compression;
- Progressively reduce the compactive effort as the height of the fill increases and load applied to the fill layer reduces. However, higher compactive effort in the upper layers of fill provides some risk management as it would be more prone to swell hence counteracting any compression that occurs deeper in the fill.
- Compact soils at optimum moisture content or wet of optimum. The intention is to maximise compression on loading by reducing the unsaturated stiffness of the soil and to maximise volume changes during construction rather than post construction. Compacting dry creates a stiff fill but long-term changes in moisture content and humidity will increase post construction internal compression.
- Rigorously mix the water into the fill to maximise its distribution. The rotary hoe method adopted by Hopkins and Beckham (1998) aims to achieve a high degree of mixing.
- Adopt thin layers and use heavy compactors in order to reduce the average particle size, maximise density and fill voids with particles.

2.4.4 *Frost action*

Swelling on freezing and loss of bearing capacity on thawing need to be considered in cold regions. Caicedo (2019) describes the freezing process as fast desaturation which creates a cryogenic suction. The suction causes potentials that move water towards the freezing fringe. In sands, most of the water freezes leaving only a small amount of unfrozen water. Accumulation of water is small and frost susceptibility is low. In silty soils and fine-grained sandy soils, some unfrozen water remains allowing water migration and accumulation into the freezing fringe. Frost susceptibility is high. In clays, a large amount of water remains unfrozen, but it cannot accumulate due to low permeability and frost susceptibility is low.

Cycles of freezing and thawing increase the soil's void ratio (Caicedo, 2019). The increase of water content during freezing reduces the resilient modulus during thawing. The water content before freezing and the number of cycles also reduces the resilient modulus. Like unsaturated soils, the rate of reduction in resilient modulus reduces with the number of freeze-thaw cycles.

The MEPDG provides methods to estimate the reduction in resilient modulus as a function of material properties, provides resilient moduli for frozen soils and suggests that the resilient modulus returns to its original value during thawing after a recovery period, the length of which depends on the material properties.

Frost heave in the cold climate region may cause serious damage to the pavement infrastructure (Schaus *et al*. 2011; Janoo and Berg 1990; Dore 2002; Roy *et al*. 1992; Dore *et al*. 1997). The resulting cracks, dips, heaving, and potholes make driving uncomfortable, damage vehicles and increase the risk of car accidents.

Three basic factors work together to generate frost heave: 1) freezing temperatures; 2) frost susceptible soils, such as silty soils or clayey soils as described above; and 3) water in the subgrade soils (Oswell 2011). Frost heave of soils is a complex coupled multi-physical process involving the coupling of the thermal-hydro-mechanical (THM) field (Li *et al*. 2000; Neaupane and Yamabe 2001; Liu *et al*. 2012; Zhou and Meschke 2013; Zhang and Michalowski 2015). The THM process is generally coupled by extending the soil mechanics under isothermal conditions theories to incorporate the effects due to thermal expansion of solid skeleton as well as the pore fluid migration (Rabin and Steif 1998; Brownell *et al*. 1977).

Frost heave is mainly caused by the formation of ice lenses. The first widely accepted theory for explaining the ice lens formation is capillary theory, which states that water is draw by the matric suction upwards to form the ice lenses (Taber, 1930). The drawback of capillary theory is that it does not account for the initiation of new ice lenses. Another model that explains the ice lens formation is the frost fringe model which proposes that frost heave can occur after ice has formed a frozen fringe by penetrating into the pores of the soil (Miller, 1972). The particle-engulfment model and geometrical supercooling model are recently developed models to simulate the periodic formation of ice lenses that have been observed in experimental work (Style *et al*. 2011).

Various models have been developed to simulate the variation of soil properties under frost effects. The distributions of temperature and water content as well as the associated volume change have been the focus of investigations. Hydrodynamic models and rigid ice models are two of the most common types

of models for this purpose. These include the CRREL model (Guymon *et al*. 1986), the Hydrodynamic model (Harlan, 1973; Taylor and Luthin, 1978; Jame and Norum, 1980; Hromadka and Yen, 1986; Noborio *et al*. 1996; Newman and Wilson, 1997; Hansson *et al*. 2004; Nishimura *et al*. 2009; Thomas *et al*. 2009), the Rigid model (Miller, 1978; O'Neill and Miller, 1985), the Semi-empirical models (Konrad and Morgenstern, 1980, 1981, 1982a, 1982b; Kujala, 1997), Poromechanical models (Coussy, 2005; Alonso *et al*. 1990; Lu and Likos, 2006; Coussy and Monteiro, 2008), Thermomechanical models (Duquennoi *et al*. 1989; Fremond and Mikkola, 1991; Li *et al.* 2000, 2002), and Multiphysics models (Song and Yu, 2018).

Methods for mitigating the frost heave in pavements include increasing the thickness of the base layer that are less susceptible to the influence of freezing/thawing process, thermally insulating the subgrade soil or base layer, and reducing the water content in subgrade soils by good drainage design (Mackay *et al*. 1992; Dore *et al*. 1999). Frost heave is an important form of environmental load that affects ride quality on pavement. In the MEPDG, the frost heave related distress is counted by the equations that predict the International Roughness Index (IRI).

In a recent study sponsored by NCHRP, the team examined the performance of the existing IRI prediction equations for road sections subjected to frost heave. The following observations were found for flexible pavement:

- Overall, current IRI prediction equation overestimates the IRI values for flexible pavement.
- The higher the frost susceptibility of the road section, the larger the prediction error with the current IRI prediction equation.
- The larger the Freezing Index for the site, the higher the segregation potential, and the larger the prediction error by the current IRI equation.

Efforts to develop and calibrate IRI equations for pavements subjected to the effects of frost heave are underway at Case western Reserve University and Arizona State University. The current effort incorporates heuristic models for Asphalt Concrete (AC), AC overlays, and Continuously Reinforced Concrete (CRCP) pavements. The new Site Factors showed improved performance when compared to the historic Site Factor equation used in the current IRI models. The calibrated equation for AC pavements is presented below:

$$IRI_{sf} = IRI_{sf_{max}} * Thickness_d * [age^{\frac{0.17}{thickness}} + 0.0005 * FI_{accum} * sin(2\pi * age + 0.04)] \quad (17)$$

$$Thickness_d = -0.188 * LN(thickness) + 0.131 \quad (18)$$

$$IRI_{sf_{max}} = 9.63 * ln(0.175 * FI + 1) * ln(0.086 * Precip + 1) * ln(0.05 * Silt_{percentage} + 1) \quad (19)$$

where, *Thickness* is the AC thickness, *FI* is the Freezing Index, *age* is the age of the pavement, *Precip* is the precipitation and *Silt* is the percentage of silt in the soil. Results showed a great improvement over the current MEPDG equation.

3 MANAGEMENT OF THE ENVIRONMENT

3.1 *Sustainability in geotechnical engineering*

Simpson and Tatsuoka (2008) reflected on discussions of the Intergovernmental Panel on Climate Change (IPCC, 2007) and suggested that production and use of energy along with climate change would be dominant themes in the near future. They also suggested that ground improvement will be critically important in future geotechnical practice to achieve reductions in quantities of material used, reduction in carbon footprint, prevention and mitigation of natural disasters, treatment and recycling of industrial wastes, remediation of polluted soils, development of brownfield sites and maintenance, and rehabilitation of existing structures.

The United Nations Rio+20 website (www.uncsd2012.org) defines sustainable development as development that meets the needs of the present without compromising the ability of future generations to meet their own needs. Sustainable development consists of three pillars: economic development, social development and environmental protection. There is tension between these pillars and between achieving simultaneous economic development and environmental protection in particular. For example, there is a trend for incorporation of principles of sustainable development into projects, particularly in government contracts. However, it is very difficult for governments tasked with obtaining value for money for taxpayers to award contracts incorporating high cost but sustainable construction, and difficult for contractors to win projects based on sustainable principles when clients award work based on lowest bid (Mitchell and Kelly, 2013).

Mitchell and Kelly (2013) identify that quantification of sustainability is a key challenge along with methods to reduce, reuse and recycle. Basu and Puppula (2015) expanded on these themes and provided examples for methods to quantify sustainability and sustainable applications.

3.2 *Carbon accounting in geotechnical infrastructure*

Carbon accounting is a relatively new but important area. Modern, robust geotechnical solutions that address the perceived issues of the past (especially but not uniquely associated with Victorian era embankments and cuttings) come at a cost – not only in terms of money, but also in terms of carbon. While a financial payback over a period of decades might be acceptable, in carbon terms it is not. Given the imminence of the threat of climate change and the urgent need to mitigate the worst effects in the next few years, the carbon payback time is more problematic. This will increasingly and urgently need to be factored into geotechnical calculations: methodologies will need to be developed discussed and generally accepted.

Current research sponsored by Network Rail in the UK is investigating, amongst other carbon related projects, the carbon impacts of cuttings and embankments. Aims include the assessment of greenhouse gas emissions associated with different interventions (maintenance, refurbishment and renewal), and the formulation of strategies for carbon mitigation over the whole life of the asset.

3.3 *Reduce, reuse, recycle in Transport Infrastructure*

3.3.1 *Reductions in materials hence carbon footprint*

Reductions in quantities can be achieved in many ways. Many forms of admixtures for soil stabilization have been used over the years including, but not limited to, lime, cement, slag, bio-grout, coal byproducts, iron oxides, lignins, zeolites and rice husk ash (Mitchell and Kelly, 2013; ICE Ground Improvement Journal more generally). Geosynthetic stabilization has developed considerably in recent years. Bio-degradable geosynthetics and vertical drains constructed from jute fibres have also been developed. Fibre reinforced soils have been explored.

These techniques are used to maximise use of poor quality subgrades and site won fills, minimize import of quarried products and reducing the quantity of materials used.

Reductions in fill materials can be achieved using vacuum consolidation. The vacuum pressure provides a similar surcharge load to an equivalent weight of fill. Reductions in fill quantities can also be achieved through steepening batter slopes using geosynthetics.

Reductions in diesel burnt during compaction can be achieved by optimizing processes using intelligent compaction.

3.3.2 *Reuse of transport infrastructure*

Reuse of brownfield sites, maintenance and rehabilitation of existing infrastructure and remediation of contaminated sites is becoming increasingly common. An example of remediation of failing earthworks slopes using discrete laterally loaded piles is provided here but there are many other examples of infrastructure reuse in the literature.

Remediation of a failing infrastructure slope using individual (discrete) piles is potentially attractive in terms of reducing cost, carbon and disruption but raises several questions relating to the maximum pile spacing at which the approach will still be effective, the pile depth needed, lateral loads and mechanisms of behaviour. Field monitoring, centrifuge modelling and numerical studies have been used to shed light these issues. Geotechnical centrifuge studies by Hayward *et al*. (2000) showed that the pile spacing could be increased up to 4 pile diameters and the method still be effective in preventing failure of the slope; a model with piles at 6 pile diameters failed with quite large slope displacements, although there was still enough interaction between adjacent piles to prevent flow-through of the soil. The inferred resultant stress acting on the upper-most sections of the piles increased monotonically with increasing pile spacing. This is in contrast to the conceptual behavioural models proposed by Ito and Matsui (1975, which indicates a decrease in the force beyond a pile spacing of two pile diameters), and by Wang and Yen (1974), which indicates a maximum force at a pile spacing of about five pile diameters).

Field studies have revealed two potential behavioural modes (Powrie and Smethurst 2015): a pile embedded into deeper, stable ground essentially resists the sliding of a top "slab" of soil, of thickness 2-3 metres; while a pile supporting a rotational slip in a scheme incorporating a surface stone blanket, or a pile responding to inward shrinkage of the embankment as a result of vegetation effects, exhibits a rather more complex bending behaviour (Smethurst *et al*., 2020). In neither the centrifuge models of Hayward *et al*. (2000) nor the field studies reported by Powrie and Smethurst (2015) did the pile bending moments approach anything like the values associated with classic limiting lateral pressures and flow through between the piles; although the spacing was deliberately low enough to prevent this.

Numerical analyses by Summersgill *et al*. (2018) of clay cutting slopes stabilised with a pile wall suggested that the piles will only ever delay the failure of slopes that are constructed over-steep, hence would not provide long-term stability. While consistent with the long-held view that first time failure of cut slopes in clay is governed by the critical state soil strength, the computed behaviour is dependent on the soil model used in the analysis, particularly the post-peak rate of softening, as also found by Rouainia *et al*. (2020). The geometric arrangement of the piles relative to the softened bands that form in the unstabilised analysis may also have had an effect: longer or differently arranged piles might have been more effective. This is a further example of the behaviour determined in a sophisticated model being crucially dependent on input parameters that are difficult to determine or characterise with confidence.

3.3.3 *Recycling of waste materials in transport infrastructure*

Mitchell and Kelly (2013) report that recycled waste materials that have been used as admixtures to stabilise soils or substitutes for natural aggregates include building rubble (crushed concrete, brick, glass, etc.), coal ash from power stations, rubber tyres, plastics, slag and rice husk ash. Collins and Ciesielski (1994) list 38 types of waste materials that have been considered for use in road construction such as embankment fill, base and subbase materials, flowable stabilized soils and concrete additives.

There is significant research being performed in this area as reflected by the 31 papers published in the ASCE GeoInstitute Geocongress 2012 (Hryciw *et al*., 2012) in a session titled 'Beneficial reuse of waste and recycled materials in sustainable geotechnical construction'. Much of the research is aimed at characterising the mechanical properties of the waste materials, an example of which is the Port Kembla Harbour reclamation.

In the past decade, the existing facilities at the Port had reached its capacity in the Inner Harbour area. The Port Kembla Port Corporation (PKPC) planned for the development of the Outer Harbour to create additional berths and storage areas by reclaiming additional land.

For the fill selection, the use of locally available granular waste materials (i.e. coalwash and steel furnace slag) was considered an economical and environmentally sustainable option to the traditionally quarried aggregates (Rujikiatkamjorn *et al*., 2013, Tasalloti *et al*., 2015a). However, the use of heterogeneous compacted waste materials such as slag and coalwash created some challenges related breakage of coalwash (CW) and swelling for steel furnace slag (SFS). Therefore, it was necessary to examine the geomechanical behaviour of these blends using a compaction field trial. The trial successfully demonstrated that the desired density, shear strength and CBR could be achieved. The fill with a higher percentage of steel slag stiffened more than fill with less slag from 30 and 170 days after compaction (Tasalloti *et al*., 2015b)

Tyre derived aggregates (TDA) or rubber crumbs (RC) present excellent engineering properties such as low unit weight, high damping and high energy absorbing capacity (Senetakis *et al*., 2012; Indraratna *et al*., 2019c; Qi *et al*., 2019a), which prevail their applications in dynamic loading projects (e.g. railways, airport runways, seismic isolation projects) to help reduce vibration and track degradation. Esmaeili *et al*. (2017) indicated adding 5% TDA into fully fouled ballast could reduce 34% ballast breakage. Sol-Sánchez *et al*. (2015) found that by adding 10% RC (by volume) into ballast layer could increase the dissipated energy significantly and reduce the ballast breakage. Signes *et al*. (2015) investigated the performance of mixed coarse aggregates with TDA as subballast through laboratory and field tests and found the inclusion of 1-10% (by weight) TDA can improve the resistance of track degradation efficiently albeit with a little reduction in bearing capacity.

Comprehensive laboratory tests have been carried out to investigate the geotechnical behaviour of SFS+CW+RC mixtures by Indraratna *et al*. (2017a) and it has been found that the addition of RC in the waste mixtures can further reduce the particle breakage of CW and the swelling potential of SFS, meanwhile increasing the ductility, damping property and energy absorbing property of the waste mixtures (e.g. Qi *et al*., 2019b).

An alternative mixture using CW+RC was proposed by Indraratna *et al*. (2019d) for use as capping for railways. In this case, the compaction energy was increased to compact the waste mixtures to a denser condition to compensate for the absence of SFS. The optimum compaction energy range for the CW+RC mixture was 900-1600 kJ/m^3. Particle breakage was less than that observed for 100% CW compacted to maximum standard dry density. Moreover, adding 10% RC by weight will significantly increase the energy absorbing property and provide comparable strength to traditional subballast materials (Indraratna *et al*., 2019b).

Constitutive models that have been tested and verified for traditional materials, cannot be directly applied when elastic and compressible recycled rubber is introduced into a matrix of relatively rigid aggregates. Recently, models have been modified to describe the behaviour of aggregate-rubber mixtures. Youwai and Bergado (2003) adopted a hypo-plasticity model within the critical state (CS) framework by modifying the original equation

for dilatancy to capture the increase in initial dilatancy with increasing mean stress when rubber is added to sand. In general, sand-rubber mixtures fail to each a clear CS unless a very large axial strain was attained which explained the deviation of this model from the experimental data at the CS. Mashiri *et al*. (2015) proposed a constant stress ratio (CSR) framework instead of the CS framework for sand-rubber blends.

These models do not fully capture the effect of rubber on the total energy absorbed by the mixture. Qi *et al*. (2019a) proposed a modified elasto-plastic model to describe the behaviour of a mixture of coal wash (CW), steel furnace slag (SFS) and rubber crumbs (RC) within the critical state framework. In this model, the critical stress ratio, M_{CS}*, is a function of total work, W_{total}, determined when the specimen achieved its point of failure. The critical state line (CSL) in the *e*-ln*p*' space also rotates clockwise as rubber content increases.

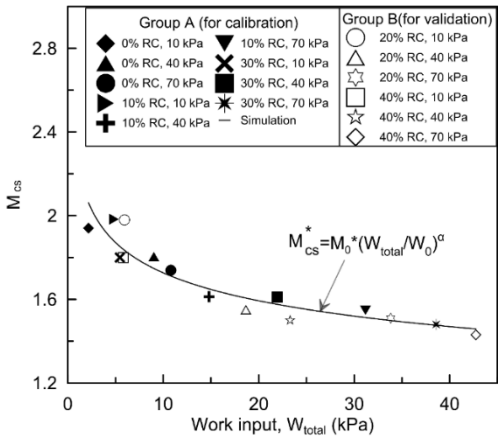

Figure 83: Relationship between the total work, W_{total}, and the critical stress ratio, M_{CS}, for CW+SFS+RC mixtures (Qi *et al*., 2018)

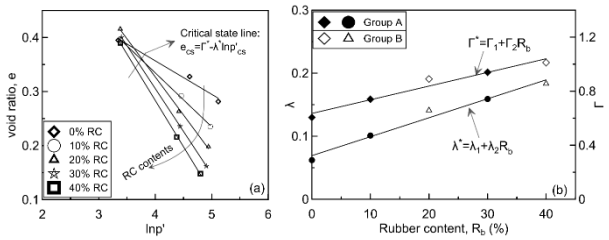

Figure 84: Effect of rubber content on the critical state of CW+SFS+RC mixtures (Qi *et al*., 2018)

Recycled rubber mats/pads can be used to modify rail track stiffness. Mats installed underneath ballast are called under ballast mat (UBM) and those placed at the interface of ballast and sleeper are called under sleeper pads (USP). The biggest advantage of using the rubber mats/pads is that they can significantly increase the contact area at the interface, and thus attenuate the dynamic and impact force, thereby reducing the ballast degradation and track deformation. Nimbalkar *et al*. (2012) evaluated the performance of the track specimen subjected to the impact force by changing the position of rubber mats and subgrade conditions. The experimental, numerical and field tests results revealed that under ballast mats are more efficient to attenuate the impact stress and mitigate the ballast degradation for a stiffer subgrade condition (e.g. tunnels and bridges), while for a softer subgrade condition, placing the rubber pads on top of ballast reduced ballast breakage and track settlement.

Field tests were carried out by Indraratna *et al*. (2014c) to investigate instrumented track sections with different geo-inclusions (e.g. UBM and geogrids) at Singleton (near Newcastle, Australia). Geogrids and a 10 mm thick UBM were installed at the bottom of ballast with changing subgrade conditions (i.e. soft alluvial deposit, concrete bridge deck and hard rock). The test result shows that the ballast breakage index (BBI) for the track incorporated UMB on the concrete bridge deck (0.039) is significantly smaller than other conditions (0.104-0.136). This verifies the effectiveness of using UBM to mitigating the ballast degradation on a stiff subgrade condition.

Indraratna *et al*. (2017b) has investigated the use of recycled truck tyres for use in rail track. They conducted plate load tests on unreinforced and tyre cell-reinforced capping layer using a large-scale prismoidal triaxial apparatus. With the increase in the thickness of the capping layer, the stress transmitted to the top of the subgrade layer was substantially reduced. The same benefit was achieved with a thinner capping layer reinforced with a tyre cell. Strain measurements on the tyre walls were small even at high loads showing the ability of the tyre cell to maintain its shape while providing the confinement. The hoop stresses in the tyre were estimated to produce an additional confining stress as high as 500 kPa at the maximum applied load of 6500 kPa.

Indraratna *et al*. (2017c) further evaluated the effect of tyre reinforcement on the ballast degradation, time-dependent resilience, damping characteristics and track deformations during cyclic load tests. Crushed basalt and spent ballast were chosen as the infill materials for the tyre cell. The number of load cycles applied in each test was 500,000 with the frequency of 15Hz and the maximum cyclic load of 370kPa as exerted by a 40-ton axle load. Settlement of the reinforced crushed basalt was smaller than the unreinforced material. However, for the spent ballast, the settlement for the reinforced specimen was more than the unreinforced specimen Figure 85. The reason for that might be that i) less particle interaction due to the internally smooth rubber tyre cell and the rolling, sliding of the particles, and ii) the size ratio.

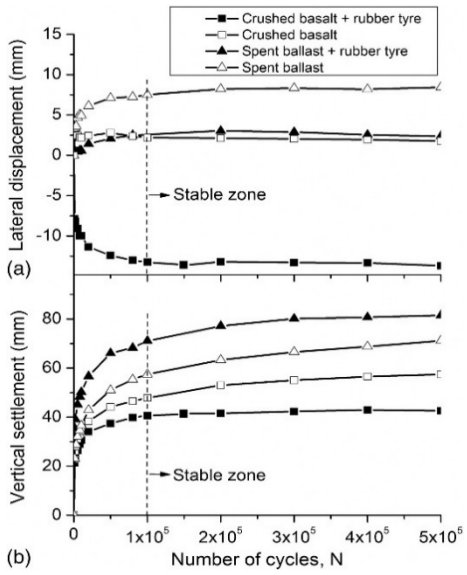

Figure 85: (a) Lateral displacements and; (b) vertical settlements of the testing specimens (Indraratna *et al*. 2017c)

Lateral tension and vertical compression forces were measured on the tyre. Although, the circumferential tensile strains were small, they helped develop additional confining stress to reduce lateral spreading. Use of rubber tyres also reduced the track modulus. Although a higher track modulus is generally desired, a lower modulus can be beneficial over a rigid substructure which must have less stiffness so that the transition

to the rail embankment is not accompanied by the large stiffness changes.

Recycled tyres have also been used to construct tracks over poor subgrade at the Ballina Soft Soil Field Testing Facility in Australia. The access track was built with 940 tyre units along with 546 tonnes of the crushed rock Figure 86 over a 10m thick soft soil deposit. Similar applications have been used for temporary platforms for piling rigs and cranes.

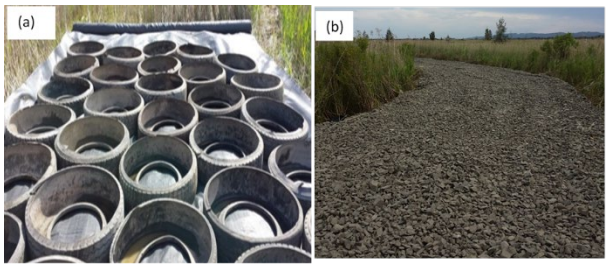

Figure 86: A view of the reinforced access track at Ballina site: (a-b) before and after infilled with crushed rock (unpublished part of a current program at the University of Technology Sydney through funding from the Australian Research Council, courtesy Ms. F. Mehmood, PhD student)

3.4 *Effects of and on the environment*

3.4.1 *The influence of vegetation and weather on earthworks*

Interest in the effects of vegetation on geotechnical infrastructure for transportation (particularly embankments and cutting slopes) arose for two reasons: (1) pore water abstraction in summer followed by re-wetting in winter causing seasonal cycles of shrinkage and swelling of clay soils that are disruptive to the infrastructure supported, and (2) the effect of vegetation on slope stability, through reduced pore water pressures as a result of water abstraction and root reinforcement effects.

Smethurst *et al*. (2012) showed that it is possible link climate data and observed pore water pressures and moisture contents in a grass or scrub-covered slope, using a simple soil water balance model of the rooting zone and surface abstraction. Grass and small shrub vegetation was not able to create a moisture deficit in summer that could be maintained through a wetter winter – relatively shallow summer drying is removed by infiltration in winter.

Trees have a deeper root zone and abstract water from greater depths. Modelling moisture abstraction by trees requires removal of the water from deep within the soil, modelling the effects of the deeper tree roots (e.g. Briggs *et al*. 2016). The greater abstraction and deeper root system of trees means that suctions in a low permeability embankment can persist through a typical winter, as infiltration does not then reach the full depth of the root zone. Tree removal from the slope, especially from the toe of an embankment, risks losing the deep suctions that maintain stability in winter. Removal of trees from the crest while leaving trees in place at the toe enables the deep suctions below the toe to be retained even through a wet winter, and should mitigate the worst effects of seasonal shrinkage / swelling in a high plasticity clay embankment (Smethurst *et al* 2015). Avoidance of high water demand tree species within 1.5 times the tree height from the track also helps mitigate damaging seasonal cycles of shrinkage and swelling (Briggs *et al*, 2013a).

Pore water pressures in a clay fill embankment are generally most detrimental to slope stability (highest) in winter. It was shown by Briggs *et al* (2013b) that the embankment foundation plays a crucial role in the wet winter pore pressures within a clay structure of permeability typical of old tipped fill embankments. If the embankment is founded on low permeability clay, pore pressures could rise towards hydrostatic below a water table close to the soil surface. If the embankment is on gravel or chalk, hence effectively under-drained, pore pressures will remain much lower – near zero in an embankment of reasonably uniform permeability with depth (Briggs *et al*. 2013b). If the embankment is of very low permeability, it is effectively impervious and suctions can be retained even in wet winter conditions (Briggs *et al*. 2013b).

The mechanical reinforcement effect of roots has been investigated experimentally using a geotechnical centrifuge (e.g. Liang *et al*. 2017) and novel shearing experiments carried out in an X-Ray CT scanner to observe root and soil behaviour (Bull *et al*. 2020). The fundamental understanding of the root and soil and behaviour gained from these experiments has allowed further development of appropriate analytical and numerical models to suitably characterise the increase in strength given by the root system (Woodman *et al*. 2020, Meijer *et al*. 2021).

3.4.2 *Failure modes likely to become more prevalent owing to climate change*

Experience over the past few years of more extreme summer and especially winter weather has suggested we will see a rise in instances of earthwork failure through

- Debris flow: possibly from a degraded / weathered near surface zone, or possibly from a downslope drain subjected to inundation flow as at Carmont (Scotland) in 2020
- “Rapid drawdown” effects, where a river level has risen adjacent to an embankment, remained high for a period of several days or weeks, and then fallen relatively quickly such that the stabilizing surface load effect is removed while high pore pressures remain within the embankment.

These mechanisms are associated with changing patterns of land use, increased intensity of rainfall and storminess, and possibly the weakening of a surface zone over a period of decades as a result of seasonal cyclic changes in pore pressure and water content. The latter mode of deterioration has been investigated using numerical models calibrated against site observations by Rouainia *et al*. (2020). Application of such an approach, even at the asset scale, is computationally intensive. Svalova *et al*. (2021) show how this difficulty can be overcome by carrying out a limited ensemble of simulations for a range of slope strengths, geometries etc., from which a statistical emulator was created to characterise the behaviour of the entire parameter space (i.e., to predict the way in which the factor of safety of a slope of any combination of strength and geometry changes over time). This can then be used to consider vulnerable earthworks at the route and network scale.

3.5 *Resilience to flooding*

Infrastructure resilience is the ability to withstand, adapt to changing conditions, and recover positively from shocks and stresses.

Flooding can affect road and rail in several ways. A flood can washout ballast, cause scour and saturate the pavement and subgrade leading to loss of strength and degradation in pavement performance as well as batter failure.

The after-effects of flooding are managed in practice in several ways:

- Shut road or rail
- Reduced speed to reduce load
- Load limits

Key considerations are

- Adopting a flood return period for design that provide satisfactory immunity at reasonable cost
- Limit damage and safety risks in larger floods
- Re-open the road or rail as soon as practicable with minimal cost.

Guidelines for the protection of flood affected road pavements have been developed by the Queensland Department of Transport and Main Roads (DTMR). These guidelines were developed based on experience of flooding in western Queensland and data from moisture probes installed in unsealed pavements. Their procedure can be summarized as:

1. Assess how many days the pavement was under water
2. Assess the structural capacity of the pavement
    a. Minor inundation: visual
    b. Moderate inundation: inspection or deflection testing
    c. Severe inundation: Deflection testing
3. Compare with historic structural data if available
4. If inspection indicates poor surface seal then adopt a higher inundation condition.
5. Decide whether to open the road or impose load restrictions
6. Depending on structural assessment main load restriction for a period of 3 to 4 weeks.

The period of load restriction is based on a 3 month pavement dry back model where the subgrade modulus increases linearly with time. Based on this model and an 80% load restriction, loss of pavement life is reduced to 33% after 1 week, 58% after 2 weeks, 74% after 3 weeks and 84% after 4 weeks. The 3 month dry back model was validated by unpublished field moisture probe data.

This short case history shows that asset owners have developed some procedures to address resilience to flooding. In contrast, the academic world has only recently started to address this issue.

Elshaer and Daniel (2018) investigated the structural response of pavements that have been inundated and the foreseen changes in capacity using a mechanistic approach using layer elastic analysis and the AASHTO empirical approach to determine the structural number. The relative impact of parameters such as unbound material type, layer thickness, traffic loads, and interlayer bond conditions on the reduction in expected strain values at critical locations were evaluated. The results showed increases of 15–80% in vertical strains at the top of subgrade layer for low volume and interstate sections and 6–15% increase in horizontal strain at the bottom of asphalt layer for low volume sections and 3–8% for interstate sections. Accurate information on the layer thicknesses, traffic type, and interlayer bond condition were found to be most important for the evaluation of the change in expected horizontal strain. The types of base and subgrade materials are the most important factors for evaluating the change in expected vertical strain.

Asadi *et al* (2021) assessed the post-flood water movement throughout its granular layers using unsaturated flow principles. They developed a numerical model for simulating the partially saturated water flow in pavements caused by surface infiltration.

Hasnayn *et al* (2020) performed laboratory tests to assess the performance of railway subgrade after flooding. They performed full-scale experimental investigation to study the behaviour of subgrade in both saturated and unsaturated conditions, and how this behaviour changes with soil suction. Further, the investigation also studies the role of sand-blanketing during and after repeated flooding events. The results showed that as soil suction reduces, flooding results in a continual reduction in both soil stiffness and track stiffness. It was shown that the introduction of a sand-blanket has limited effectiveness as a drainage material, particularly after prolonged and repeated flooding.

McKenna *et al* (2021) develop fragility functions to express the probability that an asset exceeds some serviceability or limit state as components in the quantitative risk analysis of infrastructure exposed to natural hazards. A generic granular highway embankment was modelled using the finite element method, considering various groundwater profiles and scour depths at the toe to quantify the deformation of the road surface. A probabilistic assessment of the magnitude of deformation and the groundwater level and scour depth was undertaken to derive fragility functions for the prediction of damage to assets exposed to these multiple hazards.

3.6 *Bio-geotechnics*

One of the areas that has advanced in the past two decades is bio-geotechnics. Bio-grouting processes are sustainable solutions that have the potential to replace Portland cement as binder for different soil improvement applications and reduce the CO_2 emissions associated with its production (Khodadadi Tirkolaei *et al.*, 2017).

Khodadadi *et al.* (2017) present a comprehensive review of the latest technologies developed on bio-mediated and bio-inspired improvement of granular soil via microbially induced calcium carbonate precipitation (MICP), enzyme induced calcium carbonate precipitation (EICP) and microbially induced desaturation and precipitation (MIDP). These technologies are in the research phase, but commercialization looks promising based on field trials and laboratory results at different scales.

MICP has proved to reduce the hydraulic conductivity, and increase the strength and stiffness in granular soils by mechanisms that range from urea hydrolysis (Burbank *et al*. 2011, Gomez *et al*. 2014, DeJong *et al*. 2010; Cheng *et al*. 2013) to denitrification, iron reduction and sulfate reduction (Almeida *et al*. 1995, Hamdan 2013; Karatas *et al*. 2008, O'Donnell 2016, van Paassen *et al*. 2010. Challenges to this technology that need to be addressed before implementation at a large-scale include the cost optimization of the technology, the environmental impact due to ammonium by-products and non-uniformity in the treatment due to the complexity of natural soil environments.

EICP induces carbonate precipitation by using free urease enzyme generally obtained from agricultural sources (Yasuhara *et al*. 2012, Hamdan *et al*. 2013, Neupane *et al*. 2015, Hamdan 2015, Kavazanjian and Hamdan 2015, Putra *et al*. 2016). This variant in the process eliminates the need for microbial transportation to soils and oxygen availability soils at greater depths. Challenges to the technology include the high cost of the enzyme and uniformity in the treatment.

The use of microorganisms to induce desaturation of granular soils via denitrification (MIDP) results in nitrogen and carbon dioxide gas generation, which in turn lowers the degree of saturation of the soil matrix. Given sufficient substrates, the stimulated bacteria will produce enough gas to develop a continuous gas phase. Introducing gas into the soil to reduce the degree of saturation is shown to increase the soil resistance to dynamic loading (Rebata-Landa and Santamarina 2012, He *h*. 2013, Stallings Young *et al*. 2020). The process of microbially induced desaturation and precipitation (MIDP) involves injecting an aqueous solution containing calcium, nitrate and a source of dissolved organic carbon (DOC). As a result, indigenous nitrate reducing bacteria are stimulated in-situ and convert the nitrate (NO_{3-}) into nitrogen gas (N_2), while oxidizing the organic carbon to dissolved inorganic carbon (DIC). In the presence of dissolved calcium, production of DIC results in precipitation of calcium carbonate minerals, while the energy released from the oxidation of DOC is used by the micro-organisms for growth and maintenance.

Ground improvement through MIDP occurs in two-phases (Karatas *et al*. 2008; Kavazanjian *et al*. 2015; O'Donnell *et al*. 2017a, 2017b). The first phase is microbially induced desaturation (MID). Previous research implementing MID in homogeneous sandy soils have demonstrated that a single treatment with a low concentrated solution of calcium nitrate and calcium acetate is sufficient to mitigate liquefaction via desaturation (Rebata-Landa and Santamarina 2012; He *et al*. 2013; Stallings Young *et al*. 2020; Wang *et al*. 2020; Stallings

Young 2021; Wang *et al*. 2021). The second phase of MIDP involves microbially induced carbonate precipitation (MICP), in which the sand is cemented with calcium carbonate ($CaCO_3$) minerals.

Column studies on MIDP demonstrated that the combined formation of biomass, biogas and biominerals can reduce the hydraulic conductivity by several orders of magnitude (Pham *et al*. 2018). Stallings Young et. al. (2021) performed experiments using a relatively thin tank of soil to simulate planar flow through a granular soil treated with MIDP. The treatment successfully desaturated the soil and once a continuous gas phase was formed, it remained relatively constant throughout the remainder of the experiment. Flushing with additional water did not remove a significant amount of the biogenic gas. Desaturation resulted in the reduction of hydraulic conductivity and the presence of gas affected the measured excess pore pressure and demonstrates gas formation through the system. The mechanical properties of the material were not investigated in this testing program.

The main challenge for MID is to predict and control the uniformity of the treatment in field conditions.

4.0 THE DIGITAL AGE

4.1 *Intelligent construction*

Earthworks construction refers to the tasks of excavation, transportation, spreading and compaction of geomaterial (e.g. soil, rockfill and soil-rockfill mixture). Whereas relying heavily on machinery and repetitive processes, these tasks are highly susceptible to optimization. In this context Artificial Intelligence techniques (AI), such as Data Mining and modern optimization can be applied. Parente *et al* (2016) developed a novel intelligent earthwork optimization system, capable of integrating AI and modern optimization and GIS technologies in order to optimize the earthwork processes throughout all phases of design and construction work. This integration system allows significant savings in time, cost and gas emissions contributing for a more sustainable construction.

Intelligent compaction is a process where a smooth drum roller is instrumented and the stiffness of the soil inferred from the data. Variations to vibration amplitude, frequency, roller speed, roller weight and number of passes can be varied to determine the optimum combination of factors to achieve compaction requirements while minimizing effort, time and diesel burnt. Rollers equipped with GPS can also track their path and height helping with quality control and density assessments. Data can be presented as CMV (compaction meter value) based on Fast Fourier Transform peaks from accelerometer signals or by measuring a stiffness from inferred load, displacement response obtained from the accelerometer (Briaud and Seo, 2003; Anderegg *et al*, 2006). Experience with CMV suggests some averaging (over say a 0.5 m square area) of CMV is needed to allow for measurement variability.

The fundamental problem with the stiffness measures is that they do not provide a good measure of compaction because density is not strongly correlated to stiffness. Tatsuoka *et al* (2021) show that stiffness can be near constant as density increases at near constant moisture content. Developing methods to assess density remotely is an area requiring further research.

If method compaction is used then the challenge of measuring density can be overcome and the benefits of using intelligent compaction can more readily be realized.

4.2 *Smart sensors*

4.2.1 *Airport pavements*

Many of the traditional sensors installed in airport pavement foundation layers have been multi-depth deflectometers, induction based strain coil sensors, subgrade pressure cells, etc. More recently, with the recent emphasis to develop smart sensors, such as smart rocks and bender element transducers based on shear wave propagation for determining layer stiffness properties, more detailed perspectives on the layer stiffness characteristics and rutting failure mechanisms of pavement foundation layers are gained to provide some unique perspectives, such as the depth of failure surface in a thick granular subbase by the use of strain coils installed with depth profile or the quantification of stiffened zone in a geogrid-stabilized unbound aggregate base and subbase layers (e.g. Kang *et al*. 2022).

4.2.2 *Road pavements*

Rana *et al* (2016) summarised some recent advances in sensing for road pavements. Fibre optic sensors can be used to monitor various parameters such as strain, displacement, vibration, cracks, corrosion, and chloride ion concentration, etc. An example is shown in Figure 87. Piezoelectric sensors can be incorporated in remote and inaccessible locations. They can also be used to harvest energy from pavements due to the movement of the vehicles and generated pressure (Zhao *et al*., 2013; Gholikhani el al., 2019).

A self-sensing composite has the ability to sense its own deformation and damage. Strain and damage sensing in a composite material is usually achieved through detecting change in their electrical resistivity (Rana *et al*, 2016). To achieve piezo-resistivity in a composite material, it should contain a conducting element. Different types of conducting components have been used in the existing self-sensing composite materials. Short and continuous carbon fibres (CFs), carbon particles as well as carbon nanomaterials such as carbon nanofibers (CNFs) and nanotubes (CNTs) have been utilized for this purpose. These conducting components form a conducting electrical network within the composites. When the composites are subjected to deformation or damage, this conducting network is disturbed leading to a change in the electrical resistivity.

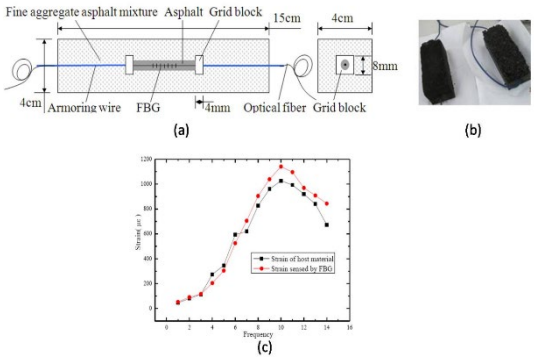

Figure 87: (a) Schematic design of fine aggregate asphalt mixture encapsulated fibre optic sensor (b) real picture (c) strain sensing capability (Rana *et al*. 2016)

CNT/cement composite sensors have been developed and applied in pavement monitoring (Yu and Kwon, 2012). These CNT sensors were installed in the road for testing the pavement monitoring capability (Figure 88). Figure 89shows the response of pre-cast and cast-in-place CNT sensors while a truck passes over the road and compares the response with that obtained in case of strain gauges. It can be observed that an abrupt change in voltage occurs when a wheel passes over the road and each wheel represents one signal peak.

A recent laboratory proof of concept was established by Abedi *et al*. (2020) using originally hybrid combination of

carbon nanotubes (CNTs) and graphene nanoplatelets (GNPs) in a cement mortar achieving high mechanical, microstructural, durability and self-sensing performances. For concentrations of 0.1, 0.3, 0.5, 0.7, and 1% CNT+GNP in the cement mortar (W/C 0,5) tested and for the different hydration times (7, 28 and 90 days) an optimum concentration of CNT+GNP around 0.5% shows the best performance in terms of durability (resistance against freeze-thaw cycles), microstructure and mechanical behavior under compression and flexural cyclic loadings. Figure 90 shows an example of the fractional change in resistivity (sensing sensibility) under cyclic flexural loading. This optimum percentage (0,25% CNT+0,25% GNP) reveals to have significant higher gauge factors when compared with the available results in literature using individual nanoparticles.

Figure 88: Installation of CNT/cement sensor in roads for testing monitoring capability (Rana *et al*. 2016)

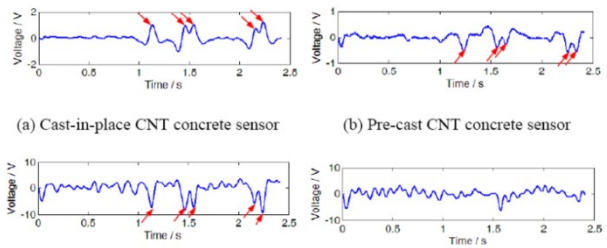

Figure 89: Response of cast-in-place and pre-cast CNT sensors (a,b) and strain gauges (c, d) while a truck passes over the road (Rana *et al*. 2016)

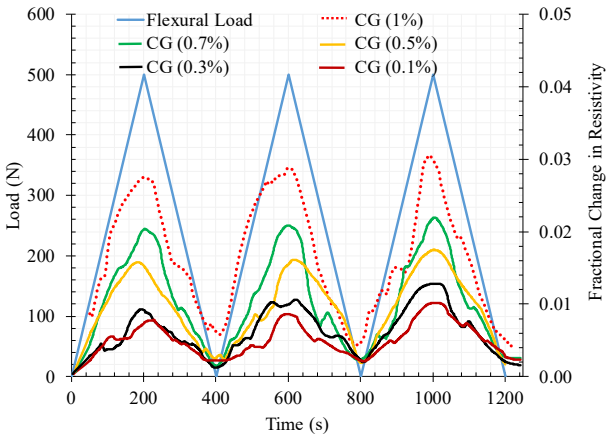

Figure 90: The fractional change in resistivity together with the cyclic flexural response for reinforced cementitious composite by different CNT+GNP concentration (Abedi *et al*, 2020)

4.3 *Data analytics*

4.3.1 *Predictive maintenance*

Use of instrumented vehicles or pavements coupled with inverse analysis or other stochastic numerical methods to predict future maintenance is an area of research that is rapidly expanding. Drivers for the research are to eliminate safety risks to maintenance workers inspecting infrastructure in heavily trafficked roads and railways, earlier identification of damage, increased inspection productivity and reduced whole of life maintenance and operational costs. Xie *et al* (2020) provide a comprehensive summary of techniques being utilized in the rail industry.

Mechanical and data-driven models are used to evaluate the track conditions for diagnostic and prognostic purposes. Mechanical models are based on engineering mechanics which allow physical understanding of a system but often rely on simplifying assumptions. Data-driven methods correlate data with maintenance events and include statistical models and machine learning models. Statistical models make inferences about the relationships between variables often described in a mechanical model, whilst machine learning models focus on making the most accurate correlation between data and maintenance events without needing a mechanical model. Both approaches can handle high dimensional and multivariate data and identify relationships between the track status and measurement data. The performance of the data-driven methods depends on the appropriate choice of data pre-processing and analysis models.

Collecting information is the first step in the application of data-driven models. Some commonly used measurement methods for railway track are summarized in Table 4.

Table 4 Methods of rail monitoring (after Xie *et al*. 2020)

Methods	**Technologies**	**Monitoring Objects**
Walking patrols	Visual, ultrasonic testing	Ballast section, ties, fasteners, rail head
Specific inspection cars	Camera-based measurement, ultrasonic testing, vibration acoustic, eddy, laser, magnetic	Track geometry, rail head, ties, fasteners, substructure
In-service vehicles	Camera-based measurement, ultrasonic testing, vibration, displacement	Track geometry, rail head, ties, fasteners
Wayside detectors	Fiber, meteorological sensor, impact load detector	Rail head, wheel-rail interactions, temperature, weather

An approximate distribution of methods used for predictive maintenance is provided in Figure 91. Data driven models comprise about 74% of the total and statistical methods about 26%.

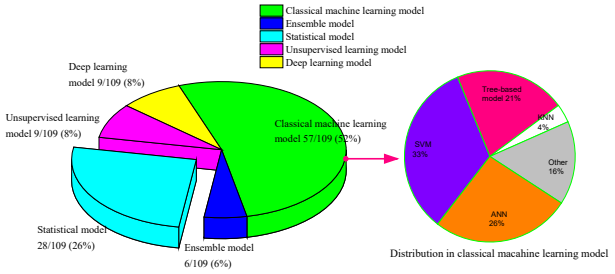

Figure 91: distribution of data-driven methods in predictive maintenance of railway track (Xie *et al*., 2020)

Some examples of statistical models are provided in Table 5 and of data driven models in Table 6. Examples of rail defects addressed by the models are provided in Table 7.

Table 5 Statistical models in predictive maintenance of railway track (Xie *et al*., 2020)

Statistical models	**Advantage**	**Disadvantage**	**Application**
Regression modeling (e.g., multivariable regression, multi-stage regression)	Simple; interpretability	Prior knowledge of the data is needed to select the best fitting model	Estimating the remaining useful life of railway track
Probability distribution model (e.g., Weibull, normal, lognormal and extreme value distributions)	Simple; interpretability	Based on specific hypotheses	Prediction of track failure time
Time series model (e.g., autoregressive (AR), autoregressive integrated moving average (ARIMA))	Interpretability	Time series is required to be stationary	Prediction of the short-term trend of track irregularity
Bayesian methods (e.g., Bayesian inference, Markov Chain Monte Carlo (MCMC))	Stable; better performance for small dataset size	Predictors are required to be independent; prior distribution assumption needed	Investigation of the rail squat failure probability using Bayesian inference
Stochastic process (e.g., Markov process, Gaussian process, Gamma process)	Better performance in process status prediction	Based on specific hypotheses; not suitable for mid to long-term system prediction	Evaluating the deterioration of track geometry based on Markov process

Table 6 Data driven models in predictive maintenance of railway track (Xie *et al*., 2020)

Classical machine learning model	**Advantage**	**Disadvantage**	**Application**
ANN	Robust; no expert knowledge is needed	Time-consuming; poor interpretability	Prediction of average track degradation rates
SVM	Efficiency in small data size; ability to deal with nonlinear characteristics	Poor interpretability, sensitive to kernel function	Fast classification and evaluation of rolling contact fatigue (RCF) defects in tracks
Tree-based model	Interpretation	Overfitting on noisy data	Prediction of tram track degradation index
K-nearest neigh-bours (KNN)	Simple; interpretation	Not easy to determine hyper-parameter k; sensitive to data distribution	Classification of tamping effectiveness

Table 7 Some recent applications (Xie *et al*, 2020)

Track Defects	**Equipment**	**Data-Driven Method**
Geometry irregularity	Track geometry recording car, operation records, maintenance records	Bayesian method
	Track geometry recording car	Ensemble of gamma process, logistic regression, and SVM
	Track geometry recording car	ANN
	Track geometry recording car	Random forest
	In-service vehicles on-board sensing device	SVM
Rail head defects	Camera	CNN
	Laser-ultrasonic technology	SVM
	Ultrasonic and rail surface photos	Bayesian inference method
	Sperry's eddy current walking stick	Clustering
Missing rail component	Camera	SVM
		Multiple signal classification
Rail break	In-service vehicles	Continuous wavelet transform

	Eddy current sensor	Bayesian network
Substructure failure: sleeper and ballast	Fiber bragg grating	Variational heteroscedastic Gaussian process
	Camera	Bayesian method

Predictive maintenance is an emerging field with many unresolved issues. Some of these are:

- Identification of the most accurate or most practical methods to assess maintenance requirements
- Reducing the rate of false positives and negatives
- Interpretation of black box methods
- Pre-processing costs of noisy input data and incorrect records
- Computational power and the time required to analyse big data sets

4.3.2 *Little data: Bayesian statistics and the observational method*

Predictive maintenance is an example of big data techniques being used in practice. However, much of the time geotechnical engineers need to make decisions based on limited information. The statistical and data driven techniques can also be used to derive best estimates and co-efficients of variance which can help understand levels of certainty and assist decision making. Bayesian statistics is one method that has particular application in the interpretation of monitoring data during construction. The Bayesian approach is essentially a mathematical version of the Observational Method.

Kelly and Huang (2015) explain that Bayes' formula can be written as follows:

$$P(\boldsymbol{\theta}|\boldsymbol{y}) \propto L(\boldsymbol{y}|\boldsymbol{\theta})P(\boldsymbol{\theta}) \quad (20)$$

where P(**θ**) is the prior probability distribution of the material parameters, L(**y**|**θ**) is the probability of measurements (**y**) conditional on the material parameters (**θ**) and P(**y**|**θ**) is the posterior distribution of the material parameters updated by measurements.

The prior distribution can be obtained by assumption, measurements or a combination of both. The prior distribution can be developed at the design stage of a project and provides a measure of uncertainty in the design predictions. The measurements can be written as:

$$y_i = g(\boldsymbol{\theta}) + \varepsilon \quad (21)$$

where ε is the "error" or difference between measurement and calculation g(**θ**). The calculation can be of any type ranging from analytical to three dimensional FEM.

If the measured error is assumed to be normally distributed, the likelihood function of measurement y_i can be written as

$$L(y_i|\boldsymbol{\theta}) = \phi\left(\frac{y_i - g(\boldsymbol{\theta}) - \mu_\varepsilon}{\sigma_\varepsilon}\right) \quad (22)$$

where μ_ε and σ_ε are the mean and standard deviation of measurement errors, ϕ is the probability density function of the standard normal distribution.

The posterior distribution is typically solved using a form of Markov Chain Monte Carlo and can be extremely computationally expensive. Often many thousands to millions of simulations need to be run to obtain accurate posterior parameters. The computational time is shorter if analytical calculations are adopted and (much) longer if complex FEM is used. Various algorithms are being explored to speed up the posterior computation along with parallel computing methods.

Examples where Bayesian methods have been used are tunnel convergence (Bjureland *et al*., 2017), braced excavations (Hsein Juang *et al*., 2013) and embankment settlement (Zheng *et al*., 2018).

Zheng *et al*. (2018) assessed predictions of future settlement performance for various amounts of monitoring data for a trial embankment constructed at Australia's soft soil field testing facility. They found that accurate predictions could be obtained after about 116 days of data despite consolidation settlement not being completed nearly 1000 days after construction. Such early accuracy allows decisions to be made regarding the performance of the embankment and whether risks need to be mitigated or opportunities can be taken advantage of, during the construction period with confidence.

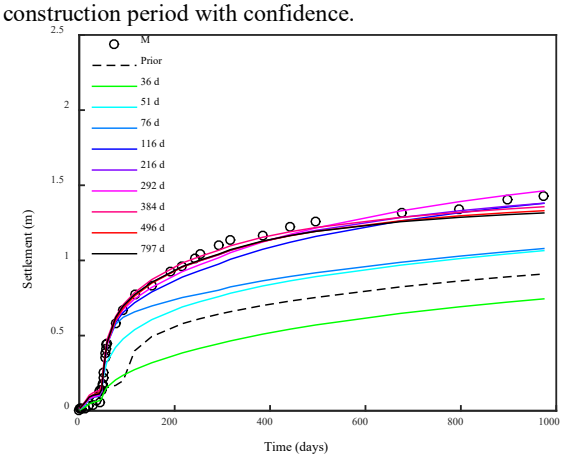

Figure 92: Long term settlement predictions at various times (Zheng *et al*., 2018)

Zheng *et al*. (2020) also used the method to back analyse, magnetic extensometer and vibrating wire piezometer data as shown in Figure 93 and Figure 94. The Bayesian method created a close match between calculation and measurement, albeit that some of the posterior material parameters lay outside ranges obtained by laboratory testing.

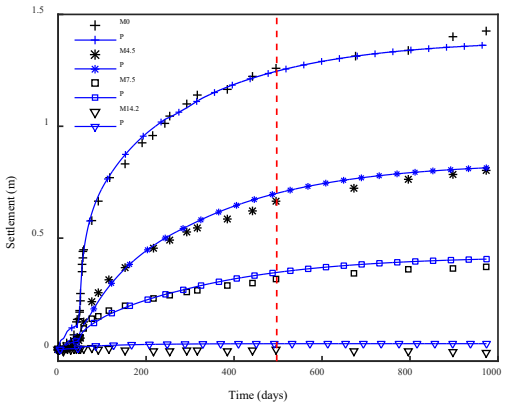

Figure 93: Back analysis of magnetic extensometer data (Zheng *et al*., 2018)

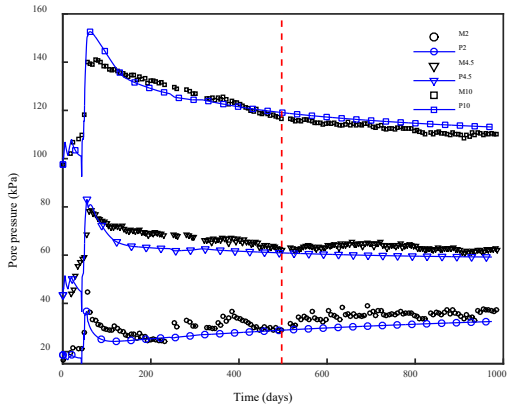

Figure 94: Back analysis of piezometer data (Zheng *et al*., 2018)

5 DISCUSSION

5.1 *Outcomes for practitioners and academics*

The USA Transportation Research Board is in the process of finalizing its critical issues report (https://www ttnews.com/articles/trb-finalize-critical-issues-report). The critical issues include:

- Transformational technologies and services
- Population trends
- Energy and sustainability
- Resilience and security
- Safety and public health
- Equity
- Governance
- System performance and asset management
- Funding and finance
- Goods movement
- Institutional and workforce capacity
- Research and innovation.

The state of practice (SOP) requires practitioners to help asset owners optimize a balance between cost, time, maintenance considerations, depleting natural construction materials, community requirements and increasingly environmental constraints for bigger, heavier, faster, longer and more automated vehicles.

Implementation of next-generation transportation technologies, such as smart sensors and energy harvesting, will mandate principles and guidelines for the design, maintenance, and rehabilitation of future physical assets such as sustainable infrastructure materials capable of directly communicating and interacting with vehicles and other types of urban infrastructure facilities. A well designed, constructed and connected transportation infrastructure is essential for smart systems, resiliency, economic competitiveness and environment-friendly operation.

Elements that practitioners and academics could adopt from this paper are summarized in the following sections.

5.2 *Reclamations for ports and airports*

When a port or offshore airport is constructed far-offshore, the depth of water will be deep. In such a case, a large amount of reclamation material will be required. For Kansai International Airport, the total geo-material volume was almost the same as the volume of two small mountains. It was pity to use such large amount of natural resources. From this introspection, the engineer involved in the project considered utilizing recycled materials such as dredged soil or broken concrete. Geomaterial solidification methods such as cement treated clay was one of the answers to the introspection.

To avoid large differential settlements, it was important to continuously supply reclamation soil to the reclamation area from the initial stage of construction.

5.3 *Airport pavements*

Increase airport pavement life by incorporating low utilization due to COVID into whole of life cycle plans.

Increase aircraft pavement life by instrumenting pavements and directing aircraft along low trafficked paths, taking into account dilation caused by aircraft wander.

Geogrids help reduce the thickness of granular layers and reduce settlement and dilation of granular layers. Construction of runways using more ductile materials with damping will offer less noise and vibrations.

Field scale comparisons of channelized and wandering traffic could provide opportunity to further develop prediction models for airport pavement prediction methods.

5.4 *Low speed rail*

Inclusion of rubber elements in the substructure can help reduce ballast degradation and transition performance and increase track longevity. They should be placed in track in such a way as to prevent interfering with maintenance equipment that needs to replenish ballast during maintenance cycles and occasionally damaged sleepers.

Ballast performance can be improved by reinforcement with random fibres or geogrids, physical confinement, increasing resistance to lateral movement by reducing sleeper spacing, widening the sleeper at the ends or using intermittent lateral restraints; or by reducing the shoulder slope below sleeper surface level, in cases where the ballast bed is raised and also by adjusting the ballast to a more well-graded distribution with greater internal friction.

In Australia and some other nations, especially along the coastal areas with high population, the possibility of constructing very long straight stretch of track will be limited. This makes it unfeasible to have very long heavy haul trains (2-3 km) operating at very high speeds on concrete slab tracks. Ballasted tracks will remain the most economical choice for heavy haul despite annual maintenance requirements. Optimum speeds should still be less than 100km/h for trains that are 2-3 km long.

For effects of track stiffness, experimental (field) validation and model parameterisation will be the key challenges for the next few years.

For effects of track stiffness, 1:1 scale physical modelling or field validation and model parameterisation will be the key challenges for the next few years. Research on new materials for construction including waste granular assemblies require more intense fundamental studies through appropriate numerical (DEM) micro-mechanical studies and greater efforts on field performance monitoring of new designs adopting recycled materials and mineral byproducts. Applied research on transition zones will require greater focus as more heavy haul networks in the future will be built over soft estuarine terrains, bridges and tunnels.

5.5 *High speed rail*

As the train speed increases the track support stiffness needed to avoid significant load and displacement magnification may also increase. In this regard, however, the use of normalised datasets can be misleading: at high speeds on a stiff trackbed, the basic static deflection being amplified is very much smaller than at a low speed on a soft trackbed, even if the ratio of train speed to critical velocity is the same.

With intensive trafficking at high speeds, ballasted track may reach its performance limit owing to issues of ballast flight and increased maintenance requirements. These effects are further magnified as the axle load increases. Thus slab track may be required more frequently in the future, particularly for higher speed, heavier trains. This will increase construction costs, hence the benefits of higher speeds will need to be clear. Most slab track forms do not have continuous bending stiffness across panels: this seems to be a potential advantage that is not currently being exploited, perhaps owing to a combination of a lack of understanding of how stiffer track systems really interact with the ground, and concerns over construction methods and quality.

Challenges remain relating to the accurate determination of effective soil stiffnesses, Rayleigh wave speeds and system critical velocities, which depend on a combination of the characteristics of potentially multiple and / or discontinuous soil strata, the track form and any earth structures (embankments or cuttings) that may be present.

The dominant frequency for pore pressure generation, and the ability to calculate realistic residual pore pressures during and after train passage, remain an ongoing debate and challenge.

The influence of wave propagation on the number of loading cycles after which the shakedown state is reached needs further research. The influence of Raleigh waves on the instability of undrained subgrade soils needs to be addressed in more detail using the multi-laminate constitutive model and needs to be integrated with Finite Element Modelling. This is required to investigate the influence of principal stress rotation due to moving trains on mud pumping behavior and stability of subgrade soils, where excess pore water pressures play an important role.

5.6 *Roads*

Advances in computing, robotics, artificial intelligence, and Internet of Things with 5G communication have enabled revolutionary technologies such as autonomous and connected vehicles to emerge, and these next-generation systems hold the promise to completely change the paradigm of transportation efficiency, sustainability, resilience, and safety. The principal opportunity from autonomous and connected systems, for example, arises from the ability to monitor both infrastructure and vehicle components of the system, and operate them in ways that maximize various societal benefits. The real-time information will be incorporated into advanced system control strategies to improve safety and mobility, and to reduce energy consumption and emissions. It also improves the resilience and reliability of the infrastructures through online monitoring and real-time management, while providing data for both on-line operations and off-line planning applications.

The use of marginal and waste materials for base and sub-base will be utilized increasingly as the availability of natural materials is becoming scarce and the capacity for expanding quarrying is becoming more challenging in the future. The use of intelligent compaction and sensor technologies will become more useful and reduce costs through optimal design and post-construction quality assurance. Roads will also benefit from the use of rubber intermixed aggregates and optimal use of geosynthetics for greater internal stability.

Future construction of roads will be advanced in terms of new materials including smart aggregates and the use of sensor technologies to monitor performance of new design. The use of synthetic inclusions including energy absorbing damping materials for increased longevity (including earthquake resistance) will become more popular as research in these areas starts to grow.

The Mechanistic Empirical Pavement Design Guide (MEPDG) by the American Association of State Highway and Transportation Officials (AASHTO) probably represents current best practice and has incorporated a design methodology for pavement systems that considers many or most elements of the state of the art. Complex coupled thermo-mechanical-hydro models as well as simplified methods will continue to be developed.

Resilient and plastic deformations are related to changes in environmental effects and water. These are complex areas that will continue to be explored over the next few years.

Quantification of the magnitudes of swell or settlement (including frost heave) and time rate of swell or settlement for engineering purposes is difficult. Further research and development of unsaturated soil models are likely to contribute to this area. Practical methods have been developed to partially manage volumetric changes in soil but new solutions are required as the volume changes are only partly predictable and controllable using low cost methods.

5.7 *Environmental management*

Two main principles of green construction involve using recycled materials and utilizing renewable resources to supply the energy needs. Current demand for recycled aggregate products like crushed concrete, glass and reclaimed asphalt aggregate, and secondary aggregates such as fly ash and slag, and mined materials like clay and shale is expected to continually grow into the future. Advances will be spurred by environmental and land use concerns favoring recycled and secondary aggregate materials, and by rising demand for specialty products such as expanded clay and shale, which are used in applications where light weight is of extreme importance. The use of lightweight aggregate will contribute significantly to sustainable development by conserving energy, lowering transportation requirements, maximizing structural efficiency and increasing service life, and, as a result, is expected promote the ability of future generations to meet their needs.

Sustainability and resilience will become increasingly important. Engineers need to optimize many competing criteria. Practice is leading academia with respect to creating infrastructure resilient to floods and drought. Potentially, critical infrastructure will attract resilience requirements in a similar fashion to areas subject to earthquakes to ensure they remain operational in the face of natural disasters. The insurance industry may also drive a higher degree of resilience in certain locations to enable risk cover to be provided at reasonable cost.

Reduce, reuse, recycle: many materials or aging infrastructure can be incorporated into new construction. In many cases the mechanical behavior of the materials is well understood and can be used with confidence. Carbon (and other waste) accounting may provide the economic impetus to accelerate the use of recycled materials and being able to quantify the cost benefit in a transparent and believable framework will be required.

Bio-grouting is an area that promise to contribute to sustainable and environmental-friendly solutions in soil improvement applications.

5.8 *Digital opportunities*

The rapid growing field of smart mobility has brought unprecedented challenges for people's demand of building smart, autonomous and multimodal transportation infrastructures. Some of emerging topics, such as connected and autonomous vehicles, smart sensors and connected road infrastructure, automatic road condition monitoring, and shared mobility are bringing both opportunities and challenges to practitioners.

Smart sensing technologies need to be developed to improve the rail industry's ability to answer critical safety and maintenance related questions related to the track infrastructure systems by monitoring and predicting track health.

Instrumentation and interpretation of big and little data sets is likely to become more prevalent in a digital world.

Understanding how the data analytics works will enable engineers to specify types and locations of instruments to maximise their utilization as well as optimizing design and construction.

Use of data to optimize construction and reduce costs is occurring now.

Predictive maintenance for rail and road pavements, driven by safety and operational needs, is likely to become prevalent. However, predictive maintenance is an emerging field with many unresolved issues. Some of these include identification of the most accurate or most practical methods to assess maintenance requirements, reducing the rate of false positives and negatives, interpretation of black box methods, pre-processing costs of noisy input data and incorrect records and computational power and the time required to analyse big data sets

A future development could be aircraft-to-pavement (A2P) connectivity. The pavement would instruct the pilot/aircraft to deliberately wander if required. This purposely-induced aircraft wander helps spread the traffic loading on the full width of the pavement. This has the potential to ultimately optimize the pavement use, extend the existing pavement life, or reduce the thicknesses of new pavements (while taking the negative impacts of wander, discussed above, into account). Development of pavement instrumentation is required for this vision to be realized.

New opportunities require broad research efforts in the technology, engineering, planning, regulatory, legal, and social spheres of next-generation transportation systems. Research is needed on (i) new technologies and innovations beyond the immediate scope of vehicle and transportation infrastructure systems; and (ii) partnership with technology companies focusing on innovative transportation ideas and coordination of machines, objects, people, and vehicles for multiple transportation modes. This will need to be accomplished through the development and implementation of embedded, wireless, "smart" infrastructure technologies capable of autonomously transmitting load-response data and "state-of-repair" exception reports. Wireless continuous monitoring for infrastructure sensing will improve safety and reliability of roads, bridges and shared mobility and establish big data for digital twin virtual models, which can in turn provide new methods for multi-scale/multi-physics modeling and simulation of transportation resiliency.

6 ACKNOWLEDGEMENTS

The authors acknowledge and thank the contribution of the following people to this paper:

- Prof. David Airey to intelligent compaction.
- Dr Alice Duley, Dr Ann Mamou, Dr John Harkness, Dr Louis Le Pen, Dr Anna Mamou, Dr David Milne, Tracey Najafpour-Navaei, Dr Joel Smethurst and Geoff Watson and Dr Trung Ngo for railways
- Prof Yoichi Watabe for ground improvement of Japanese airports.
- Prof Masaki Kitazume for ground improvement of the Tokyo Haneda airport.
- Prof Cholachat Rujikiatkamjorn for his valuable comments for roads and railway sections of the paper.

A significant number of figures have been reproduced with kind permission from various scholarly journals such as ASCE-JGGE, CGJ, Geotechnique etc.

7 REFERENCES

Abadi T.C. Le Pen L. Zervos A. and Powrie W. 2016. Improving the performance of railway tracks through ballast interventions. *Proc Inst Mech Eng, Part F: J Rail Rapid Transit*; 232(2), 337–355

Abadi T.C. Le Pen L. Zervos A. and Powrie W. 2019. Effect of sleeper interventions on railwaytrack performance. *ASCE J Geotech Geoenviron Eng*;145(4).

Abadi T.C. Madhusudhan Li. and Le Pen LM. 2021. Re-using "life expired" railway ballast: laboratory testing, shape analysis and petrographic evaluation. *Submitted to the ASCE Journal of Geotechnical and Geo-environmental Engineering*

Abedi M. Fangueiro R. Correia A.G. 2020. Ultra-sensitive affordable cementitious composite with high mechanical and microstructural performances by hybrid CNT/GNP, *Materials*, 13 (16), art. no. 3484, DOI: 10.3390/MA13163484

Ahmed S. Harkness J. Le Pen L. Powrie W. and Zervos A. 2016. Numerical modelling of railway ballast at the particle scale. *International Journal for Numerical and Analytical Methods in Geomechanics*, 40(5), 713-737. https://doi.org/10.1002/nag.2424

Allou F. Chazallon C. and Hornych P. 2007. A numerical model for flexible pavements rut depth evolution with time. *International Journal for Numerical and Analytical Methods in Geomechanics*, 31(1), 1-22.

Almeida J. Júlio S. Reis, M. and Carrondo M. 1995. Nitrite Inhibition of Denitrification by Pseudomonas fluorescens. *Biotechnol. Bioeng.*, 46(3), 194-201.

Alonso E.E. Gens A. and Josa A. 1990. Constitutive Model for Partially Saturated Soils. *Géotechnique*. 40. 10.1680/geot.1990.40.3.405.

Alonso E.E. Pinyol N.M. and Gens A. 2012. Compacted soil behaviour: initial state, structure and constitutive modelling, *Geotechnique symposium in print*, Gallipoli *ed*, 3-18

Alves Costa P. Colaco A. Calcada R. and Silva Cardoso A. 2015. Critical speed of railway tracks. Detailed and simplified approaches. *Transportation Geotechnics*, 2, 30-46

Aingaran S. Le Pen L. Zervos A. and Powrie W. 2018. Modelling the effects of trafficking and tamping on scaled railway ballast in triaxial tests. *Transportation Geotechnics* 15, 84-90. https://doi.org/10.1016/j.trgeo.2018.04.004

Ajayi O.O. Le Pen L. Zervos A. and Powrie W. 2017 A behavioural framework for fibre reinforced gravel. *Géotechnique* 67(1), 56-68, doi:10.1680/jgeot.16.P.023.

Al-Shamrani M.A. and Al-Mhaidib A.I. 1999. Prediction of potential vertical swell of expansive soils using a triaxial stress path cell. *Quarterly Journal of Engineering Geology & Hydrogeology*, 32(1). 45-54.

Anderegg R. Von Felten D.A. and Kaufmann K. 2006. Compaction monitoring using intelligent soil compactors. *GeoCongress 2006: Geotechnical Engineering in the Information Technology Age* (pp. 1-6).

Asadi M. Mallick R. and Nazarian S. 2021, Numerical modeling of post-flood water flow in pavement structures, *Transportation Geotechnics*, 27, 100468, ISSN 2214-3912, https://doi.org/10.1016/j.trgeo.2020.100468.

Aubeny C. and Long X. 2007. Moisture diffusion in shallow clay masses, *Journal of Geotechnical and Geoenvironmental Engineering*, 133(10), 1241-1248.

Australian Government Department of Infrastructure and Regional Development. 2016. Trends Transport and Australia's Development to 2040 and beyond

Balay L. Gomes Correia A. Jouve P. Hornych P. and Paute J.L. 1997. Mechanical behaviour of soils and unbound granular materials, modelling flexible pavement – Recent advances. *Proc. 8th ICAP*, Seattle, Washington, USA, 1, 823-842

Barnett I.C. and Kingsland R.I. 1999. Assignment of AS2870 Soil Suction Profile Parameters to TMI Derived Climatic Zones for NSW. *Proceedings, 8th Australia – New Zealand Conference on Geomechanics (Hobart), Expansive Soils*. 1: 149-155.

Basu D. and Puppala A.J. 2015. Principles of sustainability and their application in geotechnical engineering, *Proc. 15th PanAmerican conference in geotechnical engineering*, Buenos Aires, Argentina, 162-183

Basma A.A. Al-Homoud A.S. and Malkawi A.I. 2000. Swelling-shrinkage behaviour of natural expansive clays. *Appl. Clay Sci.*, 11: 211-227.

Basma A.A. Al-Suleiman T.I. 1991. Climatic Consideration in New AASHTO Flexible Pavement Design. *Journal of Transportation Engineering*. 117(2), 210 - 223

BBC World Service. 2013. How much bigger can container ships get? https://www.bbc.com/news/magazine-21432226

Bian X. Jiang H. Cheng C. Chen Y. Chen R. and Jiang, J. 2014. Full-scale model testing on a ballastless high-speed railway under simulated train moving loads. *Soil Dynamics and Earthquake Engineering*, 66, 368-384.

Bian X. Hu J. Thompson D. and Powrie W. 2019. Pore pressure generation in a poro-elastic soil under moving train loads. *Soil Dynamics and Earthquake Engineering*, 125, 105711.

Bian X. Li W. Qian Y. and Tutumluer E. 2020. Analysing the effect of principal stress rotation on railway track settlement by discrete element method. *Géotechnique*, 70, 803-821.

Bjureland W. Spross J. Johansson F. Prästings A and Larsson S. 2017. Reliability aspects of rock tunnel design with the observational method. *International Journal of Rock Mechanics and Mining Sciences*. 98. 102-110. 10.1016/j.ijrmms.2017.07.004.

Blackmore L. Clayton C.R. Powrie W. Priest J.A. and Otter L. 2020. Saturation and its effect on the resilient modulus of a pavement formation material. *Géotechnique*, 70(4), 292-302.

BRE (1998). Low rise buildings on fill. Part 3, *Digest 427*.

Briaud J.L. and Seo J., 2003. Intelligent compaction: overview and research needs. *Report to the Federal Highway Administration*.

Briaud J. Zhang X. and Moon S. 2003. Shrink Test–Water Content Method for Shrink & Swell Predictions. *Journal of Geotechnical & Geoenvironmental Engineering*, ASCE, 129(7), 590–600.

Briggs K.M. Smethurst J.A. Powrie W. O'Brien A.S. and Butcher, D. 2013a. Managing the extent of tree removal from railway earthwork slopes. *Ecological Engineering* 61(Part C), 690-696. https://doi.org/10.1016/j.ecoleng.2012.12.076

Briggs K.M. Smethurst J.A. Powrie W. and O'Brien A.S. 2013b. Wet winter pore pressures in railway embankments. *Proceedings of the Institution of Civil Engineers - Geotechnical Engineering*, 166(GE5), 451-465. https://doi.org/10.1680/geng.11.00106

Briggs K. Smethurst J.A. Powrie W. and O'Brien A.S. 2016. The influence of tree root water uptake on the long term hydrology of a clay fill railway embankment. *Transportation Geotechnics*, 9, 31-48. https://doi.org/10.1016/j.trgeo.2016.06.001

Brown S.F. 1996. Soil mechanics in pavement engineering. *Géotechnique*, 46(3), 383–426.

Brownell D.H. Garg S.K. and Pritchett, J.W. 1977. Governing equations for geothermal reservoirs. *Water Resources Research*, 13(6), 929-934.

Bull D. Smethurst J. Sinclair I. Pierron F. Roose T. Powrie W. and Bengough A.G. 2020. Mechanisms of root-reinforcement in soils: an experimental methodology using four-dimensional X-ray computed tomography and digital volume correlation. *Proceedings of the Royal Society A: Mathematical, Physical and Engineering Sciences*, 476(2237), 1-23. [20190838]. https://doi.org/10.1098/rspa.2019.0838

Burbank M. Weaver T. Green T. Williams B. and Crawford R. (2011). Precipitation of Calcite by Indigenous Microorganisms to Strengthen Liquefiable Soils. *Geomicrobiology Journal*, 28(4), 301-312.

Burland J.B. and Jennings J.E.B. 1962. Limitations to the Use of Effective Stresses in Partly Saturated Soils, *Geotechnique* 12(2): 125-144. DOI: 10.1680/geot.1962.12.2.125

Burmister D.M. 1943. The Theory of Stresses and Displacements in Layered Systems and Applications to the Design of Airport Runways. *HRB Proc*, 23(126)

Cai Y. Xie Z. Wang J. Wang P. and Geng X. 2015. A new approach of vacuum preloading with booster PVDs to improve deep marine clay strata. *Can. Geotech. J.* 55, 1359–1371.

Cai Y. Wu T. Guo L. and Wang J. 2018. Stiffness degradation and plastic strain accumulation of clay under cyclic load with principal stress rotation and deviatoric stress variation. *Journal of Geotechnical and Geoenvironmental Engineering*, 144, 04018021.

Caicedo B. 2019. Geotechnics of roads: fundamentals, *Taylor and Francis Group*, London

Cameron D. 2001. The extent of soil desiccation near trees in a semi-arid environment. *Geotechnical & Geological Engineering*, 19(3), 357-370

Cardoso R. Maranha Des Neves E. and Alonso E.E. 2012. Experimental behaviour of compacted marls, *Geotechnique*, 62(11), 999-1012.

Cary C. and Zapata C.E. 2011. Resilient Modulus for Unsaturated Unbound Materials. *Int. J. of Roads Materials and Pavement Design*. 12(3), 617-640.

Cary C. and Zapata C.E. 2016. Pore Water Pressure Response of Soil Subjected to Dynamic Loading under Saturated and Unsaturated Conditions, *International Journal of Geomechanics*, 16(6), doi:10.1061/(ASCE)GM.1943-5622.0000642

Chan I. and Mostyn G. 2008. Climate Factors for AS2870 for the metropolitan Sydney area, *Australian Geomechanics*, 43(1), 17-28

Chazallon C. Hornych P and Mouhoubi S. 2006. Elastoplastic model for the long term behaviour modelling of unbound granular materials in flexible pavements. *Int J. of Geomechanics*. 6(4), 279-289

Chen C. Indraratna B. McDowell G. and Rujikiatkamjorn C. 2015. Discrete element modelling of lateral displacement of a granular assembly under cyclic loading. *Computers and Geotechnics*, 69: 474-484

Chen F.H. 1975. Foundations on Expansive Soils. *Elsevier Scientific Pub. Co*., Amsterdam, New York, NY.

Cheng L. Cord-Ruwisch R. and Shahin M. 2013. Cementation of sand soil by microbially induced calcite precipitation at various degrees of saturation. *Canadian Geotechnical Journal*, 50(1), 81-90

Collins R.J. and Ciesielski S.K. 1994. Recycling and use of waste materials and by-products in highway construction. *Synthesis of Highway Practice 199. National Cooperative Research Program (NCHRP)*, Transportation Research Board, Washington, DC, USA.

Connolly D. Giannopoulos A. and Forde M. 2013. Numerical modelling of ground borne vibrations from high speed rail lines on embankments. *Soil Dynamics and Earthquake Engineering*, 46, 13-19.

Connolly D.P. Alves Costa P. Kouroussis G. Galvin P. Woodwards P.K. and Laghrouche O. 2015. Large scale international testing of railway ground vibrations across Europe. *Soil Dynamics and Earthquake Engineering*, 71, 1-12

Coronado O. Caicedo B. Taibi S. Correia A.G. and Fleureau J.M. 2011. A macro geomechanical approach to rank non-standard unbound granular materials for pavements, *Engineering Geology*, 119(1-2), 64-73.

Correia A.G. and Cunha J. 2014. Analysis of nonlinear soil modelling in the subgrade and rail track responses under HST. *Transportation Geotechnics* 1, 147-156.

Costa P.A. Calçada R. and Cardoso A.S. 2012a. Ballast mats for the reduction of railway traffic vibrations. Numerical study. *Soil Dynamics and Earthquake Engineering*, 42(0), 137-150.

Costa P.A. Calçada R. and Cardoso A.S. 2012b. Track–ground vibrations induced by railway traffic: In-situ measurements and validation of a 2.5D FEM-BEM model. *Soil Dynamics and Earthquake Engineering*, 32, 111-128.

Costa P.A. Colaço A. Calçada R. and Cardoso A.S. 2015. Critical speed of railway tracks. Detailed and simplified approaches. *Transportation Geotechnics*, 2, 30-46

Coussy O. 2005. Poromechanics of freezing materials. *J. Mech. Phys. Solids*, 53, 1689–1718. doi:10.1016/j.jmps.2005.04.001

Coussy O. and Monteiro P. 2007. Unsaturated poroelasticity for crystallization in pores. *Comput. Geotech*. 34, 279–290. doi:10.1016/j. compgeo.2007.02.007

Dareeju B. Gallage C. Ishikawa T. and Dhanasekar M. 2017. Effects of principal stress axis rotation on cyclic deformation characteristics of rail track subgrade materials. *Soils and Foundations*, 57, 423-438.

De Bruijin C.M.A. 1961. Swelling characteristics of a transported soil profile at Leeuh of Vereeniging (Transvaal). *Proc. 5th Int. Conf. Soil Mech. Found*. Eng. 1, 43-49.

De Bruijin C.M.A. 1965. Some observations on soil moisture conditions beneath & adjacent to tarred roads & other surface treatments in South Africa. *Moisture Equilibrium & Moisture Changes Beneath Covered Areas*. Butterworths, Australia. 135-142.

DeJong J. Mortensen B. Martinez B. and Nelson D. 2010. Bio-mediated Soil Improvement. *Ecological Engineering*, 36(2), 197-210.

Dhowian A.W. 1990. Field performance of expansive shale formation, *Journal of King Abdulaziz University (Engineering Sciences)*, 2: 165-82.

Dong K. Connolly D.P. Laghrouche O. Woodward P.K. and Costa, P.A. 2018. The stiffening of soft soils on railway lines. *Transportation Geotechnics*, 17, 178-191.

Dong K. Connolly D. Laghrouche O. Woodward P. and Costa P.A. 2019. Non-linear soil behaviour on high speed rail lines. *Computers and Geotechnics*, 112, 302-318.

Dong S.Y. and Yu X. 2018. Microstructure-based random finite element method simulation of frost heave: theory and implementation, *Transportation Research Record*, 2672(52), 347-357

Donovan P. Sarker P. and Tutumluer E. 2016. Rutting prediction in airport pavement granular base/subbase: A stress history based approach, *Transportation Geotechnics*, 9, 139-160

Doré G. Konrad J.M. and Roy M. 1997. Role of deicing salt in pavement deterioration by frost action. *Transportation Research Record: Journal of the Transportation Research Board*, 1596, 70-75.

Doré G. Konrad J.M. and Roy M. 1999. Deterioration model for pavements in frost conditions. *Transportation Research Record: Journal of the Transportation Research Board*, 1999 (1655), 110-117.

Doré G. 2002. Cold region pavement. *Journal of Glaciology and Geocryology*, 2002, 24(5), 593-600.

Duley A. 2018. Soil parameters for modelling critical velocity effects of railways. *PhD dissertation, University of Southampton*, UK

Duong T.V. Cui Y.-J. Tang A.M. Dupla, J.-C. Canou, J. Calon N. and Robinet A. 2014. Investigating the mud pumping and interlayer creation phenomena in railway sub-structure. *Engineering Geology*, 171, 45-58.

Duquennoi C. Fremond M. and Levy M. 1989. Modelling of thermal soil behavior. *In H. Rathmayer (ed.) Frost in geotechnical engineering, Int. Symp., Saariselk, Finland. 13–15 Mar. 1989.* VTT Symp. 94. Valtion Teknillinen Tutkimuskeskus, Espoo, Finland, 895–915.

Duriez J. and Galusinski C. 2021. A Level Set-Discrete Element Method in YADE for numerical, micro-scale, geomechanics with refined grain shapes. *Computers & Geosciences* 157, 104936.

El Kacimi A. Woodward P.K. Laghrouche O. and Medero G. 2013. Time domain 3D finite element modelling of train-induced vibration at high speed. *Computers & Structures*, 118, 66-73.

Elshaer M. and Daniel JS. 2018. Impact of pavement layer properties on the structural performance of inundated flexible pavements, *Transportation Geotechnics*, 16, 11-20, ISSN 2214-3912, https://doi.org/10.1016/j.trgeo.2018.06.002.

Erol A.O. Dhowian A. and Youssef A. 1987. Assessment of oedometer methods for heave prediction. *Proceedings of 6th International Conference on Expansive Soils, Technical Session III*. 99-105.

Esmaeili M. Aela P. and Hosseini A. 2017. Experimental assessment of cyclic behavior of sand-fouled ballast mixed with tire derived aggregates. *Soil Dynamics and Earthquake Engineering*, 98: 1-11.

Esveld C. 2001. Modern railway track, *MRT Press, The Netherlands*.

Fabre C. 2021. Effect of COVID-19 pandemic on air travel, pavement life and future outlook, *ASCE T&DI Airfield Pavement Committee (APC) Lecture Series*

Fedakar H.I. Cetin B. and Rutherford C.J. 2021. Deformation characteristics of medium-dense sand-clay mixtures under a principal stress rotation. *Transportation Geotechnics*, 30: 100616.

Feldman F. and Nissen D. 2002. Alternative testing method for the measurement of ballast fouling. *Conference on Railway Engineering*, Wollongong, RTSA.

Fityus S.G. Walsh P.F. and Kleeman P.W. 1998. The influence of climate as expressed by the Thornthwaite index on the design of depth of moisture change of clay soils in the Hunter Valley. *Conference on Geotechnical Engineering & Engineering Geology in the Hunter Valley.* Springwood, Australia, 251-265

Fityus S. Smith D.W. and Allman M.A. 2004. Expansive Soil Test Site Near Newcastle. *Journal of Geotechnical and Geoenvironmental Engineering, ASCE*, 130(7), 686-695.

Fredlund D.G. Hasan J.U. and Filson H. 1980. The prediction of total heave. *Proceedings 4th International Conference on Expansive Soils.* Denver, Colorado. 1-11

Fredlund D.G. Rahardjo H. and Fredlund M.D. 2012. Unsaturated Soil Mechanics in Engineering Practice. *John Wiley & Sons, Inc*. New Jersey.

Fremond M. and Mikkola M. 1991. Thermomechanical modeling of freezing soil. *In X. Yu and C. Wang (ed.) Ground freezing '91: Proc. Int. Symposium on Ground Freezing*, 6th, Beijing. 10–12 Sept. 1991. A.A. Balkema, Rotterdam, the Netherlands, 17–24.

Furudoi T. 2010. The second phase construction of Kansai International Airport considering the large and long-term settlement of the clay deposits, *Soils and Foundations*, 50 (6), 805–816

Gholikhani M. Nasouri R. Tahami S.A. Legette S. Dessouky S. and Montoya A. 2019. Harvesting kinetic energy from roadway pavement through an electromagnetic speed bump, *Applied Energy*, 250, 503-511, DOI: 10.1016/j.apenergy.2019.05.060

Gibbs H.J. 1973. Use of a consolidometer for measuring expansion potential of soils. *Proc. Workshop Expansive Clays & Shales in Highway Design & Construction*. Univ. Wyoming, Laramie, May, 1, 206-213.

Gomes Correia A. 1996a. Prediction of subgrade moisture conditions for purpose of pavement design. *Flexible Pavement* (A. Gomes Correia, ed.). A.A. Balkema, Rotterdam, 99.104

Gomes Correia A. (ed) 1996b. *Flexible pavements*. A.A. Balkema, Rotterdam

Gomes Correia A. (ed) 1999. Unbound Granular Materials. Laboratory testing, in-situ testing and modelling. *A.A. Balkema,* Rotterdam, Brookfield

Gomes Correia A. 2001. Soil mechanics in routine and advanced pavement and rail track rational design. *Geotechnics for roads, rail tracks and earth structures* (A. Gomes Correia and H. Brandl, eds.), Balkema, 165-187

Gomes Correia A. and Lacasse S. 2006. Marine and Transportation Geotechnical Engineering. General report – session 2e. *Proc. XVI ECSMGE*, Millpress, Rotterdam, The Netherlands, 5, 3045-3069.

Gomes Correia A. and Ramos A. 2021. A geomechanics classification for the rating of railroad subgrade performance. *Rail. Eng. Science*. https://doi.org/10.1007/s40534-021-00260-z

Gomez M. Anderson C. DeJong J. T. Nelson D. and Lau X. 2014. Stimulating In situ Soil Bacteria for Bio-Cementation of Sands. *Geo-Congress 2014 Technical Papers: Geo-characterization and Modeling for Sustainability*, ASCE, 1674-1682.

Gräbe P.J. and Clayton C.R. 2009. Effects of principal stress rotation on permanent deformation in rail track foundations. *Journal of Geotechnical and Geoenvironmental Engineering*, 135(4), 555-565.

Gräbe P.J. and Clayton C.R.I. 2014. Effects of principal stress rotation on resilient behavior in rail track foundations. *Journal of Geotechnical and Geoenvironmental Engineering*, 140(2), 1–10.

Grossoni I. Powrie W. Zervos A. Bezin Y. and Le Pen L. 2020. Modelling railway ballasted track settlement in vehicle-track interaction analysis. *Transportation Geotechnics*, 26, [100433]. https://doi.org/10.1016/j.trgeo.2020.100433

Gu C. Wang Y. Cai Y. and Wang J. 2019. Deformation characteristics of saturated clay in three-dimensional cyclic stress state. *Canadian Geotechnical Journal*, 56, 1789-1802.

Guo L. Chen J. Wang J. Cai Y. and Deng P. 2016. Influences of stress magnitude and loading frequency on cyclic behavior of K_0-consolidated marine clay involving principal stress rotation. *Soil Dynamics and Earthquake Engineering*, 84, 94-107.

Guo L. Cai Y. Jardine R.J. Yang Z. and Wang, J. 2018. Undrained behaviour of intact soft clay under cyclic paths that match vehicle loading conditions. *Canadian Geotechnical Journal*, 55(1), 90-106.

Guo Y. Markine V. and Jing G. 2021. Review of ballast track tamping: Mechanism, challenges and solutions. *Construction and Building Materials*, 300, 123940

Gupta A. Madhusudhan Zervos A. Powrie W. Harkness J. and Le Pen L.M. 2021. Grain characterisation of fresh and used railway ballast. *Submitted to Granular Matter*.

Guymon G.L. Berg R.L. and Johnston T.C. 1986. Mathematical Model of Frost Heave and Thaw Settlement in Pavements, *Report: U.S. Army Cold Regions Research and Engineering Laboratory*

Hamdan N. 2013. Carbonate Mineral Precipitation for Soil Improvement through Microbial Denitrification. *Master's Thesis, Arizona State University.*

Hamdan N. Kavazanjian E. and O'Donnell S. 2013. Carbonate Cementation via Plant Derived Urease. *18th Int. Conf. on Soil Mechanics and Geotechnical Eng*., Paris, France.

Hamdan N. 2015. Applications of Enzyme Induced Carbonate Precipitation (EICP) for Soil Improvement. *Doctoral Dissertation, Arizona State University.*

Hansson K. Šimůnek J. Mizoguchi M. Lundin L.C. and van Genuchten M.Th. 2004. Water flow and heat transport in frozen soil: *Numerical solution and freeze–thaw applications. Vadose Zone J*. 3, 693–704.

Harkness J. 2009. Potential particles for the modelling of interlocking media in three dimensions. *International Journal for Numerical Methods in Engineering*, 80(12), 1573–1594

Harkness J. Zervos A. Le Pen L. Aingaran S. and Powrie W. 2016. Discrete element simulation of railway ballast: modelling cell pressure effects in triaxial tests. *Granular Matter* 18(3), 65.

Harkness J. and Zervos A. 2019. Some effects of particle shape on the mechanical behaviour of granular materials. *DEM8*, Enschede, Netherlands.

Harlan R.L. 1973. Analysis of coupled heat–fluid transport in partially frozen soil. *Water Resour. Res*. 9, 1314–1323. doi:10.1029/WR009i005p01314

Hasnayn M.M. McCarter W.J. Woodward P.K. and Connolly D.P. 2021 Railway subgrade performance after repeated flooding – Large-scale laboratory testing, *Transportation Geotechnics*, 23, 100329, ISSN 2214-3912, https://doi.org/10.1016/j.trgeo.2020.100329.

Hayward T. Lees A. Powrie W. Richards D.J. and Smethurst J A. 2000. Centrifuge modelling of a cutting slope stabilised by discrete piles. *TRL Report 471*. Crowthorne, Berkshire: Transport Research Laboratory. 1–31.

He J. Chu J. and Ivanov V. 2013. Mitigation of liquefaction of saturated sand using biogas. *Geotechnique*, 63(4), 267.

Hendry M. Hughes D.A. and Barbour L. 2010. Track displacement and energy loss in a railway embankment. *Proceedings of the Institution of Civil Engineers-Geotechnical Engineering*, 163, 3-12.

Hopkins T.C. and Beckham T.L. 1998. Embankment construction using Shale. *Publication of Kentucky Transportation Centre*

Houston S. and Houston W. 2017. A suction-oedometer method for computation of heave & remaining heave. *Proc. of the 2nd PanAm Conf. on Unsaturated Soils*, Dallas, TX, 1, ASCE.

Houston S. and Zhang X. 2021. Review of Expansive and Collapsible Soil Volume Change Models within a Unified Elastoplastic Framework. *Soils and Rocks*, 44(3). DOI: 10.28927/SR.2021.064321.

Hromadka T.V. and Yen C. 1986. A diffusion hydrodynamic model (DHM). *Adv. Water Resour*. 9, 118–170. doi:10.1016/0309-1708(86)90031-X

Hryciw RD. Athanasopoulos-Zekkos A. and Yesiller N. (eds) 2012 *Geocongress 2012 State Of the Art and Practice In Geotechnical Engineering*. ASCE, Reston, VA, USA

HSBC 2019 Global Infrastructure Trends, Surbana Jurong SMEC internal presentation

Hsein Juang C. Luo Z. Atamturktur S. and Huang H. 2013. Bayesian Updating of Soil Parameters for Braced Excavations Using Field Observations, *ASCE J. Geotech. Geoenviron. Eng.*, 139:395-406.

Huang H. and Tutumluer E. 2011. Discrete Element Modeling for fouled railroad ballast. *Construction and Building Materials*, 25, 3306-3312.

Indraratna B. Nimbalkar S. Christie D. Rujikiatkamjorn C. and Vinod J. 2010. Field assessment of the performance of a ballasted rail track with and without geosynthetics. *Journal of Geotechnical and Geoenvironmental Engineering*, 136, 907-917.

Indraratna B. Rujikiatkamjorn C. Ameratunga J. and Boyle P. 2011a Performance and Prediction of Vacuum Combined Surcharge Consolidation at Port of Brisbane. *J. of Geotechnical & Geoenvironmental Engineering*, ASCE, 137 (11), 1009-1018.

Indraratna B. Ngo N.T. and Rujikiatkamjorn C. 2011b. Behavior of geogrid-reinforced ballast under various levels of fouling. *Geotextiles and Geomembranes*, 29(3), 313-322.

Indraratna B. Ngo N.T. and Rujikiatkamjorn C. 2013a. Deformation of coal fouled ballast stabilized with geogrid under cyclic load. *Journal of Geotechnical and Geoenvironmental Engineering*, 139(8), 1275-1289.

Indraratna, B., Balasubramaniam, A. S., Poulos, H. G., Rujikiatkamjorn, C. and Ameratunga, J. 2013b. Performance and prediction of marine clay treated with vacuum and surcharge consolidation at Port of Brisbane, *Australian Geomechanics*, 48(4), 161-180.

Indraratna B. Ngo NT. Rujikiatkamjorn C. and Vinod JS. 2014a. Behavior of Fresh and Fouled Railway Ballast Subjected to Direct Shear Testing: Discrete Element Simulation. *International Journal of Geomechanics*, 14(1), 34-44

Indraratna B. Nimbalkar S. and Neville T. 2014b. Performance assessment of reinforced ballasted rail track. *Proceedings of the Institution of Civil Engineers - Ground Improvement*, 167(1), 24-34.

Indraratna B. Nimbalkar S. and Rujikiatkamjorn C. 2014c. From theory to practice in track geomechanics–Australian perspective for synthetic inclusions. *Transportation Geotechnics* 1(4), 171-187.

Indraratna B. Qi Y. and Heitor A. 2017a. Evaluating the properties of mixtures of steel furnace slag, coal wash, and rubber crumbs used as subballast. *Journal of Materials in Civil Engineering*, 30(1): 04017251.

Indraratna B. Sun Q. and Grant J. 2017b. Behaviour of subballast reinforced with used tyre and potential application in rail tracks. *Transportation Geotechnics*, 12: 26-36.

Indraratna B. Sun Q. Heitor A. and Grant J. 2017c. Performance of rubber tire-confined capping layer under cyclic loading for railroad conditions. *Journal of Materials in Civil Engineering*, 30(3): 06017021.

Indraratna B. and Ngo N.T. 2018. Ballast Railroad Design: Smart-Uow Approach: CRC Press.

Indraratna B. Israr J. and Li M. 2018. Inception of geohydraulic failures in granular soils-an experimental and theoretical treatment. *Geotechnique*, 68(30), 233-248

Indraratna B. Sajjad MB. Ngo T. Correia AG and Kelly R. 2019a. Improved Performance of Ballasted Tracks at Transition Zones: A Review of Experimental and Modelling Approaches. *Transportation Geotechnics*, 2019. 21: p. 100260.

Indraratna B. Ngo T.N. and Rujikiatkamjorn C. 2019b. Performance of Ballast Influenced by Deformation and Degradation: Laboratory Testing and Numerical Modeling. *International Journal of Geomechanics*, 20(1), 04019138.

Indraratna B. Qi Y. Ngo N. T. Rujikiatkamjorn C. Neville T. Ferreira F. B. and Shahkolahi A. 2019c. Use of Geogrids and Recycled Rubber in Railroad Infrastructure for Enhanced Performance. *Geosciences* 9(1): 30.

Indraratna B. Rujikiatkamjorn C. Tawk M. and Heitor A. 2019d. Compaction, degradation and deformation characteristics of an energy absorbing matrix. *Transportation Geotechnics*, 19: 74-83.

Indraratna B. Singh M. Nguyen T. Ngo N.T. Leroueil S. Abeywickrama A. Kelly R. and Neville T. 2020a. A laboratory study on fluidization of subgrade under cyclic train loading. *Canadian Geotechnical Journal,* Online First 1-46

Indraratna B. Korkitsuntornsan W. and Nguyen T. 2020b. Influence of kaolin content on the cyclic loading response of railway subgrade. *Transportation Geotechnics*: 100319. doi: https://doi.org/10.1016/j.trgeo.2020.100319.

Institution of Civil Engineers UK 2019 What should be in the National Infrastructure Strategy? https://www.ice.org.uk/ getattachment /news-and- insight/policy/what-should-national-infrastructure-strategy/What-should-be-in-the-National-Infrastructure-Strategy-ICE-July-2019.pdf.aspx

IPCC (Intergovernmental Panel on Climate Change) (2007) Climate Change 2007: Synthesis Report. *Contribution of Working Groups I, II and III to the Fourth Assessment Report of the Intergovernmental Panel on Climate Change* (Pachauri RK and Reisinger A (eds)). IPCC, Geneva, Switzerland

Israr J. and Indraratna B. 2019. Study of Critical Hydraulic Gradients for Seepage-Induced Failures in Granular Soils. *J. Geotech. Geoenviron. Eng.*, 145 (7): 04019025.

Ito T. and Matsui T. (1975). Methods to estimate lateral force acting on stabilizing piles. *Soils and Foundations*, 15(4), 43–59.

Jaksa M.B. Kaggwa W.S. Woodburn J.A. and Sinclair R. 2002g. Influence of large gum trees on the soil suction profile in expansive soils. *Australian Geomechanics*, 37(1), 23-33

Jame Y.W. and Norum D.I. 1980. Heat and mass transfer in a freezing unsaturated porous medium. *Water Resources Research*, 16(4), 811-819.

Janoo V.C. and Berg R.L. 1990. Thaw weakening of pavement structures in seasonal frost areas. *Transportation Research Record: Journal of the Transportation Research Board*, 1286, 217-233.

Jayatilaka R. Gay D. Lytton R. and Wray W. 1992. Effectiveness of controlling pavement roughness due to expansive clays with vertical moisture barriers. *Research Study No. 2/11-8-88-1165. Texas Depart of Transportation*, Texas Transportation Institute, & Texas Tech University, 230

Jefferies M. Shuttle D. and Been K. 2015. Principal stress rotation as cause of cyclic mobility. *Geotechnical Research*, 2, 66-96.

Jennings J.E.B and Knight K. 1957. The prediction of total heave from double oedometer test, *In Proceedings of Symposium on Expansive Clays*. South African Institution of Civil Engineers, Johannesburg, 13-19.

Jennings J.E.B. Firtu R.A. Ralph T.K. and Nagar N. 1973. An improved method for predicting heave using the oedometer test. *Proc. 3rd Int. Conf. Expansive Soils*, Haifa, Israel, 2, 149-154.

Jia W. Markine V. Guo Y. and Jing G. 2019. Experimental and numerical investigations on the shear behaviour of recycled railway ballast. *Construction and Building Materials*, 217, 310-320

Jing P. Nowamooz H. and Chazallon C. 2018. Permanent deformation behaviour of a granular material used in low-traffic pavements, *Road Materials and Pavement Design*, 19(2), 289-314.

Johnson L.D. and Snethen D.R. 1978. Prediction of potential heave of swelling soils. *Geotechnical Testing Journal*, 1(3), 117-124.

Jones C.W. 1954. The permeability and settlement of laboratory specimens of sand and sand-gravel mixtures. *ASTM: Special Technical Publication,* 163, 68-78.

Kang M. Qamhia IIA. Tutumluer E. Garg N. and Villafane W. 2022. Airport Pavement Stiffness Monitoring and Assessment of Mechanical Stabilization using Bender Element Field Sensor, *submitted Transport Research Record*

Kang YS. Yang SC. Lee H.S. Kim Y.B. Jang S.Y. and Kim E. 2008. A study of track and train dynamic behavior of transition zone between concrete slab track and ballasted track, *in SPARK. 2008, Korea Railroad Research Institute*, Uiwang, South Korea. p. 1-7.

Karatas I. Kavazanjian E. and Rittmann B. (2008). Microbially induced precipitation of calcite using Pseudomonas denitrificants. *Proc., 1st International Conference on Bio-Geo-Civil Engineering*, 58-66.

Karunarathne A. Rajeev P. Chan D. and Kodikara J. 2012. Ground-atmosphere Interaction Modelling for Long-Term Prediction of Soil Moisture and Temperature. *Canadian Geotechnical Journal*. 49(9), DOI: 10.1139/T2012-068

Kausel E. Estaire J. and Crespo-Chacón I. 2020. Proof of critical speed of high-speed rail underlain by stratified media. *Proc. R. Soc. A* 476: 20200083. http://dx.doi.org/10.1098/rspa.2020.0083

Kavazanjian E. and Hamdan N. 2015. Enzyme Induced Carbonate Precipitation (EICP) Columns for Ground Improvement. *IFCEE*, ASCE, San Antonio, TX.

Kavazanjian E. O'Donnell S. T. and Hamdan N. 2015. Biogeotechnical mitigation of earthquake-induced soil liquefaction by denitrification: a two-stage process. *In Proceedings of 6th International Conference on Earthquake Geotechnical Engineering*, Christchurch, New Zealand, 20-28

Kelly R. and Huang J. 2015. Bayesian updating for one-dimensional consolidation measurements, *Canadian Geotechnical Journal*, 52: 1318–1330 (2015) dx.doi.org/10.1139/cgj-2014-0338

Khodadadi Tirkolaei H. Kavazanjian E. van Paassen L. and DeJong, J. 2017. Bio-grout materials: A review. *Grouting*, 1-12.

Kianfar K. Indraratna B. and Leroueil S. (2015) Radial consolidation response upon the application and removal of vacuum and fill loading, *Canadian Geotechnical Journal*, 52 (12), 2156 - 2162

Kitazume M. and Terashi M. 2013. The Deep Mixing Method, *CRC Press, Taylor & Francis Group*, 410p.

Komornik A. and David D. 1969. Prediction of Swelling Pressure of Clays, *Journal of the Soil Mechanics and Foundations Division*, 95, 209-226

Konrad J.M. and Morgenstern N.R. 1980. A mechanistic theory of ice lens formation in fine-grained soils. *Canadian Geotechnical Journal*, 17(4), 473-486.

Konrad J.M. and Morgenstern N.R. 1981. The segregation potential of a freezing soil. *Canadian Geotechnical Journal*, 18(4), 482-491.

Konrad J.M. and Morgenstern N.R. 1982a. Prediction of frost heave in the laboratory during transient freezing. *Canadian Geotechnical Journal*, 19(3), 250-259.

Konrad J.M. and Morgenstern N.R. 1982b. Effects of applied pressure on freezing soils. *Canadian Geotechnical Journal*, 19(4), 494-505.

Kouroussis G. Van Parys L. Conti C. and Verlinden O. 2014. Using three-dimensional finite element analysis in time domain to model railway-induced ground vibrations. *Advances in Engineering Software*, 70, 63-76.

Kouroussis G. and Verlinden O. 2015. Prediction of railway ground vibrations: accuracy of a coupled lumped mass model for representing the track/soil interaction. *Soil Dynamics and Earthquake Engineering* 69, 220-226.

Kujala K. 1997. Estimation of frost heave and thaw weakening by statistical analyses and physical models. *In: Knutsson, S. Ž . Ed. , Ground Freezing '97, Proceedings of the International Symposium on Ground Freezing and Frost Action in Soils*, Lulea, Sweden. A.A. Balkema, The Netherlands, 31–42

Kumara JJ. and Hayano K. 2016. Deformation characteristics of fresh and fouled ballasts subjected to tamping maintenance, *Soils and Foundations*, 56(4), 652-63.

Lackenby J. Indraratna B. McDowell G.R. and Christie D. 2007. Effect of confining pressure on ballast degradation and deformation under cyclic triaxial loading. *Geotechnique*, 57(6), 527–536.

Lakuši S. Ahac M. and Haladin I. (2010) Experimental investigation of railway track with under sleeper pad. *Proceedings of the 10th Slovenian Road and Transportation Congress*, 386-393.

Lamas-Lopez F. Cui Y.-J. Calon N. D'Aguiar S.C. De Oliveira M.P. and Zhang T. 2016. Track-bed mechanical behaviour under the impact of train at different speeds. *Soils and Foundations*, 56, 627-639.

Lee K.H. and Pande G.N. 2004. Development of a two-surface model in the Multi-laminate framework. *Proceedings of the 11th Conference on Numerical Models in Geomechanics*, Ottawa, 139-144.

Le Pen L. Powrie W. Zervos A. Ahmed S. and Aingaran S. 2013. Dependence of shape on particle size for a crushed rock railway ballast. *Granular Matter*, 15(6), 849-861. https://doi.org/10.1007/s10035-013-0437-5

Le Pen L. Ahmed S. Zervos A. Harkness J. and Powrie W. 2014. Resin recovery and the use of computed tomography for quantitative image analysis of railway ballast. *Proceedings of the Second International Conference on Railway Technology: Research, Development and Maintenance*, France Ed. J. Pombo. https://doi.org/10.4203/ccp.104.130

Le Pen L. Milne D. Watson G. Harkness J. and Powrie W. (2020). A model for the stochastic prediction of track support stiffness. *Proceedings of the Institution of Mechanical Engineers*, Part F: Journal of Rail and Rapid Transit, 234, 468-481

Li D. Hyslip J. Sussmann T. and Chrismer S. 2015. *Railway geotechnics:* CRC Press.

Li L. Nimbalkar S. and Zhong, R. 2018. Finite element model of ballasted railway with infinite boundaries considering effects of moving train loads and Rayleigh waves. *Soil Dynamics and Earthquake Engineering*, 114, 147-153.

Li H. and McDowell G. 2020. Discrete element modelling of two-layered ballast in a box test. *Granular Matter*, 22(4), 76

Li J. Cameron D. and Ren G. 2013. Case study and back analysis of a residential building damaged by expansive soils, *Computers and Geotechnics*, 56, 89-99.

Li N. Chen B. Chen F. and Xu X. 2000. The coupled heat-moisture-mechanic model of the frozen soil. *Cold Regions Science and Technology*, 31(3), 199-205.

Li, N., Chen, F., Su, B., & Cheng, G. (2002). Theoretical frame of the saturated freezing soil. Cold Regions Science and Technology, 35(2), 73-80.

Li T. Su Q. Kaewunruen S. 2019. Saturated ground vibration analysis based on a three-dimensional coupled train-track-soil interaction model. *Applied Sciences*, 9, 4991.

Li X. Ekh M. and Nielsen J.C. 2016. Three-dimensional modelling of differential railway track settlement using a cycle domain constitutive model. *International Journal for Numerical and Analytical Methods in Geomechanics*, 40, 1758-1770.

Liang T. Bengough A.G. Knappett J.A. Muir-Wood D. Loades K.W. Hallett P.D. Boldrin D. Leung A.K. and Meijer G.J. 2017. Scaling of the reinforcement of soil slopes by living plants in a geotechnical centrifuge. *Ecological Engineering*, 109(Part B), 207-227. https://doi.org/10.1016/j.ecoleng.2017.06.067

Liu J.K. and Xiao J.H. 2010. Experimental study on the stability of railroad subgrade with increasing train speed. *J. Geotech. Geoenviron*. ASCE, 136(6), 833-841.

Liu S. Huang H. Qiu T. and Gao L. 2016a. Comparison of laboratory testing using SmartRock and discrete element modeling of ballast particle movement, *Journal of Materials in Civil Engineering*, 29(3), D6016001.

Liu Z. Yu X.B. Tao J.L. and Sun Y. 2012. Multiphysics extension to physically based analyses of pipes with emphasis on frost actions. *Journal of Zhejiang University-Science A*, 13(11), 877-887.

Lopes D. and Karunarathne A. 2017. New Conditioned Soil Index Test and Characteristic Ground Movement Calculation Model. *Geotechnical Special Publication: Proceedings of the Second Pan-American Conference on Unsaturated Soils (PanAm Unsaturated Soils 2017)*, Dallas, Texas, GSP 303, 81-89

López-Acosta N.P. Espinosa-Santiago A.L. Pineda-Núñez V.M. Ossa A. Mendoza M.J. Ovando-Shelley E. and Botero E. 2019. Performance of a test embankment on very soft clayey soil improved with drain-to-drain vacuum preloading technology, *Geotextiles and Geomembranes*, 47 (5), 618-631.

Lu N. and Likos W.J. 2006. Suction stress characteristic curve for unsaturated soil. *J. Geotech. Geoenviron. Eng.* 132, 131–142. doi:10.1061/(ASCE)1090-0241(2006)132:2(131)

Lytton R. Aubeny C. and Bulut R. 2005. Design Procedures for Soils on Expansive Soils: Volume 1. *FHWA/TX-05/0-4518*. Texas Department of Transportation.

Lytton R.L. Pufahl D.E. Michalak C.H. Liang H.S. and Dempsey K.J. 1990. An Integrated Model of the Climatic Effects on Pavement. *Report No. FHWA-RD-90-033.* Federal Highway Administration, Texas Transportation Institute, Texas A&M University McLean, VA.

MacKay M.H. Hein D.K. and Emery J.J. 1992. Evaluation of frost action mitigation procedures for highly frost-susceptible soils. *Transportation Research Record: Journal of the Transportation Research Board*, 1362, 79-89.

Malisetty R.S. Indraratna B. and Vinod, J. 2020a. Behaviour of ballast under principal stress rotation: Multi-laminate approach for moving loads. *Computers and Geotechnics*, 125, 103655.

Malisetty R.S. Indraratna B. and Vinod J.S. 2020b. Multi-laminate Mathematical Framework for Analyzing the Deformation of Coarse Granular Materials. *International Journal of Geomechanics,* 20(6): 06020004.

Mamou A. Powrie W. Priest J.A. and Clayton C.R.I. 2017. The effects of drainage on the behaviour of railway track foundation materials during cyclic loading. *Géotechnique*, 67(10) 845–854.

Mamou A. Priest J.A. Clayton C.R.I. and Powrie W. 2018. Behaviour of saturated railway track foundation materials during undrained cyclic loading. *Canadian Geotechnical Journal*, 55(5), 689 697.

Mamou A. Clayton C. Powrie W. and Priest J. 2019a. The role of clay content on the response of railway track foundations during free-to-drain cyclic changes in principal stress rotation. *Transportation Geotechnics*, 20: 100246.

Mamou A. Powrie W. Priest J.A. and Clayton, C.R.I. 2019b. The use of the hollow cylinder apparatus to study stress paths relevant to railway track foundations. In *Proceedings of the 7th International Symposium on Deformation Characteristics of Geomaterials*, Glasgow, UK.

Mamou A. Powrie, W. Clayton C.R.I. Priest J.A. 2021. Suitability of empirical equations for estimating permanent settlement of railway foundation materials subjected to cyclic loading with principal stress rotation. *Canadian Geotechnical Journal*. 58(10), 1603-1610.

Mashiri M.S. Vinod J.S. Sheikh M.N. and Tsang H.H. 2015. Shear strength and dilatancy behaviour of sand–tyre chip mixtures. *Soils and Foundations*, 55(3), 517-528.

McDowell G.R. and Li H. 2016. Discrete element modelling of scaled railway ballast under triaxial conditions. Granular Matter 18(3), 66

McKeen R.G. and Johnson L.D. 1990. Climate-Controlled Soil Design Parameters for Mat Foundations. *J. of Geotechnical Eng.*, 116(7), 1073-1094.

McKenna G. Argyroudis S.A. Winter M.G. and Mitoulis S.A. 2021, Multiple hazard fragility analysis for granular highway embankments: Moisture ingress and scour, *Transportation Geotechnics*, 26, 100431, ISSN 2214-3912, https://doi.org/10.1016/ j.trgeo.2020.100431.

Meijer G. Muir-Wood D. Knappett J.A. Bengough G.A. and Liang T. (Accepted/In press). Root reinforcement: continuum framework for constitutive modelling. *Geotechnique*.

Miller R.D. 1972. Freezing and heaving of saturated and unsaturated soils. *Highway Research Record, In Proc. Int. Conf. Permafrost, 2nd, Yakutsk*, Siberia. 13–28 July 1973. Natl. Acad. Sci., Washington, DC.1972, 344-452(393).

Miller R.D. 1978. Frost heaving in non-colloidal soils. *In Proc. Int. Conf. on Permafrost, 3rd, Edmonton, AB, Canada*. Natl. Res. Counc. of Canada, Ottawa, ON, 708–713.

Milne D. Le Pen L. Thompson D. and Powrie W. (2017). Properties of train load frequencies and their applications. *Journal of Sound and Vibration* 397, 123-140. https://doi.org/10.1016/j.jsv.2017.03.006

Milne D. Harkness J. Le Pen L. and Powrie W. (2019). The influence of variation in track level and support system stiffness over longer lengths of track for track performance and vehicle track interaction. *Vehicle System Dynamics*. https://doi.org/10.1080/ 00423114. 2019.1677920

Mitchell J. and Kelly R. 2013. Addressing some current challenges in ground improvement, *Proc ICE Ground Improvement*, 1, 1-11

Mitchell P.W. 1980. The Concepts Defining the Rate of Swell of Expansive Soils. *Proceedings of the 4th International Conference on Expansive Soils. Denver, USA*. 1, 106-116.

Mitchell P.W. 2008. Footing Design for Residential Type Structures in Arid Climates. *Australian Geomechanics*, 41(4). 51-68.

Mitchell P.W. 2013. Climate Change Effects on Expansive Soil Movements. *Proceedings of the 18th International Conference on Soil Mechanics and Geotechnical Engineering*. Paris, 1159-1162.

Muttuvel T. Kelly R. Malorey D. Litvin E. and Pineda J. 2020. Internal compression of fill materials originating from Bringelly Shale. *Proc. Australian Geomechanics Society Sydney Symposium*

National Academies of Sciences, Engineering, and Medicine 2019. Critical Issues in Transportation 2019. Washington, DC: The National Academies Press. https://doi.org/10.17226/25314

Navaratnarajah S.K. Indraratna B. and Ngo, N.T. 2018. Influence of Under Sleeper Pads on Ballast Behavior Under Cyclic Loading: Experimental and Numerical Studies. *Journal of Geotechnical and Geoenvironmental Engineering*, 144(9), 04018068.

Navy, Dept. of, Naval Facilities Engineering Command. 1971. Design Manual-Soil Mechanics, Foundations & Earth Structures. *U.S. Naval Publications & Forms Center*, NAVFAC DM-7.

Nayak N.V. and Christensen R.W. 1971. Swell characteristics of compacted expansive soils. *Clay & Clay Minerals*. 19(4), 251-261.

Neaupane K.M. and Yamabe T. 2001. A fully coupled thermo-hydro-mechanical nonlinear model for a frozen medium. *Computers and Geotechnics*, 28(8), 613-637.

Nelson J.D. and Miller D.J. 1992. *Expansive Soils: Problems and Practice in Foundation and Pavement Engineering*. John Wiley & Sons, Inc.

Nelson J.D. Overton D.D. and Durkee D.B. 2001. Depth of Wetting & the Active Zone. *Proceedings of Expansive Clay Soils & Vegetative Influence on Shallow Foundations*, Houston, Texas, USA, ASCE, 95-109.

Neupane D. Yasuhara H. Kinoshita N. and Ando Y. 2015. Distribution of Mineralized Carbonate and Its Quantification Method in Enzyme Mediated Calcite Precipitation Technique. *Soils and Foundations*, 55(2), 447-457.

Newman G.P. and Wilson G.W. 1997. Heat and mass transfer in unsaturated soils during freezing. *Can. Geotech. J*. 34, 63–70

Ngo N.T. Indraratna B. and Rujikiatkamjorn C. 2014. DEM simulation of the behaviour of geogrid stabilised ballast fouled with coal. *Computers and Geotechnics*, 55, 224-231

Ngo N.T. Indraratna B. and Rujikiatkamjorn C. 2016. Modelling geogrid-reinforced railway ballast using the discrete element method. *Transportation Geotechnics*, 8, 86-102

Ngo N.T. Indraratna B. and Rujikiatkamjorn C. 2017. Simulation Ballasted Track Behavior: Numerical Treatment and Field Application. *International Journal of Geomechanics*, 17(6), 04016130.

Ngo N.T. Indraratna B. and Rujikiatkamjorn C. 2019. Improved performance of ballasted tracks under impact loading by recycled rubber mats. *Transportation Geotechnics*, 20, 100239.

Ngo, N.T. and Indraratna B. 2020. Mitigating ballast degradation with under-sleeper rubber pads: Experimental and numerical perspectives. *Computers and Geotechnics*, 122, 103540

Nguyen K. Villalmanzo D. Goicolea J. and Gabaldon F. 2016. A computational procedure for prediction of ballasted track profile degradation under railway traffic loading. *Proceedings of the Institution of Mechanical Engineers, Part F: Journal of Rail and Rapid Transit*, 230, 1812-1827.

Nguyen T.T. and Indraratna B. 2020. A coupled CFD-DEM approach to examine the hydraulic critical state of soil under increasing hydraulic gradient. *ASCE International Journal of Geomechanics*, 20(9): 04020138-1:15. doi: https://doi.org/10.1061/ (ASCE)GM.1943-5622.0001782.

Nimbalkar S. Indraratna B. Dash S.K. and Christie D. 2012. Improved Performance of Railway Ballast under Impact Loads Using Shock Mats. *Journal of Geotechnical and Geoenvironmental Engineering*, 138(3), 281-294.

Nimbalkar S. and Indraratna B. 2016. Improved performance of ballasted rail track using geosynthetics and rubber shockmat. *Journal of Geotechnical and Geoenvironmental Engineering*, 142(8): 4016031.

Nishimura S. Gens A. Olivella S. and Jardine R.J. 2009. THM-coupled finite element analysis of frozen soil: Formulation and application. *Geotechnique* 59, 159–171. doi:10.1680/geot.2009.59.3.159

Nobel C.A. 1966. Swelling measurements & prediction of heave for a lacustrine clay. *Can. Geotechnical Journal*, 3(1), 32-41.

Noborio K. McInnes K.J. and Heilman J.L. 1996. Two-dimensional model for water, heat and solute transport in furrow-irrigated soil: I. Theory. *Soil Sci. Soc. Am. J.* 60, 1001–1009. doi:10.2136/sssaj1996.03615995006000040007x

OECD Futures Project on Transcontinental Infrastructure Needs to 2030/50. 2011 Strategic Transport Infrastructure Needs to 2030: Main Findings

O'Donnell S.T. 2016. Mitigation of Earthquake-Induced Soil Liquefaction via Microbial Denitrification: A Two-Stage Process. *Doctoral Dissertation, Arizona State University*.

O'Donnell S.T. Rittmann B.E. and Kavazanjian E. 2017a. MIDP: Liquefaction Mitigation via Microbial Denitrification as a Two-Stage Process. I: Desaturation. *Journal of Geotechnical and Geoenvironmental Engineering*, 143(12).

O'Donnell S.T. Kavazanjian E. and Rittmann B.E. 2017b. MIDP: Liquefaction Mitigation via Microbial Denitrification as a Two-Stage Process. II: MICP. *Journal of Geotechnical and Geoenvironmental Engineering*, 143(12).

Olaiz A.H. Singhar S.H. Vann J.D. and Houston S.L. 2016. Comparison & applications of the Thornthwaite moisture index using GIS. *Proc. of the 2nd PanAm Conf. on Unsaturated Soils*, Dallas, TX, 1, ASCE

Olaiz A.H. 2017. *Evaluation of Testing Methods for Suction-Volume Change of Natural Clay Soils.* Arizona State University.

Olaiz A.H. Mosawi M. and Zapata C.E. 2021. An improved framework for volume change of shrink/swell soils subjected to time-varying climatic effects. *Soils and Rocks*, 44(3), [e2021065621]. https://doi.org/10.28927/SR.2021.065621

O'Neill K. and Miller R.D. 1985. Exploration of a rigid ice model of frost heave. *Water Resour. Res*. 21, 281–296. doi:10.1029/WR021i003p00281

Oswell J.M. 2011. Pipelines in permafrost: geotechnical issues and lessons. *Canadian Geotechnical Journal*, 48(9), 1412-1431.

Paixão A. Alves Ribeiro C. Pinto N. Fortunato E. and Calçada R. (2014). On the use of under sleeper pads in transition zones at railway underpasses: experimental field testing. *Structure and Infrastructure Engineering*, 1-17.

Parente M. Correia A.G. Cortez P. 2016. A Novel Integrated Optimization System for Earthwork Tasks. *Transportation Research Procedia*, 14, pp. 3601-3610, DOI: 10.1016/j.trpro.2016.05.428

Perera Y.Y. Zapata C.E. Houston W.N. and Houston S.L. 2004. Moisture Equilibria beneath Highway Pavements, *Transportation Research Board 83rd Annual Meeting CD-ROM*, National Research Council, Washington D.C.

Pham V.P. van Paassen L.A. Star W.R.L.v.d. and Heimovaara T.J. 2018. Evaluating Strategies to Improve Process Efficiency of Denitrification-Based MICP. *Journal of Geotechnical and Geoenvironmental Engineering*, 144(8).

Picornell M. and Lytton R.L. 1984. Modeling the heave of a heavily loaded foundation. *Proceeding of 5th International Conference on Expansive Soils.* Adelaide, Australia. 104-108

Pineda J.A. Alonso E.E and Romero E. 2014. Environmental degradation of claystones, *Geotechnique*, 64(1), 64-821

Porter A.A. and Nelson J.D. 1980. Strain controlled testing of soils. *Proc. 4th Int. Conf Expansive Soils*, ASCE & Int. Soc. Soil Mech. Found. Eng. Denver, CO. 34-44

Post-Tensioning Institute. 2004. *Design of Post-Tensioned Slabs-on-Ground. Phoenix: 3rd Edition*, Post-Tensioning Institute.

Post-Tensioning Institute, 2008. *Design & construction of post-tensioned slabs-on-ground, 3rd edition*. Post Tensioning Institute, Phoenix.

Potticary M. Zervos A. and Harkness J. 2014. A numerical investigation into the effect of particle form on the strength of granular materials. *22nd UK National Conference of the Association for Computational Mechanics in Engineering*, United Kingdom.

Potticary M. Zervos A. and Harkness J. 2015. An investigation into the effect of particle platyness on the strength of granular materials using the discrete element method. *IV International Conference on Particle-based Methods. Fundamentals and Applications (PARTICLES 2015),* Spain. 767-778.

Potticary M. Zervos A. and Harkness J. 2016. The effect of particle elongation on the strength of granular materials. *24th Conference on Computational Mechanics*, United Kingdom, 239-242.

Potticary M. 2018. A Numerical Investigation of the Effect of Particle Shape on the Strength of Coarse Granular Materials. *PhD Thesis*, University of Southampton, UK.

Powrie W. Yang L.A. and Clayton C.R.I. 2007. Stress changes in the ground below ballasted railway track during train passage. *Proceedings of the Institution of Mechanical Engineers: Part F: Journal of Rail and Rapid Transit*, 247-261.

Powrie W. 2014. On track: the future for rail infrastructure systems. *Proceedings of the Proceedings of the Institution of Civil Engineers-Civil Engineering.* Thomas Telford Ltd, 167, 177-185.

Powrie W. and Smethurst J.A. 2015. Discrete passive piles for infrastructure slope stabilization. *International Conference on Soft Ground Engineering* (ICSGE 2015), Singapore.

Powrie, W., Le Pen, L., Milne, D., Watson, G., & Harkness, J. (2019a). Behaviour of under-track crossings on ballasted railways. *Transportation Geotechnics*, 21, [100258]. https://doi.org/10.1016/j.trgeo.2019.100258

Powrie W. Le Pen L. Milne D. and Thompson D. (2019b). Train loading effects in railway geotechnical engineering: ground response, analysis, measurement and interpretation. *Transportation Geotechnics*, 21, 1-12. [100261]. https://doi.org/10.1016/j.trgeo.2019.100261

Priest J.A. Powrie W. Yang, L. Grabe, P.J. and Clayton, I. (2010). Measurements of transient ground movements below a ballasted railway line. *Géotechnique*, 60(9), 667–677.

Putra H. Yasuhara H. Kinoshita N. Neupane D. and Lu C. 2016. Effect of Magnesium as Substitute Material in Enzyme-Mediated Calcite Precipitation for Soil-Improvement Technique. *Front. Bioeng. Biotechnol.*, 4.

Qi Y. Indraratna B. and Vinod J S. 2018. Behavior of Steel Furnace Slag, Coal Wash, and Rubber Crumb Mixtures with Special Relevance to Stress-Dilatancy Relation. *Journal of Materials in Civil Engineering* 30(11): 04018276.

Qi Y. Indraratna B. Heitor A. and Vinod J. 2019a. The influence of rubber crumbs on the energy absorbing property of waste mixtures. *Geotechnics for Transportation Infrastructure*. Sundaram R., S. J., Havanagi V. Singapore, Springer. 29: 271-281.

Qi Y. Indraratna B. and Coop M.R. 2019b. Predicted Behavior of Saturated Granular Waste Blended with Rubber Crumbs. *International Journal of Geomechanics* 19(8): 04019079.

Qian Y. Mishra D. Tutumluer E. and Kazmee HA. 2015. Characterization of geogrid reinforced ballast behavior at different levels of degradation through triaxial shear strength test and discrete element modeling. *Geotextiles and Geomembranes* 43(5), 393-402

Qian J.G. Wang Y.G. Yin Z.Y. and Huang M.S. 2016. Experimental identification of plastic shakedown behavior of saturated clay subjected to traffic loading with principal stress rotation. *Engineering Geology*, 214, 29-42.

Rabin Y. and Steif P.S. 1998. Thermal stresses in a freezing sphere and its application to cryobiology. *Journal of Applied Mechanics*, 65(2), 328-333.

Ramos A. Gomes Correia A. Indraratna B. Ngo T. Calçada R. and Alves Costa P. 2020. Mechanistic-empirical permanent deformation models: Laboratory testing, modelling and ranking. *Transportation Geotechnics*. 23. 100326. 10.1016/j.trgeo.2020.100326.

Rana S. Subramani P. Fangueiro R. and Correia A.G. 2016. A review on smart self-sensing composite materials for civil engineering applications, *AIMS Materials Science*, Vol 3(2), 357-379

Ranganathan B.V. and Satyanarayana B. 1965. A rational method of predicting swelling potential for compacted expansive clays. *Proceedings of the 6th International Conference on Soil Mechanics & Foundation Engineering.* International Society for Soil Mechanics & Geotechnical Engineering, London, 1, 92-96.

Rebata-Landa V. and Santamarina J.C. 2012. Mechanical effects of biogenic nitrogen gas bubbles in soils. *Journal of Geotechnical and Geoenvironmental Engineering*, 138(2), 128-137.

Rosenbalm D.C. and Zapata C.E. 2013. Incorporation of the Soil-Water Characteristic Curve Hysteresis in Pavement Design. *Advances in Unsaturated Soils. Caycedo et al. (eds). Proc. of the First Pan-American Conf. on Unsaturated Soils*, ASCE, Cartagena, Colombia, Taylor & Francis Group, 461-467.

Rosenbalm D.C. and Zapata C.E. 2017. Effect of wetting and drying cycles on the behavior of compacted expansive soils, *Journal of Materials in Civil Engineering*, 29(1), 04016191. https://doi.org/10.1061/(ASCE)MT.1943-5533.0001689

Rouainia M. Helm P. and Davies O. 2020. Deterioration of an infrastructure cutting subjected to climate change. *Acta Geotechnica* 15, 2997–3016. https://doi.org/10.1007/s11440-020-00965-1

Roy M. Crispin J. Konrad J.M. and Larose G. 1992. Field study of two road sections during a freeze-thaw cycle. *Transportation Research Record: Journal of the Transportation Research Board*, 1992, (1362), 71-78

Rujikiatkamjorn C. Indraratna B. and Chiaro G. 2013. Compaction of coal wash to optimise its utilisation as water-front reclamation fill. *Geomechanics and Geoengineering*, 8, 36-45.

Salour F. Erlingsson S. and Zapata C.E. 2014. Modelling Resilient Modulus Seasonal Variation of Silty Sand Subgrade Soils with Matric Suction Control. *Canadian Geotech. J.* 51(12), 1413-1422.

Salour F. Erlingsson S. and Zapata C.E. 2015. Model for Seasonal Variation of Resilient Modulus in Silty Sand Subgrade Soil: Evaluation with Falling Weight Deflectometer. *Transportation Research Record: J. of the Transportation Research Board, No. 2510*. Transportation Research Board of the National Academies, Washington, D.C, 65-73.

Sampson E. Schuster R.L. and Budge W.D. 1965. A method of determining swell potential of an expansive clay. *Proc. Engineering*

Effects of Moisture Changes in Soils. Int. Res. Eng. Conf Expansive Clay Soils. Texas A & M Univ. Press, College Station, TX, 255-275.

Sarker P. and Tutumluer E. 2020. A Stress-history-based Approach for Predicting Deformation Potentials of Granular Base and Subbase Layers in Airport Pavements (NAPTF CC5 data analysis), *FAA Final Report FAA_UILU-ENG-2020-2013*

Sayeed M.A. and Shahin M.A. 2016. Three-dimensional numerical modelling of ballasted railway track foundations for high-speed trains with special reference to critical speed. *Transportation Geotechnics*, 6, 55-65.

Schaus L. Eng P. Popik M. and Eng M. 2011. Frost heaves: a problem that continues to swell. *In Conference and Exhibition of the Transportation Association of Canada. Transportation Successes: Let's Build on Them*.

Schneider G.L. and Poor A.R. 1974. The prediction of soil heave & swell pressures developed by an expansive clay. *Research Report, No: TR-9-74.* Construction Research Center, Univ. of Texas.

Seed H.B. Woodward R.J. and Lundgren R. 1962. Prediction of Swelling Potential for Compacted Clays. *Journal of the Soil Mech. Found. Div., ASCE*, 88, SM4, 57-59.

Selig E.T. and Waters J.M. 1994. Track geotechnology and substructure management, Thomas Telford, London.

Senetakis K. Anastasiadis A. and Pitilakis K. 2012. Dynamic properties of dry sand/rubber (SRM) and gravel/rubber (GRM) mixtures in a wide range of shearing strain amplitudes. *Soil Dynamics and Earthquake Engineering*, 33(1): 38-53.

Shanker N.B. Ratnam M.V. and Rao A.S. 1987. Multi-dimensional swell behaviour of expansive clays. *Proc. 6th Int. Conf. Expansive Soils*. New Delhi, India.

Sheng X. Jones C.J.C. and Thompson D.J. 2004. A theoretical study on the influence of the track on train-induced ground vibration. *Journal of Sound and Vibration*, 272, 909-936

Sheng D. Fredlund D.G. and Gens A. 2008. A new modelling approach for unsaturated soils using independent stress variables. *Canadian Geotechnical Journal*, 45(4): 511–534. doi:10. 1139/T07-112.

Shi S. Gao L. Cai X. Yin H. and Wang X. 2020. Effect of tamping operation on mechanical qualities of ballast bed based on DEM-MBD coupling method. *Computers and Geotechnics*, 124, 103574

Shih J.-Y. Thompson D. and Zervos A. 2016. The effect of boundary conditions, model size and damping models in the finite element modelling of a moving load on a track/ground system. Soil Dynamics and Earthquake Engineering, 89, 12-27.

Signes C.H. Fernández P.M. Perallón E.M. and Franco R.I. 2015. Characterisation of an unbound granular mixture with waste tyre rubber for subballast layers. *Materials and Structures*, 48(12): 3847-3861.

Simpson B. and Tatsuoka F. 2008. Geotechnics: the next 60 years. The Essence of Geotechnical Engineering: *60 Years of Geotechnique*. Thomas Telford, London, UK, 49–60

Singhal S. 2010. Expansive Soil Behavior: Property Measurement Techniques & Heave Prediction Methods. *Ph.D. Dissertation, Arizona State University*, Tempe, AZ, USA

Smethurst J.A. Clarke D. and Powrie W. 2012. Factors controlling the seasonal variation in soil water content and pore water pressures within a lightly vegetated clay slope. *Géotechnique*, 62(5), 429-446. https://doi.org/10.1680/geot.10.p.097

Smethurst J.A. Briggs K.M. Powrie W. Ridley A. and Butcher D.J.E. 2015. Mechanical and hydrological impacts of tree removal on a clay fill railway embankment. *Géotechnique*, 65(11), 869-882. https://doi.org/10.1680/jgeot.14.P.010

Smethurst J. Bicocchi N. Powrie W. and O'Brien. A. S. 2020. Behaviour of discrete piles used to stabilise a tree-covered railway embankment. *Géotechnique*, 70(9), 774-790. [18-P-150R1]. https://doi.org/10.1680/jgeot.18.P.150

Smith A.W. 1973. Method for determining the potential vertical rise, PVR. Proc. *Workshop Expansive Clays & Shales in Highway Design & Construction.* Univ. of Wyoming, Denver, CO, 245-249.

Sol-Sánchez M. Moreno-Navarro F. and Rubio-Gámez M.C. 2015. The use of elastic elements in railway tracks: A state of the art review. *Construction and Building Materials*, 75, 293-305.

Sridharan A. Sreepada Rao A. and SivapuUaiah, P.V. 1986. Swelling pressure of clays. *Geotechnical Testing Journal, GTJODJ*, 9(1), 24-33.

Stallings Young E.G. Zapata C.E. and van Paassen L. 2020. Unsaturated Fluid Flow through Granular Soils Treated with Microbial Induced Desaturation and Precipitation. *In Proceedings of the 4th European Conference on Unsaturated Soils (E-UNSAT 2020)* Online Conference, 195, 05003 (2020), October 19-21st, 2020, DOI: https://doi.org/10.1051/e3sconf/202019505003

Stallings Young E.G. 2021. Fluid Flow through Granular Soils Treated with Microbial Induced Desaturation and Precipitation. *Doctor of Philosophy Dissertation*, Arizona State University, ProQuest.

Stallings Young E.G. Mahabadi N. Zapata C.E. and Paassen L.A.v. 2021. Microbial-Induced Desaturation in Stratified Soil Conditions. *International Journal of Geosynthetics and Ground Engineering*, 7(37), 1-17.

Style R.W. Peppin S.S. Cocks A.C. and Wettlaufer, J.S. 2011. Ice-lens formation and geometrical supercooling in soils and other colloidal materials. *Physical Review E*, 84(4), 041402

Su Y. and Cui Y-J. 2022. Modelling the suction-dependent plastic shakedown limit of unsaturated fine/coarse soil mixture with consideration of soil-water retention curve. *Transportation Geotechnics*, 32, art. no. 100698

Subba Rao K.S. and Tripathy S. 2003. Effect of aging on swelling & swell-shrink behavior of a compacted expansive soil. *ASTM Geotechnical Testing Journal*, 26(1), 36-46.

Suhr B. Marschnig S. and Six K. 2018. Comparison of two different types of railway ballast in compression and direct shear tests: experimental results and DEM model validation. *Granular Matter*, 20(4), 70

Sullivan R.A. and McClelland B. 1969. Predicting heave of buildings on unsaturated clay. *Proc. 2nd Int. Res. Eng. Conf. Expansive Soils*. Texas A & M Univ. Press, College Station, TX, 404-420.

Summersgill F.C. Kontoe S. and Potts D.M. 2018. Stabilisation of excavated slopes in strain-softening materials with piles. *Géotechnique* 68, No. 7, 626–639, https://doi.org/10.1680/jgeot.17.P.096.

Sun Q. Indraratna B. and Ngo T.N. 2019. Effect of increase in load and frequency on the resilience of railway ballast. Géotechnique, 69(9), 833-840.

Sun. Xi. Li. Jie. and Zhou A. 2017. Evaluation and Comparison of Methods for Calculating Thornthwaite Moisture Index. *Australian Geomechanics Journal.* 52(2), 61-75

Svalova A. Prangle D. Wilkinson D.J. Helm P. Rouainia M. and Glendinning S. (2021). Emulating computer experiments of infrastructure slope stability in the London-Bristol rail corridor using Gaussian processes and Bayesian inference, *Data-Centric Engineering*, 2:e12.

Taber, S. The mechanics of frost heaving. *The Journal of Geology*, 1930, 38(4), pp. 303-317.

Tang Y. Xiao S. and Yang Q. 2019a. Numerical study of dynamic stress developed in the high speed rail foundation under train loads. Soil Dynamics and Earthquake Engineering, 123, 36-47.

Tang Y. Yang Q. Ren X. and Xiao S. 2019b. Dynamic response of soft soils in high-speed rail foundation: in situ measurements and time domain finite element method model. Canadian Geotechnical Journal, 56, 1832-1848.

Tasalloti S.M.A. Indraratna B. Rujikiatkamjorn C. Heitor A. and Chiaro G. 2015a. A laboratory study on the shear behavior of mixtures of coal wash and steel furnace slag as potential structural fill, *Geotechnical Testing Journal*, 38(4), 1-12.

Tasalloti S.M.A. Indraratna B. Chiaro G. and Heitor A. 2015b, Field investigation on compaction and strength performance of two coal wash-BOS slag mixtures, *ASCE Geotechnical Special Publication*, 256, 2359-2368 (Proc. of the 2015 International Foundations Congress. & Equipment Expo,, 17-21 March 2015, San Antonio, Texas, USA).

Tatsuoka F. Hashimoto T. and Tateyama K. 2021, Soil stiffness as a function of dry density and the degree of saturation for compaction control, *Soils and Foundations*, 61, 989-1002

Taylor G.S. and Luthin J.N. 1978. A model for coupled heat and moisture transfer during soil freezing. *Can. Geotech. J.* 15, 548–555. doi:10.1139/t78-058

Teng T.C.P. and Clisby M.B. 1975. Experimental work for active clays in Mississippi. Transport. *Eng. J. ASCE 101 (TEI)*: 77-95.

Teng T.C.P. Mattox R.M. and Clisby M.B. 1972. A study of active clays as related to highway design. *Research & Development Division, Mississippi State Highway Dept., Engineering & Industrial Research Station,* Mississippi State University, MSHD-RD-72-045, 134.

Teng T.C.P. Mattox R.M. and Clisby M.B. 1973. Mississippi's experimental work on active clays. *Proc. Workshop on Expansive Clays & Shales in Highway design & Construction*. Univ. of Wyoming, Laramie. 1-17

Tennakoon N. Indraratna B. Rujikiatkamjorn C. Nimbalkar S. and Neville T. 2012. The role of ballast-fouling characteristics on the drainage capacity of rail substructure. Geotechnical Testing Journal, 35(4), 1-11.

The Communist Party of China Central Committee and the State Council 2019. Program of Building National Strength in Transportation. http://www.gov.cn/xinwen/2019-09/19/content_5431432.htm (in Chinese)

Thomas H.R. Cleall P. Li Y.C. Harris C. and Kern-Luetschg M. 2009. Modelling of cryogenic processes in permafrost and seasonally frozen soils. *Geotechnique* 59, 173–184. doi:10.1680/geot. 2009.59.3.173

Thornthwaite C. 1948. An Approach Toward A Rational Classification of Climate, *Geographical Review*, 38(1), 55-94.

Thornthwaite C. and Mather J. 1955. The Water Balance, *Publications in Climatology*, 8(1)

Torres-Hernandez G. 2011. Estimating the Soil–Water Characteristic Curve using Grain Size Analysis and Plasticity Index. *Master's Thesis. Arizona State University*, Tempe, AZ.

Track Stiffness Working Group (2016). A Guide to Track Stiffness, Edited by W. Powrie & L Le Pen on behalf of the *cross industry track stiffness working group (TSWG)*. Southampton, UK; University of Southampton. ISBN: 9780854329946.

Trani L.D.O. and Indraratna B. 2012. A New Method of Filtration Design on Rail Track Subballast. *J. Geotech. Geoenviron. Eng*, 136(11), 1519-1528.

Tutumluer E. Huang H. and Bian X. 2012. Geogrid-Aggregate Interlock Mechanism Investigated through Aggregate Imaging-Based Discrete Element Modeling Approach. *International Journal of Geomechanics*, 12(4), 391-398.

Tutumluer E. Qian Y. Hashash YMA. Ghaboussi J. and Davis DD. 2013. Discrete element modelling of ballasted track deformation behaviour. *International Journal of Rail Transportation*, 1(1-2), 57-73.

University of Southampton (2013). Confidential report on Sand mitigation measures efficiency track resilience test carried out for Etihad Rail for the Shah-Habshan-Ruwais Railway Project

USA Army Corps of Engineers. 1948. Field Moisture Content Investigation. *T.M. 3-401, Interim Report No. 1*, Waterways Experiment Station

USA Army Corps of Engineers. 1955. Field Moisture Content Investigation. *T. M. 3-401, Report No. 2, October 1945 -November 1952 Phase*, Waterways Experiment Station

Van Der Merwe D.H. 1964. The prediction of heave from the plasticity index & percentage clay fraction of soils. *Civil Engineers in South Africa*, 6, 337-42.

van Paassen L. Daza C. Staal M. Sorokin D. van der Zon W. and van Loosdrecht M. 2010. Potential Soil Reinforcement by Biological Denitrification. *Ecological Engineering*, 36(2), 168-175.

Vanapalli S. and Lu L. 2012. A State-of-the Art Review of 1-D Heave Prediction Methods for Expansive Soils. *International Journal of Geotechnical Engineering*, 6(1), 15-41.

Vann J. Houston S. Houston W. Singhar S. Cuzme A. and Olaiz A. 2018. A soil suction surrogate & its use in the suction-oedometer method for computation of volume change of expansive soils. *Proc. of the 7th International Conference on Unsaturated Soil.* Hong Kong. 1205-1210

Vann J.D. 2019. A Soil Suction-Oedometer Method and Design Soil Suction Profile Recommendations for Estimation of Volume Change of Expansive Soils, *Doctoral Dissertation, Arizona State University*, Tempe, AZ.

Vann J.D. and Houston S. 2021. Field Suction Profiles for Expansive Soil, *J. of Geotechnical and Geoenvironmental Engineering*, 147(9), doi:10.1061/(ASCE)GT.1943-5606.0002570.

Varandas J.N. Paixão A. Fortunato E. and Hölscher P. 2016. A numerical study on the stress changes in the ballast due to train passages. *Procedia engineering*, 143, 1169-1176.

Varandas J. Paixão A. Fortunato E. Coelho B.Z. and Hölscher, P. 2020. Long-term deformation of railway tracks considering train-track interaction and non-linear resilient behaviour of aggregates–a 3D FEM implementation. *Computers and Geotechnics*, 126, 103712.

Walker R.T. Indraratna B. 2018. Moving loads on a viscoelastic foundation with special reference to railway transition zones. *International Journal of Geomechanics*, 18, 04018145.

Wang J. Zhou Z. Hu X. Guo L. and Cai Y. 2019. Effects of principal stress rotation and cyclic confining pressure on behavior of soft clay with different frequencies. *Soil Dynamics and Earthquake Engineering*, 118: 75-85.

Wang L. Van Paassen L. Gao Y. He J. Gao Y. and Kim, D. 2020. Laboratory tests on mitigation of soil liquefaction using microbial induced desaturation and precipitation. *Geotechnical Testing Journal*, 44(2).

Wang L. Gao Y. He J. Gao Y. and van Paassen L.A. 2021. Effect of Biogenic Gas Formation through Microbial Induced Desaturation and Precipitation on the Static Response of Sands with Varied Relative Density. *Journal of Geotechnical and Geoenvironmental Engineering*, 147(8), 04021071.

Wang W.L. and Yen B.C. 1974. Soil arching in slopes. *Journal of the geotechnical Engineering division* ASCE, 100(GT1), 61–78.

Ward Wilson, G. 1990. Soil Evaporative Fluxes for Geotechnical Engineering Problems. *PhD Thesis, University of Sasketchewan*, Canada.

Weston D.J. 1980. Expansive roadbed, treatment for Southern Africa. *Proceeding of the 4th International Conference on Expansive Soils*, 1, 339-360.

Witczak M.W. Zapata C.E. and Houston W.N. 2006. Models Incorporated into the Current Enhanced Integrated Climatic Model: *NCHRP 9-23 Project Findings and Additional Changes after Version 0.7. Final Report*. Project NCHRP 1-40D.

Woldringh R. and New B. 1999. Embankment design for high speed trains on soft soils. *Twelfth European Conference on Soil Mechanics and Geotechnical Engineering, Geotechnical Engineering for Transport Infrastructure*. Amsterdam. Rotterdam: Balkema

Woodman N. Smethurst J. Roose T. Powrie W. Meijer G. Knappett J. and Dias T. 2020. Mathematical and computational modelling of vegetated soil incorporating hydraulically-driven finite strain deformation. *Computers and Geotechnics*, 127, [103754]. https://doi.org/10.1016/j.compgeo.2020.103754

Wong H.Y and Yong R.M. 1973. A study of swelling & swelling force during unsaturated flow in expansive soils. *Proc. 3rd Int. Conf. Expansive Soils*, Haifa, Israel, 1, 143-151.

Wu, T. Cai Y. Guo L. Ling D. and Wang J. 2017. Influence of shear stress level on cyclic deformation behaviour of intact Wenzhou soft clay under traffic loading. *Engineering Geology*, 228, 61-70.

Xiao J. Juang C.H. Wei K. and Xu S. 2014. Effects of principal stress rotation on the cumulative deformation of normally consolidated soft clay under subway traffic loading. *Journal of Geotechnical and Geoenvironmental Engineering*, 140(4), 04013046.

Xie J Huang J Zeng C Jiang S-H and Podlich N. 2020. Systematic Literature Review on Data-Driven Models for Predictive Maintenance of Railway Track: Implications in Geotechnical Engineering, *Geosciences*, 10, 425; doi:10.3390/geosciences 10110425

Xu S. Liang R. and Edil T. (2015) Innovative Soft Soil Improvement Method through Intelligent Use of Vacuum De-Watering and Dynamic Compaction Techniques, *Geotechnical Engineering* 46(4), 57-67.

Yang L. Powrie W. Priest J. 2009. Dynamic stress analysis of a ballasted railway track bed during train passage. *Journal of Geotechnical and Geoenvironmental Engineering* 135, 680-689.

Yang Y.B. Liu S.J. Li Q.M. and Ge P.B. 2019. Stress waves in half-space due to moving train loads by 2.5D finite/infinite element approach. *Soil Dynamics and Earthquake Engineering*, 125, 105714.

Yasuhara H. Neupane D. Hayashi K. and Okamura M. 2012. Experiments and Predictions of Physical Properties of Sand Cemented by Enzymatically-induced Carbonate Precipitation. *Soils and Foundations*, 52(3), 539-549.

Youwai S. and Bergado D.T. (2003). Strength and deformation characteristics of shredded rubber tire-sand mixtures. *Canadian Geotechnical Journal*, 40(2), 254-264.

Yu X. and Kwon E. 2012. Carbon nanotube based self-sensing concrete for pavement structural health monitoring, *Research report University of Minnesota,* Duluth, Contract Number: US DOT: DTFH161-10-C-00911

Zapata C.E. Andrei D. Witczak M.W. and Houston W.N. 2007. Incorporation of Environmental Effects in Pavement Design. *Int. J. of Road Materials and Pavement Design*, 8(4). 667-693

Zapata C.E. Perera Y.Y. and Houston W.N. 2009. Matric Suction Prediction Model Used in the New AASHTO Mechanistic-Empirical Pavement Design Guide. *Transportation Research Record: J. of the Transportation Research Board, No. 2101, Geology and Properties of Earth Materials*, 53-62.

Zapata, C.E. 2018. Empirical approach for the use of unsaturated soil mechanics in pavement design. *Geotechnical Special Publication, 2017-November (GSP 300)*, 149-173. https://doi.org /10.1061/9780784481677.008

Zeng K. Qiu T. Bian X. Xiao M. and Huang H. 2019. Identification of ballast condition using SmartRock and pattern recognition, *Construction and Building Materials*, 221, 50-59.

Zhao H.D. Ling J.M. Fu P.C. 2013. A review of harvesting green energy from road. *Advanced Materials Research*, 723, 559-566, DOI: 10.4028/www.scientific.net/AMR.723.559

Zhao HY. Indraratna B. and Ngo N.T. 2021. Numerical simulation of the effect of moving loads on saturated subgrade soil, *Computers and Geotechnics* https://doi.org/10.1016/j.compgeo.2020.103930.

Zhang X. and Lytton R. 2009. Modified State-Surface Approach to the Study of Unsaturated Soil Behaviour. Part I: Basic Concept. *Canadian Geotechnical Journal*, 46, 1-17.

Zhang X. Zhao C. and Zhai W. 2017. Dynamic behavior analysis of high-speed railway ballast under moving vehicle loads using discrete element method. *International Journal of Geomechanics*, 17, 04016157.

Zhang Y. Gu C. Wang J. and Cai Y. 2021. Three-dimensional cyclic behavior of saturated clays: comparison between undrained and partly drained conditions. *Canadian Geotechnical Journal*, ahead of print

Zhang Y. and Michalowski R.L. 2015. Thermal-hydro-mechanical analysis of frost heave and thaw settlement. *Journal of Geotechnical and Geoenvironmental Engineering*, 141(7), 04015027.

Zhai W. Wang K. and Lin J. 2004. Modelling and experiment of railway ballast vibrations, *Journal of Sound and Vibration*, 270(4-5), 673-683.

Zheng D. Huang J. Li D-Q. Kelly R. and Sloan S.W. 2018, Embankment prediction using testing data and monitored behaviour: A Bayesian updating approach, *Computers and Geotechnics*, 93, 150–162,

Zhou M.M. and Meschke G. 2013. A three-phase thermo-hydro-mechanical finite element model for freezing soils. *International Journal for Numerical and Analytical Methods in Geomechanics*, 37(18), 3173-3193